THEORETICAL INVESTIGATION OF ALTINI TERNARY CLUSTERS: DENSITY FUNCTIONAL THEORY CALCULATIONS AND MOLECULAR DYNAMICS SIMULATIONS

A THESIS SUBMITTED TO
THE GRADUATE SCHOOL OF NATURAL AND APPLIED SCIENCES
OF
MIDDLE EAST TECHNICAL UNIVERSITY

BY

HÜSEYİN OYMAK

IN PARTIAL FULFILLMENT OF THE REQUIREMENTS FOR THE DEGREE OF

DOCTOR OF PHILOSOPHY

IN

PHYSICS

JUNE 2004

Approval of the Graduate School of Natural and Applied Sciences.

Prof. Dr. Canan Özgen
Director

I certify that this thesis satisfies all the requirements as a thesis for the degree of Doctor of Philosophy.

Prof. Dr. Sinan Bilikmen
Head of Department

This is to certify that we have read this thesis and that in our opinion it is fully adequate, in scope and quality, as a thesis for the degree of Doctor of Philosophy.

Prof. Dr. Şakir Erkoç
Supervisor

Examining Committee Members

Prof. Dr. Cemal Yalabık	(Bilkent University)	
Prof. Dr. Şakir Erkoç	(METU)	
Prof. Dr. Demet Gülen	(METU)	
Prof. Dr. O. Amdulla Mehrabov	(METU)	
Prof. Dr. Lemî Türker	(METU)	

"I hereby declare that all information in this document has been obtained and presented in accordance with academic rules and ethical conduct. I also declare that, as required by these rules and conduct, I have fully cited and referenced all material and results that are not original to this work."

Name Surname : HÜSEYİN OYMAK

Signature :

ABSTRACT

THEORETICAL INVESTIGATION OF AlTiNi TERNARY CLUSTERS: DENSITY FUNCTIONAL THEORY CALCULATIONS AND MOLECULAR DYNAMICS SIMULATIONS

OYMAK, HÜSEYİN

Ph.D., Department of Physics

Supervisor: Prof. Dr. Şakir Erkoç

June 2004, 156 pages.

This doctoral study consists of three parts. In the first part, structural and electronic properties of $Al_kTi_lNi_m$ $(k+l+m=2,3)$ microclusters have been investigated by performing density functional theory (DFT) calculations within the B3LYP [which comprises the Becke–88 exchange functional and the correlation functional of Lee, Yang, and Parr] and the effective core potential (ECP) level. Dimers and trimers of the elements aluminum, titanium, and nickel, and their binary and ternary combinations have been studied in their ground states. The optimum geometries, possible dissociation channels, vibrational properties, and electronic structure of the clusters under study have been obtained.

In the second part, after an empirical potential energy function (PEF) has been parametrized for the AlTiNi ternary system, stable (minimum–energy) structures of $Al_kTi_lNi_m$ $(k+l+m=4)$ microclusters have been determined by molecular dynamics (MD) simulations. The energetics of the microclusters in 1 K and 300 K have been

discussed. By performing, again, DFT calculations (within the B3LYP and ECP level), the possible dissociation channels and electronic properties of the obtained clusters have been calculated.

In the last part, using the empirical PEF parametrized previously for the AlTiNi ternary system, minimum–energy structures of $Al_nTi_nNi_n$ (n = 1–16) ternary alloy nanoparticles have been determined by performing MD simulations. The structural and energetic features of the obtained nanoparticles have been investigated.

Keywords: Transition metal clusters, aluminum, nickel, titanium, empirical potential energy functions, density functional theory, molecular dynamics simulations.

ÖZ

AlTiNi ÜÇLÜ TOPAKLARIN KURAMSAL OLARAK İNCELENMESİ: YOĞUNLUK FONKSİYONELİ KURAMI HESAPLARI VE MOLEKÜLER DİNAMİK SİMÜLASYONLARI

OYMAK, HÜSEYİN

Doktora, Fizik Bölümü

Tez Yöneticisi: Prof. Dr. Şakir Erkoç

Haziran 2004, 156 sayfa.

Bu doktora çalışması üç kısımdan oluşmaktadır. İlk kısımda, $Al_kTi_lNi_m$ $(k+l+m=2,3)$ yapısındaki mikrotopakların yapısal ve elektronik özellikleri incelenmiştir. Çalışmalar yoğunluk fonksiyoneli kuramı (YFK) hesapları yapılarak [etkili çekirdek potansiyeli (EÇP) düzeyinde ve B3LYP değiş–tokuş ve kaçınım katkısı dahil edilerek] gerçekleştirilmiştir. Alüminyum, nikel ve titan elementlerinin homonükleer ikili ve üçlü ve heteronükleer ikili ve üçlü bileşikleri temel seviyelerinde incelenmiştir. Çalışılan mikrotopakların minimum enerji geometrileri, mümkün ayrışma kanalları, ayrışma enerjileri, titreşim frekansları ve bazı elektronik yapı özellikleri hesaplanmıştır.

Çalışmanın ikinci kısmında, AlTiNi üçlü sistemi için bir ampirik potansiyel enerji fonksiyonu (PEF) parametrize edildikten sonra, $Al_kTi_lNi_m$ $(k+l+m=4)$ yapısındaki mikrotopakların minimum enerji yapıları moleküler dinamik (MD) simülasyonu ile belirlenmiştir. 1 K ve 300 K sıcaklıklarında elde edilen mikrotopakların genel enerji özellikleri tartışılmıştır. Mikrotopakların mümkün ayrışma kanalları, ayrışma enerjileri

ve bazı elektronik özellileri YFK hesapları (yine EÇP düzeyinde ve B3LYP katkısıyla) ile elde edilmiştir.

Çalışmanın son kısmında ise, ikinci kısımda AlTiNi üçlü sistemi için parametrize edilen ampirik PEF kullanılarak, $Al_nNi_nTi_n$ ($n = 1 - 16$) yapısındaki nano–parçacıkların minimum enerji yapıları MD simülasyonu ile belirlenmiştir. Elde edilen nano–parçacıkların genel yapısal özellikleri tartışılmıştır.

Anahtar Kelimeler: Geçiş elementleri topakları, alüminyum, nikel, titan, ampirik potansiyel enerji fonksiyonları, yoğunluk fonksiyoneli kuramı, moleküler dinamik simülasyonları.

aux mémoires de mon père, *Mehmet Oymak*

et

ma mère, *Fatma Oymak*

ACKNOWLEDGMENTS

I would like to express my sincere feelings to my supervisor, *Prof. Dr. Şakir Erkoç*. I am grateful to him for his painstaking care in the course of this project, for his meticulous effort in teaching me very precious, numerous concepts. I could have done nothing without him. I would like to thank also TÜRK PETROL VAKFI for the partial support they granted.

TABLE OF CONTENTS

LIST OF TABLES

LIST OF FIGURES

CHAPTER 1

INTRODUCTION

1.1 Al–Ti–Ni Binary and Ternary Materials and Their Importance

In this work, we deal with the microclusters of aluminum, nickel, and titanium. Recently their binary and ternary alloy systems have become very popular from the metallurgical point of view. Their crystal structure and phase diagram data, electronic structure, optical properties, etc. have been investigated intensely. There exist some recent experimental and theoretical studies about Al–Ti–Ni binary and ternary alloy systems [1–3], the Ni–Ti alloy system [4, 5], the Al–Ti alloy system [6, 7], and the Al–Ni alloy system [8, 9].

Atomistic studies of the structures of intermetallic materials have been of great value in the modeling and understanding of alloy behavior. With the advent of extremely fine–grained eutectic microstructures, Al–Ti–Ni alloys have attracted attention as soldering or brazing materials for Ni–based superalloy devices as well as for TiAl–based structural intermetallics [1]. Ni–based superalloys is of great

importance in many applications such as gas turbines, demolition devices, metal cutting and welding, and emergency beacons and flares [8]. Ni–Al and Ti–Al intermetallic alloys are candidate alloys for structural applications and consequently received theoretical interest [3]. Several Al–Ti intermetallic compounds have a number of outstanding high–temperature properties (such as high melting point, low density and good oxidation resistance) which make them desirable candidates for high temperature applications [6, 7]. In addition to their technologically useful properties, Al–Ti–Ni binary and ternary intermetallics also exhibit scientifically interesting complex structures. Noteworthy among these alloys are quasicrystals, ordered structures displaying crystallographically forbidden icosahedral or decagonal symmetry [9].

One of the most important reason of the intense interest in the Al–Ti–Ni binary and ternary intermetallics is their *shape–memory–alloy* (SMA) properties which render them industrially important [10, 11]. SMAs are "strange" materials exhibiting some novel properties. The most striking one is that they have the ability to return to a predetermined shape when heated. In other words, they "remember" and transform back to their original shape upon heating. When an SMA is cold, or when it is under its transformation temperature T_t, it has a very low *yield strength*. Therefore, it can readily be deformed into any shape at low temperatures. As long as the temperature is kept below T_t, the SMA will retain

its shape. However, when it is heated above T_t, its crystal structure undergoes a change which causes the SMA to return to its original shape. Furthermore, if the SMA encounters any resistance during this transformation, it can generate extremely large forces. Obviously, this property of SMAs can be fully exploited when a remote actuation or a sensor mechanism is needed; and this is only one among the very diverse current applications of SMAs.

The most famous SMA is the intermetallic Ni–Ti (usually called *nitinol*) alloys. It has been studied extensively due to its technological importance and its peculiar structural phase transition[1] that has been found in alloys near equiatomic stoichiometry. This transformation is associated with shape–memory effect. This transition also shows large hysteresis in electrical resistivity, Hall coefficient, sound velocity, magnetic susceptibility upon cooling or heating [5]. (There are lots of explanation trying to account for this unusual phase transition. A good review can be found in Ref. [5].) Additional stimulus for the research on Ni–Ti alloys is the finding that alloys on the Ti–rich side possesses glass–forming ability. Furthermore, a metastable quasicrystal can be formed near the stoichiometry $NiTi_2$ [4].

[1] Technically described as a martensitic transformation from the austenitic $B2$ phase at high temperature ($\geq$ 333 K) to the martensitic $B19'$ phase upon cooling [5].

Understanding of the microscopic origins of this type of structural properties of Al–Ti–Ni binary and ternary intermetallics has been at the core of chemistry, metallurgy, and condensed matter physics for a long time. Both technological need and fundamental scientific interest motivate study of these systems. Our interest in Al–Ti–Ni ternary clusters is to determine the very basic building blocks of and to explore the clustering phenomenon in these economically promising alloy systems. We desired to investigate systematically the simpler potential candidates for the building blocks, namely Al_2, Ti_2, Ni_2, AlTi, AlNi, TiNi, Al_3, Ti_3, Ni_3, Al_2Ti, $AlTi_2$, Al_2Ni, $AlNi_2$, Ti_2Ni, $TiNi_2$, as we did in the first part of our study (Section 2.2 and Ref.[12]); and the more involved candidates Al_4, Ti_4, Ni_4, Al_3Ti, Al_2Ti_2, $AlTi_3$, Al_3Ni, Al_2Ni_2, $AlNi_3$, Ti_3Ni, Ti_2Ni_2, $TiNi_3$, Al_2TiNi, $AlTi_2Ni$, $AlTiNi_2$, as we did in the second part of our study (Section 4.2 and Ref.[13]). In this regard, we continued our research series toward the larger clusters of Al–Ti–Ni ternary system, as we did in the last part (Section 4.3 and Ref.[14]). Our general objective is to get a general understanding of geometrical and electronic properties about these clusters, which is believed to lead valuable insights into the evolution from small clusters to bulk Al–Ti–Ni binary and ternary alloy systems. Accordingly, we have embarked on this study.

1.2 Clusters of Metal Atoms

In the past thirty years or so, a new type of chemical entity has come under both experimental and theoretical examination: clusters of metal atoms. The cluster area has been one of the most actively studied research field especially after 1980s; it today occupies an interdisciplinary place in the intersection point of quantum chemistry, solid–state physics, surface science, atomic and molecular physics, metallurgical sciences, etc. Although there is actually no need to point out it, it should not be superfluous, we think, to highlight the importance of the studies aimed at understanding structural and electronic properties of clusters.

Quantum molecular methods in cluster theory has proven its usefulness in quantum chemical investigations of the structural and electronic properties of small atomic and molecular clusters. The literature of past two decades is full of numerous theoretical and experimental studies devoted to characterize these unexamined species. The theoretical and experimental results of these studies, their far–reaching consequences, their practical and possible industrial applications have been collected in several reviews [15–21] and books [22–37]. At the fundamental level, these investigations are being carried out in order to reveal the very general physical and chemical properties of atoms under the specific conditions existing in clusters and therefore to reach a consensus in interpreting the

basic properties of clusters. Among these studies are abundances [20, 38], catalysis [28, 34, 39–51], chemisorption and substrate adsorption [43–46, 50, 52–65], crystal growth [16, 66–71], electronic structures, equilibrium structures, evolution of surface properties [72, 73], laser applications [46], magic numbers [16, 19, 28, 74–89], magnetism [62, 81, 84, 85, 90–99], nucleation [41, 42, 46, 65, 70, 72, 100–103], photographic processes [42, 46, 51], reactivity [28, 51, 104–106], properties as a function of clusters size [17, 45, 56, 73, 74, 85, 90, 91, 105, 107–116]. All the other information about the studies not mentioned above can be drawn from Refs. [15–37]. Notwithstanding the fact that a large and still increasing number of researches are at the moment being conducted with the aim of providing further theoretical contribution to the understanding of the cluster field, there will always be much yet to be studied. Each new study usually gives such results that cause new problems and questions to rise in this field. Although a substantial amount of information has been collected so far on clusters, all the facts about them have not understood completely yet. The cluster area is thus relatively young compared to the more established traditional areas of chemistry and physics.

The quantum molecular methods in efforts of revealing the properties of clusters are, of course, not alone. In addition to the theoretical studies (see Ref. [117] for a somewhat detailed description of the methods), experiments constitute the very indispensable part of the field of cluster research. They either precede theoretical studies giving them experimental results and thus offering impetus to researchers, or follow a theoretical study providing test confirming or refuting the results of it. This ceaseless interplay between theory and experiment leads to new scopes in understanding of the properties of clusters.

Clusters are generally defined as small aggregates of atoms. Their sizes are intermediate between constituent atoms and bulk matter. The number of atoms, N, making up a cluster is no more than a few hundred or at most a thousand; beyond this enters the field of nano–scale materials. *Small* clusters have structural and electronic properties which depend strictly on N. It is hardly possible to correlate these properties with smoothly varying functions of N. There are lots of experimental and theoretical studies which showed that the geometrical and electronic properties of small clusters exhibits no similarity at all compared with the properties corresponding bulk. This is one of the reasons that has rendered the cluster area being one of the most actively studied research field. The properties of a *large* cluster usually approach those of the corresponding bulk material. This puts the large clusters in front of the main door to the realm of the solid state.

Consequently, clusters can be thought to be on the border separating atoms and molecules from liquids and solids and this fact is perhaps the most important reason for the indispensability of the cluster area. From atoms and molecules to liquids and solids, it is possible only with the help of the studies of clusters to understand the evolution of structural and electronic properties of solid state [30, 31, 115]. (For a good discussion, the reader is recommended to have a look also at Reference [80], where clusters are described to be in the *mesoscopic* region between the microscopic region of atoms or molecules and the macroscopic region of the condensed matter. In that review, the authors build a bridge, for this mesoscopic region of clusters, between microscopic and macroscopic regions. They discuss *analytic cluster models* enabling simple interpolation formulas for the size dependence of various stationary cluster properties. The verification of the given interpolation formulas for electronic, geometrical, kinetic, optical, electrical, and magnetic properties are presented. They show how beautifully the cluster properties approach those of bulk.)

There is another intriguing phenomenon so–called *magic numbers* that has given intense impetus to many researchers. Speaking simplest, at magic numbers, clusters are unusually stable. In the mass–spectroscopic detection of clusters, it is usually the case that one finds especially high abundances for certain cluster sizes. The existence of magic numbers is still waiting for a concrete explanation.

The increasing knowledge about the properties of clusters has a potential to contribute to the theory of crystal growth. In determining the stability of clusters of a given size, it is likely that an understanding of the electronic structure of the clusters will offer new aspects and thus will help to suggest possible growth sequences.

The structural and electronic properties of trimers and higher clusters have been less well investigated compared to those of dimers in the literature of clusters. Structural properties of these bear particular importance because one can begin only with the trimer to compare between cluster properties and those of the bulk [118]. For example, the structure of small clusters of group IA and IB metals have been predicted to be linear. Therefore one can expect some *critical* cluster sizes to exist at which some drastic structural changes takes place leading to the closed–packed of the bulk [20, 84, 95, 97, 118, 119]. Geometrical arrangement of the atoms and the charges on them in small clusters constitute another aspect of the importance in understanding of some catalytic processes [41]. Therefore, determining geometrical and electronical properties of small clusters is worthwhile.

Despite all the recent breakthroughs in experimental techniques, the advent of sophisticated supercomputers and theoretical methods, our current understanding of clusters is still little compared to our knowledge of other fields of chemistry. In the regard of augmenting our understanding of clusters, the task is heavily on theoreticians because it is likely that experimental progresses will not reach in near future the proper sophistication to probe the structures of clusters. For this reason, the developing of new methods for the structural properties of clusters is the ultimate goal for theorists.

1.3 Transition Metals and Their Clusters

Titanium and nickel, two of the three elements under consideration in this work, are so–called *transition metal* (TM) elements. It would not be superfluous to repeat here briefly general properties of TMs [120]. The major characteristic of TMs is that they have incompletely filled d subshells or readily give rise to ions with incompletely filled d subshells. Most of TM elements have a close–packed structure in which each atom has a coordination number of 12. Furthermore, they have relatively small atomic radii. The combined effect of closest packing and small atomic size leads to strong metallic bonds. These in turn causes TMs to possess higher densities, higher melting and boiling points, and higher heats of fusion and vaporization than the Group IA and IIA metals, as well as the Group

IIB metals. Due to their incompletely filled d subshells, most TM compounds are paramagnetic. Many of transition metals and their compounds are good catalysts both for inorganic and organic reactions and for electrochemical processes [120].

Titanium is a Group IVB element with the electron configuration $[Ar]3d^24s^2$. It is the most abundant TM after iron (0.63 percent of Earth's crust by mass). It is a strong, lightweight, corrosion–resistant metal that is used in the construction of rockets, aircrafts, and jet engines. It also has applications in the chemical and polymer industry [120].

Nickel is a Group VIIIB element with the electron configuration $[Ar]3d^84s^2$. It is a rare element (0.01 percent of Earth's crust by mass). It has high electrical and thermal conductivities and is mainly used in making alloys. It also finds applications as a catalyst in hydrogenation reactions and as electrodes in batteries and fuel cells [120].

As to aluminum, which is not a TM, it is a Group IIIA element with the electronic configuration $[Ne]3s^23p^1$. It is the most abundant metal and the third most plentiful element (7.5 percent of Earth's crust by mass). Aluminum is one of the most versatile metals known. It has a low density (2.7 g/cm^3) and high

tensile strength; it is malleable, it can be rolled into thin foils, and it is an excellent conductor so that it is widely used in high–voltage transmission lines. One of its chief use is in aircraft construction. Mechanical properties of aluminum can be greatly improved by alloying it with small amounts of metals such as copper, magnesium, manganese, silicon, nickel, as well as titanium [120].

In the literature, the transition metal clusters have a special place because of their physical, chemical, and obvious economical importance. For this reason, transition metal clusters have drawn very intense interest. Three monumental reviews, Refs. [15–17], present the experimental data and theoretical results concerning transition metal clusters. (Another well–known review [19] giving both theoretical and experimental information about the heavy p–block dimers and trimers is also very precious.) Because of their wide–spread use in the studies of the catalysis processes, chemisorption and substrate adsorption, nucleation, the photographic processes, and possible laser applications, the chemistry of transition metals, especially that of bare metal clusters and of metallic surfaces is attached a great importance [34, 41, 47, 100]. In addition, the diatomic transition metals are source of information about the metal–metal bond and organometallic complexes [121]. These dimers have an important place in solid–state physics; they play a key role in exploring how the atomic properties change as the atoms

are clustered [47]. Homonuclear transition metal diatomics are the simplest models for metallic clusters and binuclear transition metal complexes. They also have theoretical, astronomical and high temperature importance [122, 123]. Therefore studying their properties would be very useful and instructive.

Unfortunately, isolation of these molecules from the bulk metal is very difficult to do in a manner that allows proper characterization. Experimental data on these molecules are scarce and quite inconclusive. The paucity of experimental data on transition metal microclusters, particularly beyond dimers, was a notable feature of the literature search for this work. Such data are needed in order to challenge researchers' interest to get a deep understanding of metallic clusters and small particles. Metal atom clusters have been first observed experimentally in vaporization and sublimation of solids [124] (observations from this research were later used o determine the dissociation energies of some diatomic molecules [125]), in rf–spark sources [126] and in sputtering ion sources[127]. Later small metal molecules have been isolated in rare–gas matrices, and in this way a number of spectra of these species have been investigated [42, 122, 128–131]. The matrix isolation methods has furthermore been utilized when studying the processes of catalysis and chemisorption [40, 132, 133].

1.4 Abbreviations Mentioned Frequently in This Work and Elsewhere

At present many *ab initio* and semiempirical methods are ceaselessly introduced by quantum chemists and physicists and they are now customarily abbreviated to initials. In the below list we give some of them which are mentioned frequently in this work and elsewhere [15]:

- AREP: Averaged relativistic core potential.
- CAS–SCF: Complete active space—self–consistent field.
- CI: Configuration interaction.
- CNDO: Complete neglect of differential overlap.
- CVP: Core valence polarization (pseudopotential).
- DFT: Density functional theory.
- DIM: Diatomics–in–differential overlap.
- DVM: Discrete variational method.
- ECP: Effective core potential (pseudopotential).
- EH: Extended Hückel.
- GMO: Generalized molecular orbital.
- GVB–vdw: Generalized valence bond–van der Waals.

- HFS: Hatree–Fock–Slater.
- LCAO: Linear combination of atomic orbitals
- LCGTO: Linear combination of Gaussian–Type orbitals.
- LD: Local density.
- LSD: Local spin density.
- MC–SCF: Multiconfigurational—self–consistent field.
- MD: Molecular–dynamics.
- MEH: Modified extended Hückel.
- MINDO: Modified intermediate neglect of differential overlap.
- MP: Model potential
- MRD: Multi–reference double excitation.
- NRMP: Nonrelativistic model potential.
- PEF: Potential energy function
- POL–CI: Polarized configuration interaction.
- QRMP: Quasirelativistic model potential.
- RECP: Relativistic effective core potential.

- RHF: Restricted Hartree–Fock.
- SC–CMS: Self–consistent cellular multiple scattering.
- SCF–Xα–SW: Self–consistent field–Xα–scattered wave.
- SC–LSD: Self–consistent Local spin density.
- SH: Simple Hückel.
- Xα: A local density method, α is a parameter.

CHAPTER 2

DENSITY FUNCTIONAL THEORY CALCULATIONS

This chapter is composed of two main sections. In the first section, which is largely compiled from the book *Lecture Notes on Molecular Physics*, by Ş. Erkoç [134], we will give, at some length, introductory information about the fundamentals of density functional theory (DFT). In the second section we will present the first part of our study carried out by using DFT calculations.

2.1 Density Functional Theory

2.1.1 Introduction

One of the main aim of quantum physics and quantum chemistry is, given a system, to solve the electronic Schrödinger equation for the electronic wave function

$$\hat{H}\Psi_e = E_e\Psi_e \tag{2.1}$$

more or less accurately. The (approximate) solution Ψ_e is an N–electron wave function and depends accordingly on $3N$ position–space coordinates and N spin coordinates. For just medium–sized systems this function is therefore extremely complex: for a water molecule, it is a function of 30 position–space coordinates and 10 spin coordinates; for a benzene molecule it depends on 126 position–space coordinates and 42 spin coordinates; for a crystal it depends on of the order of 10^{24} coordinates [117].

Having obtained the wave function Ψ_e, it is, in principle, possible to calculate any experimental observable although, due to practical limitations, many of the calculated properties are less accurate than may be desirable. A basic problem is that the wave function Ψ_e is very much more complex than is necessary when calculating experimental observables. Most operators for the experimental observables depend on the coordinates of only one or two electrons, i.e., of the

$3N$ position–space and N spin coordinates, at most 6 position–space and 2 spin coordinates are required. That is, for the operators of the form [117]

$$\hat{A} = \sum_{n=1}^{N} \hat{a}(n)\,, \tag{2.2}$$

when calculating the expectation values, $\langle \Psi_e | \hat{A} | \Psi_e \rangle$, most of the complexity of Ψ_e is redundant.

A particularly simple case occurs when $\hat{A}$ is written as in Eq.(2.2) and when, furthermore, $\hat{a}$ depends only on position–space coordinates,

$$\hat{a}(n) = a\left(\mathbf{r}_n\right)\,. \tag{2.3}$$

This is actually the case for many physically and chemically relevant observables. Since

$$a\left(\mathbf{r}_n\right) = \int a(\mathbf{r}')\,\delta\left(\mathbf{r}_n - \mathbf{r}'\right)\,d\mathbf{r}'\,, \tag{2.4}$$

we find

$$\begin{aligned}
\langle \Psi_e | \hat{A} | \Psi_e \rangle &= \int\int\cdots\int \Psi_e^*\left(\mathbf{r}_1, \mathbf{r}_2, \ldots, \mathbf{r}_N\right) \Psi_e\left(\mathbf{r}_1, \mathbf{r}_2, \ldots, \mathbf{r}_N\right) \\
&\quad \times \sum_{n=1}^{N} a\left(\mathbf{r}_n\right)\,d\mathbf{r}_1\,d\mathbf{r}_2\,\ldots d\mathbf{r}_N \\
&= \int \left[\int\int\cdots\int \Psi_e^*\left(\mathbf{r}_1, \mathbf{r}_2, \ldots, \mathbf{r}_N\right) \Psi_e\left(\mathbf{r}_1, \mathbf{r}_2, \ldots, \mathbf{r}_N\right)\right. \\
&\quad \left. \times \sum_{n=1}^{N} a(\mathbf{r}')\,\delta\left(\mathbf{r}_n - \mathbf{r}'\right)\,d\mathbf{r}_1\,d\mathbf{r}_2\,\ldots d\mathbf{r}_N\right] d\mathbf{r}'
\end{aligned}$$

$$= \int \left[\int \int \cdots \int \Psi_e^* \left(\mathbf{r}_1, \mathbf{r}_2, \ldots, \mathbf{r}_N \right) \Psi_e \left(\mathbf{r}_1, \mathbf{r}_2, \ldots, \mathbf{r}_N \right) \right.$$
$$\left. \times \sum_{n=1}^{N} \delta \left(\mathbf{r}_n - \mathbf{r}' \right) \, d\mathbf{r}_1 \, d\mathbf{r}_2 \, \ldots d\mathbf{r}_N \right] a(\mathbf{r}') \, d\mathbf{r}'$$

$$\langle \Psi_e | \, \hat{A} \, | \Psi_e \rangle = \int \rho(\mathbf{r}') \, a(\mathbf{r}') \, d\mathbf{r}' \, . \tag{2.5}$$

In this result, we identify the quantity $\rho(\mathbf{r}')$ as the *electron density* of the electronic system under question; it is of great importance in the density functional theory. Its formula in terms of Ψ_e is

$$\rho(\mathbf{r}') = \sum_{n=1}^{N} \int \int \cdots \int \left| \Psi_e \left(\mathbf{r}_1, \mathbf{r}_2, \ldots, \mathbf{r}_N \right) \right|^2 \delta \left(\mathbf{r}_n - \mathbf{r}' \right) \, d\mathbf{r}_1 \, d\mathbf{r}_2 \, \ldots d\mathbf{r}_N \, . \tag{2.6}$$

It is a nonnegative simple function of three variables, x, y, z, integrating to the total number of electrons,

$$\int \rho(\mathbf{r}') \, d\mathbf{r}' = N \, . \tag{2.7}$$

Recapitulating our simple finding, Eq.(2.5), we draw a conclusion that *for the expectation value of the most of the physically and chemically relevant observables, we need only the electronic density* $\rho(\mathbf{r}')$ [117].

We may now suggest that, somehow, we may avoid determining the complete N–electron wave function Ψ_e but instead can determine only the position–space density ρ and from that obtain all information that is of interest. This means that instead of solving the Schrödinger equation (2.1) for the wave function Ψ_e, we would have to solve another equation that determines the electron density ρ.

2.1.2 Basic Theory

The proposal for the use of electronic density goes back to the beginning of the modern quantum theory [135]. Thomas and Fermi suggested [136–138] that for larger systems (for N not too small), the number of electrons was so large that the system could be treated using statistical arguments. Then the electron density is the number of electrons per small volume element; and by assuming that this number is large, a statistical treatment is justified. Furthermore, one can then derive an approximate expression for the total energy of a such a gas of electrons that move in a given external field (which in our case is the electrostatic field generated by the nuclei). This total–energy expression then becomes one depending solely on the electron density ρ. In its original form, it is

$$E_{TF}[\rho] = T[\rho] + \int v(\mathbf{r})\,\rho(\mathbf{r})\,d\mathbf{r} + J[\rho]\,, \tag{2.8}$$

where $T[\rho]$ is the kinetic energy

$$T[\rho] = C_F \int \rho^{5/3}(\mathbf{r})\,d\mathbf{r}\,, \qquad C_F = \frac{3}{10}\left(3\pi^2\right)^{2/3}\,, \tag{2.9}$$

$J[\rho]$ is the Coulombic electrostatic interactions between the electrons

$$J[\rho] = \frac{1}{2}\int\int \frac{\rho\,(\mathbf{r})\;\rho\,(\mathbf{r}')}{|\mathbf{r}-\mathbf{r}'|}\,d\mathbf{r}\,d\mathbf{r}'\,, \tag{2.10}$$

and $v(\mathbf{r})$ is the external Coulombic potential generated by nuclei

$$v(\mathbf{r}) = \sum_{k=1}^{M} \frac{-Z_k}{\mathbf{R}_k - \mathbf{r}}\,. \tag{2.11}$$

For the electron density ρ, it is assumed that the ground state of an atom of interest, ρ minimizes the energy functional $E_{TF}[\rho]$, under the constraint (2.7). Using the method of Lagrange multipliers, it is seen that the ground–state electron density must satisfy the variational principle

$$\delta \left\{ E_{TF}[\rho] - \mu_{TF} \left[\int \rho(\mathbf{r})\, d\mathbf{r} - N \right] \right\} = 0 \tag{2.12}$$

which leads to the Euler–Lagrange equation

$$\mu_{TF} = \frac{\delta E_{TF}[\rho]}{\delta \rho(\mathbf{r})} = \frac{5}{3} C_F\, \rho^{2/3}(\mathbf{r}) - \phi(\mathbf{r})\,, \tag{2.13}$$

where $\phi(\mathbf{r})$ is the electrostatic potential at point $\mathbf{r}$ due to the nucleus and the entire electron distribution

$$\phi(\mathbf{r}) = \frac{Z}{r} - \int \frac{\rho\,(\mathbf{r}')}{|\mathbf{r} - \mathbf{r}'|}\, d\mathbf{r}'\,. \tag{2.14}$$

Equation (2.13) can then be solved with the constraint (2.7), and the resulting electron density ρ is inserted into $E_{TF}[\rho]$ to give the total energy[1]. This is the *Thomas–Fermi theory* of the atom.

We may now attempt to use E_{TF} for a given system, but for those of interest here it turns out that the results are very inaccurate. After all, the whole formalism is constructed as being approximate, and only as long as the approximations

[1] To calculate the electronic density (of atoms) for some basic problems, the Hartree–Fock wave functions are conventionally and frequently used. Hartree–Fock results are available for most atoms and ions [139]. More accurate (e.g. variational or configuration–interaction) atomic functions could also be used; but these accurate functions are available only for small atoms. Recently a work was presented offering *general atomic density distribution for atoms* [140]. Using these density distribution functions, one can easily do his/her calculations without referring to Hartree-Fock wave functions.

are valid we can expect reasonable results. First of all, the assumption that there is a large number of electrons per small volume element is rarely justified. The Thomas-Fermi approach is a pure density–based one, where the problem of calculating the N–electron wave function is replaced by calculating the electron density in three–dimensional position space. It is not constructed as being an exact alternative to solving the Schrödinger equation, but rather as an approximation; therefore also the results are at most approximate.

Numerous modifications and improvements for the Thomas–Fermi theory have been made over the years. The accuracy for atoms was not high as that with other methods, which caused the method to be viewed as an oversimplified model of much real importance for quantitative predictions in atomic and or molecular solid–state physics. The situation, however, changed with the work of Hohenberg and Kohn in 1964 [141]. They proved the fundamental theorems showing that, for ground states, the Thomas–Fermi theory was merely an approximation to an *exact* theory, the **density functional theory** (DFT).

2.1.3 The Hohenberg–Kohn Theorems

For an N–electron system described by the Hamiltonian

$$H = \sum_{i=1}^{N} \left(-\frac{1}{2} \nabla_i^2 \right) + \sum_{i=1}^{N} v\left(\mathbf{r}_i\right) + \sum_{i<j}^{N} \frac{1}{|\mathbf{r}_i - \mathbf{r}_j|}\,, \tag{2.15}$$

where $v\left(\mathbf{r}_i\right)$ is the external potential (associated with the electron–nucleus interaction) acting on the ith electron, both ground–state energy E_0 and the ground–state wave function ψ_0 are determined, using the variational method, by minimizing the energy functional

$$E[\psi] = \frac{<\psi|H|\psi>}{<\psi|\psi>} \tag{2.16}$$

with the result

$$E[\psi] \geq E_0\,. \tag{2.17}$$

It is clear that for an N–electron system, the external potential v completely fixes the Hamiltonian; thus N and v determine all the properties for the ground state.

In lieu of N and v, the *first Hohenberg–Kohn theorem* [141] considers the use of the electron density ρ as the basic variable. It simply states that *the external potential v is determined, within an additive constant, by the electron density ρ.* Since ρ and N are interrelated via Eq.(2.7), then ρ determines the ground–state wave function ψ_0 and all the other electronic properties of the system. The total

energy is expressed as

$$E[\rho] = T[\rho] + V_{ne}[\rho] + V_{ee}[\rho] = \int \rho(\mathbf{r})\, v(\mathbf{r})\, d\mathbf{r} + F_{HK}[\rho]\,, \tag{2.18}$$

with

$$F_{HK}[\rho] = T[\rho] + V_{ee}[\rho]\,, \tag{2.19}$$

where $T[\rho]$ is the kinetic energy of N noninteracting electrons, $V_{ne}[\rho]$ and $V_{ee}[\rho]$ are respectively the potential energy of associated with the electron–nucleus and the electron–electron interactions. The functional for the electron–electron interaction can be written as

$$V_{ee}[\rho] = J[\rho] + \text{nonclassical term}\,, \tag{2.20}$$

where $J[\rho]$ is the Coulombic electrostatic interactions between the electrons

$$J[\rho] = \frac{1}{2} \int\int \frac{\rho\,(\mathbf{r})\ \rho\,(\mathbf{r}')}{|\mathbf{r} - \mathbf{r}'|}\, d\mathbf{r}\, d\mathbf{r}'\,, \tag{2.21}$$

and the nonclassical term, a very important term, includes the exchange functional and all the many–body terms of the interacting electron system.

The *second Hohenberg–Kohn theorem* [141] provides the energy variational principle: *For a trial density ρ, such that $\rho \geq 0$ and $\int \rho(\mathbf{r})\, d\mathbf{r} = N$, it is always true that $E[\rho] \geq E_0$, where E_0 is the ground–state energy of the system and $E[\rho]$ is the energy functional resulted from the trial density ρ.* This provides the justification for the variational principle in Thomas–Fermi theory that $E_{TF}[\rho]$ is

an approximation to $E[\rho]$. The variational principle, $E[\rho] \geq E_0$, requires that the ground–state density satisfies the stationary principle

$$\delta \left\{ E[\rho] - \mu \left[\int \rho(\mathbf{r})\, d\mathbf{r} - N \right] \right\} = 0 \tag{2.22}$$

which leads to the Euler–Lagrange equation

$$\mu = \frac{\delta E[\rho]}{\delta \rho(\mathbf{r})} = v(\mathbf{r}) + \frac{\delta F_{HK}[\rho]}{\delta \rho(\mathbf{r})}\,, \tag{2.23}$$

where the quantity μ is the *chemical potential* which measures the escaping tendency of an electron cloud; it is a constant, through all space for the ground–state of an atom, or solid, and equals the slope of E versus N curve at constant $v(\mathbf{r})$.

If the functional $F_{HK}[\rho]$ happens to be known, the stationary principle (2.22) will be an exact equation for the ground–state electron density. We note from Eq.(2.19) that $F_{HK}[\rho]$ is defined independently of the external potential $v(\mathbf{r})$; this means that $F_{HK}[\rho]$ is a universal functional of ρ.

Once the functional $F_{HK}[\rho]$ is explicitly known (approximate or accurate), the DFT method can be applied to any system. Equation (2.23) is the basic working equation of DFT. Accurate calculational implementations of DFT are still far from easy to achieve because of the unfortunate (though challenging) fact that the functional form of $F_{HK}[\rho]$ is hard to come by in explicit form. Various

methods have been developed to implement DFT in real systems. The most commonly used one is the so–called *Kohn–Sham method* [142]. They thereby turned DFT into a practical tool for rigorous calculations.

2.1.4 The Kohn–Sham Method

To recapitulate, we have four interrelated equations:

$$E[\rho] = \int \rho(\mathbf{r})\, v(\mathbf{r})\, d\mathbf{r} + F[\rho]\,, \tag{2.24}$$

$$F[\rho] = T[\rho] + V_{ee}[\rho]\,, \tag{2.25}$$

$$\mu = v(\mathbf{r}) + \frac{\delta F_{HK}[\rho]}{\delta \rho(\mathbf{r})}\,, \tag{2.26}$$

$$N = \int \rho(\mathbf{r})\, d\mathbf{r}\,. \tag{2.27}$$

Kohn and Sham [142] introduced orbitals into the problem in such a way that the kinetic energy functional

$$T = \sum_{i}^{N} n_i \left\langle \psi_i \right| -\frac{1}{2}\nabla_i^2 \left| \psi_i \right\rangle\,, \tag{2.28}$$

where ψ_i are natural spin orbitals and n_i are their corresponding occupation numbers (the Pauli principle requires that $0 \leq n_i \leq 1$), can be computed to a good accuracy. T in Eq.(2.28) is a functional of the total electron density

$$\rho(\mathbf{r}) = \sum_{i}^{N} n_i \sum_{s} \left|\psi_i(\mathbf{r}, s)\right|^2\,. \tag{2.29}$$

Kohn and Sham showed that one can built a theory using simpler formulas, namely

$$T_s[\rho] = \sum_i^N \langle \psi_i | -\frac{1}{2}\nabla_i^2 | \psi_i \rangle \tag{2.30}$$

and

$$\rho(\mathbf{r}) = \sum_i^N \sum_s |\psi_i(\mathbf{r}, s)|^2 \ . \tag{2.31}$$

The latter two equations are the special case of the former two equations with $n_i = 1$ for N orbitals and $n_i = 0$ for the rest. This representations of kinetic energy and density holds true for the determinantal wave function that exactly describes N *noninteracting* electrons, with the Hamiltonian

$$H_s = \sum_i^N \left(-\frac{1}{2}\nabla_i^2 \right) + \sum_i^N v_s(\mathbf{r}_i) \ , \tag{2.32}$$

in which there are no electron–electron repulsion terms, and for which the ground–state electron density is exactly ρ. For this system there will be an exact determinantal ground–state wave function

$$\Psi_s = \frac{1}{\sqrt{N!}} | \psi_1 \, \psi_2 \, \ldots \psi_N | \tag{2.33}$$

where ψ_i are the N lowest eigenstates of the one–electron Hamiltonian h_s:

$$h_s \, \psi_i = \left[-\frac{1}{2}\nabla^2 + V_s(\mathbf{r}_i) \right] \psi_i = \varepsilon_i \, \psi_i \, . \tag{2.34}$$

The kinetic energy functional is, as given in Eq.(2.30),

$$T_s[\rho] = \sum_i^N \langle \Psi_s | -\frac{1}{2}\nabla_i^2 | \Psi_s \rangle = \sum_i^N \langle \psi_i | -\frac{1}{2}\nabla_i^2 | \psi_i \rangle \ , \tag{2.35}$$

and the density is decomposed as in Eq.(2.31).

In order to produce the separation out of $T_s[\rho]$ as the kinetic energy component, Eq.(2.25) is rewritten as

$$F[\rho] = T_s[\rho] + J[\rho] + E_{xc}[\rho] \tag{2.36}$$

where

$$E_{xc}[\rho] = T[\rho] - T_s[\rho] + V_{ee}[\rho] - J[\rho]\,. \tag{2.37}$$

The defined quantity $E_{xc}[\rho]$ is called the *exchange–correlation energy*; it contains the difference between T and T_s, and the nonclassical part of V_{ee}, Eq.(2.20).

The Euler equation now becomes

$$\mu = v_{\text{eff}}(\mathbf{r}) + \frac{\delta T_s[\rho]}{\delta \rho(\mathbf{r})} \tag{2.38}$$

where the Kohn–Sham effective potential is defined by

$$v_{\text{eff}}(\mathbf{r}) = v(\mathbf{r}) + \frac{\delta J[\rho]}{\delta \rho(\mathbf{r})} + \frac{\delta E_{xc}[\rho]}{\delta \rho(\mathbf{r})} = v(\mathbf{r}) + \int \frac{\rho(\mathbf{r}')}{|\mathbf{r} - \mathbf{r}'|}\, d\mathbf{r}' + v_{xc}(\mathbf{r}) \tag{2.39}$$

with the exchange–correlation potential

$$v_{xc}(\mathbf{r}) = \frac{\delta E_{xc}[\rho]}{\delta \rho(\mathbf{r})}\,. \tag{2.40}$$

The explicit form of $T_s[\rho]$ in terms of density is as yet unknown. We follow the indirect approach designed by Kohn and Sham.

The Kohn–Sham treatment runs as follows. For a given $v_{\text{eff}}(\mathbf{r})$, one obtains the $\rho(\mathbf{r})$ that satisfies Eq.(2.38) simply by solving the N one–electron equations (the Kohn–Sham orbital equations)

$$\left[-\frac{1}{2}\nabla^2 + v_{\text{eff}}(\mathbf{r})\right]\psi_i = \varepsilon_i \psi_i \tag{2.41}$$

and setting

$$\rho(\mathbf{r}) = \sum_i^N \sum_s |\psi_i(\mathbf{r}, s)|^2 \ . \tag{2.42}$$

Here, $v_{\text{eff}}(\mathbf{r})$ depends on $\rho(\mathbf{r})$ through Eq.(2.40); hence Eqs.(2.39), (2.41), and (2.42), must be solved self–consistently. During the self–consistency procedure mixing of density should be taken into account:

$$\rho_{in}^{i+1} = (1-\alpha)\rho_{in}^{i} + \alpha \rho_{out}^{i} \tag{2.43}$$

The mixing parameter α is usually taken as ~ 0.15 [143]. One begins with a guessed $\rho(\mathbf{r})$, constructs $v_{\text{eff}}(\mathbf{r})$ from Eq.(2.39), and then finds a new $\rho(\mathbf{r})$ from Eqs.(2.41) and (2.42). The total energy can be computed directly from Eq.(2.24) with Eq.(2.36), or indirectly from

$$E = \sum_i^N \epsilon_i - \frac{1}{2}\int \frac{\rho(\mathbf{r})\,\rho(\mathbf{r}')}{|\mathbf{r}-\mathbf{r}'|}\, d\mathbf{r}\, d\mathbf{r}' + E_{xc}[\rho] - \int v_{xc}(\mathbf{r})\,\rho(\mathbf{r})\, d\mathbf{r}\,, \tag{2.44}$$

where

$$\sum_i^N \epsilon_i = \sum_i^N \langle \psi_i | -\frac{1}{2}\nabla^2 + v_{\text{eff}}(\mathbf{r}) \,|\psi_i\rangle = T_s[\rho] + \int v_{\text{eff}}(\mathbf{r})\,\rho(\mathbf{r})\, d\mathbf{r}\,. \tag{2.45}$$

Just as in Hartree–Fock theory, the total electronic energy is not the sum of the orbital energies.

The computational effort to solve Kohn–Sham equations is not much more than to solve the Hartree equations—less than for the Hartree–Fock equations. The Hartree–Fock equations contain a nonlocal potential operator in the one–electron Hamiltonian and hence are not a special case of the Kohn–Sham equations. All the three theories, Hartree–SCF, Hartree–Fock, and Kohn–Sham, provide one–electron equations for describing many–electron systems. The Kohn–Sham theory, exact in principle, is distinguished from the Hartree–Fock theory in its capacity to fully incorporate the exchange–correlation effect of electrons.

2.1.5 Local–Density Approximation

The Kohn–Sham equations

$$[-\frac{1}{2}\nabla^2 + v_{\text{eff}}]\psi_i = \varepsilon_i\,\psi_i \tag{2.46}$$

$$v_{\text{eff}}(\mathbf{r}) = v(\mathbf{r}) + \int \frac{\rho(\mathbf{r}')}{|\mathbf{r}-\mathbf{r}'|}\,d\mathbf{r}' + v_{xc}(\mathbf{r}) \tag{2.47}$$

$$\rho(\mathbf{r}) = \sum_i^N \sum_s |\psi_i(\mathbf{r},s)|^2 \tag{2.48}$$

while exactly incorporating the kinetic energy $T_s[\rho]$, still leave the exchange–correlation functional $E_{xc}[\rho]$ of Eq.(2.36) unsettled. An explicit form for $E_{xc}[\rho]$

is needed to specify the Kohn–Sham equations. The simplest approximation, the local approximation to $E_{xc}[\rho]$ has been proposed by Kohn and Sham. The so called *local–density approximation* (LDA) for exchange and correlation energy,

$$E_{xc}^{\mathrm{LDA}}[\rho] = \int \rho(\mathbf{r})\, \varepsilon_{xc}(\rho)\, d\mathbf{r}\,, \tag{2.49}$$

where $\varepsilon_{xc}(\rho)$ indicates the exchange and correlation energy per particle of a uniform electron gas of density ρ. The corresponding exchange–correlation potential of Eq.(2.39) then becomes

$$v_{xc}^{\mathrm{LDA}}(\mathbf{r}) = \frac{\delta E_{xc}^{\mathrm{LDA}}[\rho]}{\delta\rho(\mathbf{r})} = \varepsilon_{xc}(\rho(\mathbf{r})) + \rho(\mathbf{r})\, \frac{\delta\varepsilon_{xc}(\rho)}{\delta\rho(\mathbf{r})} \tag{2.50}$$

and the Kohn–Sham orbital equations read

$$\left[-\frac{1}{2}\nabla^2 + v(\mathbf{r}) + \int \frac{\rho(\mathbf{r}')}{|\mathbf{r}-\mathbf{r}'|}\, d\mathbf{r}' + v_{xc}^{\mathrm{LDA}}(\mathbf{r})\right] \psi_i = \varepsilon_i\, \psi_i\,. \tag{2.51}$$

The self–consistent solution of this equation defines the Kohn–Sham local density approximation (KS–LDA), which in the literature is usually simply called the *LDA method.*

The function $\varepsilon_{xc}(\rho)$ can be divided into *exchange* and *correlation* contributions,

$$\varepsilon_{xc}(\rho) = \varepsilon_x(\rho) + \varepsilon_c(\rho)\,. \tag{2.52}$$

The exchange part is already known, given by the Dirac exchange–energy functional of the form

$$\varepsilon_x(\rho) = -C_x\,(\rho(\mathbf{r}))^{1/3}\,, \qquad C_x = \frac{3}{4}\left(\frac{3}{\pi}\right)^{1/3}\,. \tag{2.53}$$

Accurate values of $\varepsilon_c(\rho)$ are available. These values have been interpolated to provide an analytic form for $\varepsilon_c(\rho)$.

The DFT method is not this much, here we just gave some introductory information about the method, a detailed discussion of the theory and its applications on atoms and molecules and much more can be found in Ref. [135].

2.1.6 Functionals Used in the DFT Method

Total energy of a many–electron system can be written in DFT as

$$E[\rho] = \int v_{\text{ext}}(\mathbf{r})\,\rho(\mathbf{r})\,d\mathbf{r} + T_s + V_{\text{class}}[\rho] + E_{xc}[\rho]\,. \tag{2.54}$$

Up to this point there is no approximation. All of this development comes out directly from the Schrödinger equation. All of the functionals but E_{xc} in Eq.(2.54) are known. Once E_{xc} is happened to be known, the total energy E can be minimized with respect to the density ρ, yielding the Kohn–Sham equations that can be solved self–consistently

$$\left[-\frac{1}{2}\nabla^2 + v_{\text{ext}} + v_{\text{class}} + v_{xc}\right]\phi_i = \varepsilon_i\,\phi_i\,, \tag{2.55}$$

where v_{class} and v_{xc} are the potentials corresponding to the classical Coulomb repulsive energy between the electrons and to the exchange–correlation energy,

respectively,

$$v_{\text{class}}(\mathbf{r}) = \int \frac{\rho(\mathbf{r}')}{|\mathbf{r} - \mathbf{r}'|}\, d\mathbf{r}', \qquad v_{xc}(\mathbf{r}) = \frac{\delta E_{xc}[\rho(\mathbf{r})]}{\delta \rho(\mathbf{r})}\,. \tag{2.56}$$

The Kohn–Sham orbitals, $\{\phi_i\}$, in this procedure are the solutions for the non-interacting system of electrons that feel the effective potential v_{eff}

$$v_{\text{eff}} = v_{\text{ext}} + v_{\text{class}} + v_{xc}\,. \tag{2.57}$$

Therefore,

$$E_s = \sum_{i=1}^{N} \varepsilon_i = T_s + V_s = \sum_{i=1}^{N} \langle \phi_i | -\frac{1}{2}\nabla^2 | \phi_i \rangle + \int v_{\text{eff}}(\mathbf{r})\, \rho(\mathbf{r})\, d\mathbf{r}\,, \tag{2.58}$$

where E_s, T_s, and V_s are respectively the total, kinetic, and potential energies of the noninteracting system. The wave function of this noninteracting system is exactly the determinant composed from the orbitals ϕ_i,

$$\Psi_s(\mathbf{r}_1, \mathbf{r}_2, \cdots, \mathbf{r}_N) = \frac{1}{\sqrt{N!}} |\phi_1 \phi_2 \cdots \phi_N|\,. \tag{2.59}$$

It should always be kept in mind that Ψ_s is not the wave function of the real system, nor are the $\{\phi_i\}$ related to real electrons, except that they yield the same density through the sum

$$\rho(\mathbf{r}) = \sum_{i=1}^{N} |\phi_i(\mathbf{r})|^2\,. \tag{2.60}$$

The total energy for the real system will be evaluated from Eq.(2.54), where one should use those orbitals that yield the minimum energy.

2.1.6.1 Functionals

The first functionals related to E_{xc} were not created with DFT in mind, but rather were oriented to the description of exchange effects. Therefore, for practical reasons, the partition,

$$E_{xc}[\rho] = E_x[\rho] + E_c[\rho] \tag{2.61}$$

is invoked, with the implicit warning that we are defining at least one term (E_c) that does not correspond to the *ab initio* E_c, while E_x follows closely the HF definition of exchange. The partition can be made according to convenience.

The calculation of exchange functionals is as old as quantum theory itself. The first *ab initio* functional to be calculated for the exchange was the one for the ground state of a uniform gas of electrons. Given a uniform density of electrons, assumed to have a Fermi distribution, Bloch [144] obtained an exchange potential energy proportional to $\rho^{1/3}$; later Dirac [145] used it to include the exchange in the Thomas–Fermi atom [136, 146]; in both cases, no intention of a DFT procedure was in mind as yet. Later, Slater [147] used the $\rho^{1/3}$ relation as a functional to simplify the HF method, substituting for the more complicated HF exchange. Slater [148] introduced a proportionality constant α to $\rho^{1/3}$ to reproduce the HF exchange energy. This last method is called $X\alpha$ or HFS (HF–Slater) method, and it can be regarded as an approximation to the Kohn–Sham procedure.

The exchange energy using the formula for the uniform electron gas is the local density approximation (LDA), written as

$$E_x^{\mathrm{LDA}}[\rho] = -\int \frac{3}{4}\left(\frac{3}{\pi}\right)^{1/3} \rho^{4/3}\, d\mathbf{r}\,. \tag{2.62}$$

The corresponding potential is

$$v_x^{\mathrm{LDA}}(\mathbf{r}) = -\left[\frac{3}{\pi}\rho(\mathbf{r})\right]^{1/3}. \tag{2.63}$$

The above formulas and the following ones are often expressed using a parameter r_s, equivalent to the radius of a sphere with constant charge density ρ and a total charge of one electron, also known as the *Wigner–Seitz radius*:

$$r_s = \left(\frac{4}{3}\pi\rho\right)^{-1/3}. \tag{2.64}$$

Therefore,

$$v_x^{\mathrm{LDA}}(\mathbf{r}) = -\left(\frac{3}{2\pi}\right)^{2/3}\frac{1}{r_s}\,. \tag{2.65}$$

Equation (2.62) indicates that E_x scales homogeneously when the coordinates are scaled by a factor λ:

$$E_x[\rho_\lambda] = \lambda\, E_x[\rho]\,. \tag{2.66}$$

Therefore another way to define the exchange functional is as that portion of the E_{xc} that scales linearly. The remainder will be defined as the correlation functional E_c.

The uniform electron gas model gives us the first approximation for E_{xc}

$$E_{xc}^{\mathrm{LDA}} = \int \varepsilon_{xc}^{\mathrm{LDA}}[\rho(\mathbf{r})]\,\rho(\mathbf{r})\,d\mathbf{r}\,, \tag{2.67}$$

where $\varepsilon_{xc}^{\mathrm{LDA}}$ is the exchange–correlation energy distribution per unit volume, which depends on the density only at the point where it is evaluated.

In principle, the ideal electron gas of uniform density requires a uniform positive charge of equal density but without exchange effects. This idealized system is known as *jellium*. Because of the interaction of the positive charge with itself and with the electron distribution, Eq.(2.54), reduces only to

$$E[\rho] = T_s + E_{xc}[\rho]\,. \tag{2.68}$$

This equation can be solved numerically as accurate as is needed for any situation by using plane waves, and analytically for some limiting cases. Therefore it will be possible to obtain E_{xc}, and by subtracting the E_x already known, the E_c can be calculated.

In the literature there are many exchange and correlation functional; their explicit forms with their limitations can be found in Refs. [117, 135, 149] and the references therein. We here give only those that have been used in our DFT calculations. They are the Becke–88 exchange functional [150]

$$\varepsilon_x^{\mathrm{B88}} = \varepsilon_x^{\mathrm{LDA}} \left[1 - \frac{\beta x^2}{2^{1/3}\,A_x \left(1 + 6\,\beta\,x\,\sinh^{-1} x\right)}\right]\,, \tag{2.69}$$

where

$$x = \frac{2^{1/3}\,|\nabla\rho|}{\rho^{4/3}}\,, \quad A_x = \frac{3}{4}\left(\frac{3}{\pi}\right)^{1/3}\,, \quad \beta = 0.0042\,,$$

and the correlation functional of Lee, Yang, and Parr [151]

$$\varepsilon_c^{\mathrm{LYP}} = -\frac{a}{1+d\,\rho^{-1/3}}\left\{\rho + b\rho^{-2/3}\left[C_{_F}\,\rho^{5/3} - 2t_w + \frac{1}{9}\left(t_w + \frac{1}{2}\nabla^2\rho\right)\right]e^{-c\rho^{-1/3}}\right\} \quad (2.70)$$

where

$$t_w = \frac{1}{8}\left(\frac{|\nabla\rho|^2}{\rho} - \nabla^2\rho\right)\,, \qquad C_{_F} = \frac{3}{10}\left(3\pi^2\right)^{2/3}\,,$$

$$a = 0.04918\,, \quad b = 0.132\,, \quad c = 0.2533\,, \quad d = 0.349\,.$$

We have been used these two functionals because of their best performance over the years [152].

2.1.6.2 Classification of Functionals

The simplest type of DFT exchange treatment is to use a local functional, most commonly the *Dirac–Slater* or $X\alpha$ functional [153], which gives the exact exchange energy for the uniform electron gas. Moving to a *gradient–corrected exchange functional* usually results in an improvement; one of the most widely used such functionals is due to Becke [150]. The simplest way to treat the correlation is to ignore it entirely, by using a "null" functional. A more sensible approach is to use either a local functional such as the uniform gas correlation parametrization of Vosko, Wilk and Nusair [154] or a gradient–corrected functional, an example

of which is the functional of Lee, Yang and Parr [151]. Each pair of exchange and correlation treatment gives a different type of exchange–correlation functional. A general hierarchy of exchange and correlation functionals is represented in a diagram as shown in Figure 2.1. In particular, two of these methods have been in wide use for some time; S–null corresponds to Hartree–Fock–Slater theory, while S–VWN is commonly referred to as LSDA.

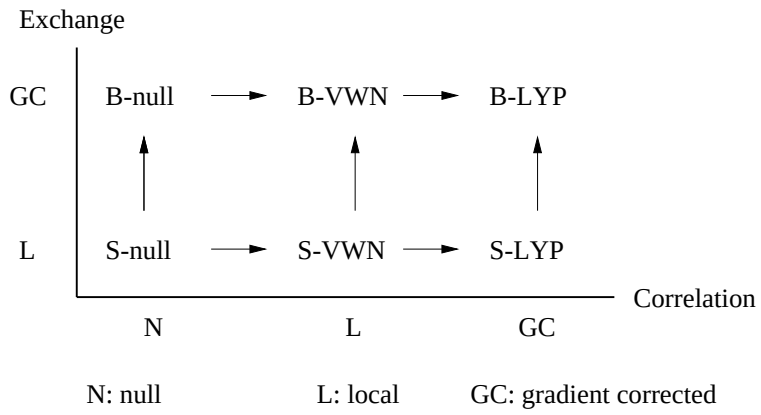

Figure 2.1: The hierarchy of exchange and correlation functionals.

2.1.6.3 Comparison of Functionals

It has long been recognized that HF theory frequently gives bond lengths which are too short. The bond lengths by the various DFT methods are mostly too long, with some methods giving systematically long bond lengths. Some general trends can also be discerned for bond angles. All of the functionals gave smaller bond angle. The DFT dipole moments are often significantly in error, the calculated values are all too small. All of the DFT methods are remarkably successful in reproducing fundamental vibrational frequencies. It is well known that HF frequencies are systematically too high. The atomization energies show a large variation with theoretical method. HF method gives binding energies which are too low, primarily because of inadequate treatment of electron correlation. Overall, B–VWN and B–LYP are the DFT methods exhibiting the best performance. More information about the comparison of functionals for various molecular properties may be found in Ref. [152].

2.2 Structural and Electronic Properties of $Al_kTi_lNi_m$ $(k+l+m=2,3)$ Microclusters: Density Functional Theory Calculations

2.2.1 Introduction

In the first part of our doctoral study, structural and electronic properties of sixteen different microclusters of the type $Al_kTi_lNi_m$ $(k+l+m=2,3)$ have been investigated. The dimers (Al_2, Ti_2, Ni_2), trimers (Al_3, Ti_3, Ni_3) of elements aluminum, titanium, and nickel, and their binary combinations (AlNi, AlTi, NiTi, Al_2Ni, $AlNi_2$, Al_2Ti, Ni_2Ti, $AlTi_2$, $NiTi_2$), and the ternary combination (AlTiNi) have been studied in their ground states. The density functional theory (DFT) calculations have been performed within the effective core potential (ECP) level [with B3LYP exchange–correlation contribution]. All the calculations have been carried out by using the GAUSSIAN–98 package [155]. The calculated spectroscopic constants (binding energy D_e, equilibrium interatomic separation r_e, and fundamental frequency w_e) of the dimers, the minimum energy configurations of the trimers (bond lengths and bond angles, as well as their fundamental frequencies w_n) are reported. For all the microclusters considered, the possible dissociation channels and the corresponding dissociation energies, the calculated HOMO (highest occupied molecular orbital), LUMO (lowest unoccupied molecular orbital), and HOMO–LUMO gap energies are presented. The calculated dipole moments and excess charges on the atoms of the trimers are also given.

The calculated values are compared with the previously reported ones computed by various other approximate methods and estimated experimentally. Several discrepancies appear between the present calculations and some literature values.

2.2.2 Method of Calculation

Why *density functional theory* and *effective core potential* methods? When the standard quantum–mechanical methods are too time–consuming or incapable, DFT provides us with the formal framework for energy calculations with predictive value. Even when working with DFT, one usually encounters some great computational difficulties in treating systems with atoms having many electrons. The ECP or *pseudopotential* methods have been indispensable in overcoming partially these difficulties. In these methods, instead of considering all the electrons (all–electron *ab initio* methods), one treats only valence electrons explicitly; the remaining "effective core" electrons are thought to modify the potential in which the valence electrons move. (For a good review, see Ref. [16] and references therein.) The ECP methods have proven their accuracy and reliability over many years; they give good results for chemical systems, with error relative to the experiment comparable to corresponding error obtained from all–electron *ab initio* methods [45].

In this first part, $Al_kTi_lNi_m$ $(k+l+m=2,3)$ microclusters have been investigated theoretically by performing DFT calculations. The exchange and correlation potentials contributions have been considered at B3LYP level [135]. The compact effective potential (CEP) basis functions with ECP triple–split basis, namely, CEP-121G [156–158], have been used in the calculations. The exchange term of B3LYP consists of hybrid Hartree-Fock and local spin density (LSD) exchange functions with Becke's gradient correlation to LSD exchange [150]. The correlation term of B3LYP consists of the Vosko, Wilk, Nusair (VWN3) local correlational functional [154] and Lee, Yang, Parr (LYP) correlation correction functional [151]. The BLYP method gives a better improvement over the SCF–HF results, as we mentioned earlier. Its predictions are in qualitative agreement with experiment. In general, the DFT method overestimates the energies, and it gives shorter bond lengths than the experimental values. However, the optimized structures predicted at BLYP level are in good agreement with the experiment[159, 160].

CEP–121G basis functions are becoming widely used in quantum chemistry, particularly in the study of compounds containing heavy elements [156–158]. The CEP basis sets have been used to calculate the equilibrium structures and spectroscopic properties of several small molecules [156]. The standard basis set of CEP theory was consistent for the entire series not only within the lanthanide

series but also with the second and third row metals. The quality of the CEP–121G basis set does not degrade when going from the second to third row of the periodic table. In the present calculations, CEP–121G basis set and the number of primitive Gausssians used in CEP–121G vary from atom to atom, depending on the valence structure of atoms considered.

2.2.3 Results and Discussions

2.2.3.1 Dimers

The calculated results, as well as some experimental and theoretical outcomes from the literature, related to homonuclear dimers Al_2, Ni_2, and Ti_2 are presented in Tables 2.1–2.3.

Al_2: The Al–Al bond in the bulk metal is 2.86 Å [176], as compared with our value of 2.65 Å. The corresponding experimental value, estimated from vibrational spectra of aluminum, is 2.70 Å [163], which is very close to the present calculation. As is seen from Table 2.1, both experimental and theoretical values for Al–Al bond are all in a good range of 2.45–2.95 Å, most of them are close to the experimental value of 2.70 Å. This is not surprising because aluminum is almost an ideal free electron metal. It is light and has only one isotope. These properties render it being one of the model systems for testing and developing ideas about metal

Table 2.1: Spectroscopic constants of Al_2. Binding energy D_e is in eV, equilibrium interatomic separation r_e is in Å, and the fundamental frequency ω_e is in cm^{-1}.

D_e	r_e	ω_e	Method	Reference
0.4531	2.6520	274.3	DFT	This work
1.5	2.466	350.0	Exp.	[161]
1.55			Exp.	[162]
	2.70	284.2	Exp.	[163]
1.33	2.51	354	*ab initio* (pseudopotential)	[56]
	2.95	246	*ab initio* MD	[74]
1.425	2.73	277	SOCI + Q BIG–ANO	[109]
	2.51		first princ. calc.	[110]
1.51	2.519		*ab initio* & par. emp. pot.	[111]
2.03	2.70	290	LSD (pseudopot.) + MD	[112]
1.19	2.779	270	MCSCF+FOCI	[164]
2.0			LDA	[165]
0.08	2.65		CI (all–electron & ECP)	[166]
1.35	2.717	285	CCD + ST	[167]
1.30	2.493	338	MRCI+D	[168]

Table 2.2: Spectroscopic constants of Ni_2. Binding energy D_e is in eV, equilibrium interatomic separation r_e is in Å, and the fundamental frequency ω_e is in cm^{-1}.

D_e	r_e	ω_e	Method	Reference
1.2581	2.4948	222.2	DFT	This work
		330	Exp.	[42]
2.068	2.200		Exp.	[47]
2.08			Exp.	[114]
		192	Exp.	[122]
2.3			Exp.	[161]
2.38			Exp.	[162]
2.03			Exp. & abs. ent. meth.	[169]
2.36	2.30	325	Exp. & second law calc.	[169]
		381	Exp.	[170]
		280	Exp.	[171]
2.62	2.5		EH	[39]
	2.5		MO	[41]
1.42	2.20	289	CI	[43]
0.97	2.60	236	HF	[43]
1.89	2.26	(190)	ECP–GVB–CI	[44]
1.43	2.33	211	ECP–CI	[45]
1.21	2.36	201	ECP–1-pair CI	[45]
0.92	2.33	216	ECP–SCF	[45]
	2.28	240	RHF	[46]
	2.49		ECP–MCSCF	[53]
3.32	2.00		DFT (LCAO-MO)	[91]
2.4			CNDO	[107]
2.92	2.04	344	ECP–GVB–CI	[121]
2.78	2.21	395	MEH	[123]
2.45	2.21	370	EH	[172]
2.70	2.18	320	DFT (LSD)	[173]

Table 2.3: Spectroscopic constants of Ti_2. Binding energy D_e is in eV, equilibrium interatomic separation r_e is in Å, and the fundamental frequency ω_e is in cm^{-1}.

D_e	r_e	ω_e	Method	Reference
2.8979	1.8537	482.4	DFT	This work
		407.9	Exp.	[100]
1.3			Exp.	[161]
1.31			Exp.	[162]
1.23			Exp. & second law calc.	[174]
1.42	2.65	288	Exp. & third law calc.	[174]
	3.0		MO	[41]
	1.87	580	RHF	[46]
1.88	2.30	250	EH	[172]
2.30	2.52	220	DFT (LSD)	[173]
	1.96		DV–Xα	[175]

clusters. It is possible to perform reasonably reliable theoretical calculations on aluminum clusters [177]. The calculated binding energy D_e for Al_2 of 0.45 eV is significantly lower than the experimental estimate of $\sim$ 1.5 eV [161, 162]. This is in contrast with the general trend of the DFT methods because, as it was mentioned before, the DFT methods, in general, overestimate the energies with respect to the experimental values. The reason for this discrepancy might be due to the ECP method itself since ECP considers only the valance electrons of the system. In this work Al atom has the least number of electrons among the atoms considered. If we had used an all-electron formalism, with an extended basis set, we might have obtained a result closer to the experimental value for the binding

energy D_e of Al_2. The fundamental frequency ω_e is calculated to be 274.3 cm^{-1}, in reasonable agreement with the experimental value of 284.2 cm^{-1} [163]. For more rigorous treatments for Al_2, involving low–lying states, the reader is recommended to go over Refs. [109, 164, 166–168].

Ni_2: The ground state is found to be a bond length of 2.4948 Å, which is surprisingly (and incidentally) almost equal to the bulk value of 2.4919 Å [176]. The discrepancy between the present result and the seemingly best estimate of 2.200 Å of the experiment [47], which was on jet–cooled Ni_2, is not too severe. On the other hand, the case for the binding energy cannot, however, be seen reliable: the ground state is found to has a binding energy of 1.2581 eV, which is not at all close the corresponding experimental value of 2.068 eV. Similar to Al_2, the present binding energy is much lower than the experimental one, again not consistent with the general trend of the DFT method. As is seen from Table 2.2, the other calculated D_e values vary in a large range from 1.42 to 3.42 eV; i.e., there is no unanimous answer concerning the binding energy of Ni_2 in the literature. The situation for the fundamental frequency ω_e is even more severe: both experimental estimates and other theoretical calculations exhibit a great diversity; the present value of 222.2 cm^{-1} lies between the two extrema of 192 and 395 cm^{-1}.

Ti_2: The Ti–Ti bond is calculated to be 1.8537 Å, lower than the bulk value of 2.95Å [176] and the conjectured value of 2.65 Å used by Kant [174] in his semiempirical calculations. We have not encountered any other experimental value for the bond length to compare. The other calculated results for r_e taken from the literature again do not show any unanimity. The binding energy D_e of Ti_2 is calculated as 2.8979 eV, which is significantly overestimated compared with the experimental estimate of $\sim$ 1.3 eV [161, 162, 174] and with the other theoretical calculations. In this case the results for both bond length and binding energy is consistent with the typical outcomes of the DFT method. The fundamental frequency ω_e is calculated to be 482.4 cm^{-1}, which may be considered to be much closer to the experimental prediction of 407.9 cm^{-1} [100] (matrix–isolated Ti_2) than the other calculated values cited in Table 2.3.

We have seen in Ni_2 and Ti_2 cases that their binding energies were significantly different from the corresponding experimental values. A possible reason might be the use of the ECP scheme instead of an all-electron approach, similar to the Al_2 case. Another possible reason could be that the B3LYP exchange and correlation functionals might not properly take into account spin polarization (which leads to magnetism in some TM elements) in Ni and Ti elements [178] and this might account for the observed binding energy discrepancies in Ni_2 and Ti_2.

Table 2.4: Spectroscopic constants of heteronuclear diatoms. Binding energy D_e is in eV, equilibrium interatomic separation r_e is in Å, and the fundamental frequency ω_e is in cm^{-1}.

Diatom	D_e	r_e	ω_e	Method	Reference
Al–Ni	3.3511	2.5331	263.5	DFT	This work
Al–Ti	2.0708	2.7480	202.9	DFT	This work
Ni–Ti	2.8032	2.0567	349.3	DFT	This work

AlNi, AlTi, NiTi: For these heteroneuclear diatoms there was no experimental and theoretical data to compare in the literature. However, relatively much information are available about many of the homonuclear metal dimers. To our best knowledge, the present calculated values are the first for these species. Calculated spectroscopic constants for these dimers are given in Table 2.4.

2.2.3.2 Trimers

The present calculated results for the homonuclear trimers Al_3, Ni_3, and Ti_3, with some experimental and theoretical values from the literature, are tabulated in Table 2.5. The geometry adoption, with $a = b$, is as shown in Figure 2.2. In the following discussion, we will focus mainly on the structure of the trimers considered. This is not only the most intriguing question in the short history of the clusters, but also one of the most difficult aspects to probe. Because

of the approximations made, the theoretical calculations usually result in the equilibrium geometries which are not accepted unanimously. Even in the simplest case of homonuclear trimers, we have seen that there was no consensus about the question of whether the considered species is linear, isosceles triangle, or equilateral triangle.

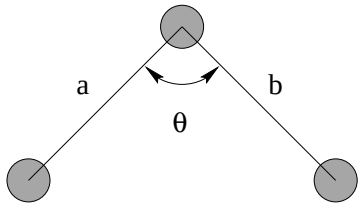

Figure 2.2: Geometry of triatom with parameters.

Al_3: With an *ab initio* pseudopotential method, Upton [56] conjectured the triangular form of Al_3 as being most stable. Considering an *ab initio* calculation, Basch [181] found that the Al_3 trimer having lowest energy is in triangular form (nearly equilateral triangle); similarly in his perturbed electron drop model calculation, Upton [110] also obtained the same result. Pettersson *et al.* [111] considered both *ab initio* and parametric empirical potential calculations for Al_n clusters, and they also found that the triangular configuration for Al_3 is energetically most stable. Pacchioni and Koutecký [180] considered pseudopotential

Table 2.5: Trimers Al_3, Ni_3, and Ti_3 at minimum energy configurations. Bond lengths $a = b$ are in Å, bond angle θ is in degree, and the vibration with maximum amplitude ω^* is in cm^{-1}. The geometry, with $a = b$, is as shown in Figure 2.2. (The abbreviations in the "Structure" column are as E: equilateral, T: triangular, L: linear.)

Trimer	Structure	a	θ	ω^*	Method	Reference
Al_3	E	2.64		200.7	DFT	This work
	E (D_{3h})	2.802			Exp. & MO	[179], or
	T (C_{2v})	2.709	72.6		Exp. & MO	[179]
	T	2.61	60.5		*ab initio* (pseudopotential)	[56]
	E	2.52		255	first princ. calc.	[74]
	E	2.916			MRD CI	[108, 180]
	T (C_{2v})	2.62	60.5		first princ. calc.	[110]
	T	2.619	71.0		*ab initio* & par. emp. pot.	[111]
	E	2.46			DFT	[112]
	T (C_{2v})	2.47	63		MD	[113]
	T	2.55	63		MCSCF/MRCI	[168]
	T (D_{3h})	2.569	56.2		MCSCF	[181]
	T (D_{3h})	2.584			empirical PEF	[182]
	E (D_{3h})	2.58			MD	[183]
Ni_3	E	2.21		227.8	DFT	This work
				202	Exp.	[42]
	T (C_{2v})		90–100	232.3	Exp.	[118]
	E	2.5			EH	[39]
	L	2.5			MO	[41]
	L				ECP–MCSCF–CI	[45]
	T	2.15	61.14		DFT	[91]
	E				CNDO	[107]
	L	2.25			MO	[123]
	T (D_{3h})	2.253			empirical PEF	[182]
	L & E				SCF/CCI	[184]
Ti_3	T	2.30	67.97	75.2	DFT	This work
	E	3.1			MO	[41]

calculations and found that linear and equilateral triangle forms of the Al_3 trimer are energetically almost degenerate. On the other hand, Howard *et al.* [179] in their ESR spectroscopy experiment observed that the equilateral triangle geometry of Al_3 has lowest energy. The finding of Tse [168] is the triangular form for Al_3. In his empirical PEF calculation Erkoç [182, 183] found the triangular form of Al_3 as most stable. Jones [112], using DFT calculation, found that the equilateral triangle form of Al_3 is energetically most stable. El–Bayyari and Erkoç [113], with the molecular dynamics technique, found the triangular form of Al_3 with $C_{2\nu}$ symmetry as the energetically most stable structure. Finally, with a first principle calculation, Yang *et al.* [74] found an equilateral triangular structure for the ground state of Al_3. In the present study, we found the ground state to be an equilateral triangle with a bond length of 2.64 Å, which may be seen to be consistent with the other calculations. We also tried a linear geometry for Al_3 and found that its energy is about 0.3 eV above from that of the equilateral one. We note that our bond length for Al_3 is very close to that for Al_2 dimer, 2.6520 Å. Our result for the vibration with the maximum amplitude, $\omega^* = 200.7$ cm^{-1} is in reasonable agreement with that of Yang *et al.* [74], 255 cm^{-1}. For a more rigorous treatment of Al_3, see Ref. [181]; and for a detailed information about Al clusters see Ref. [177].

Ni_3: There exists a controversy between theory and experiment for this microcluster. With semiempirical methods Anderson [41, 123] and with *ab initio* methods Basch *et al.* [45] predicted the linear structure to be most stable. Basch *et al.* found that the linear form is more stable by 0.17 eV than the triangular form. In solid argon matrix, Moskovits and DiLella [118] found, on the other hand, the geometry of Ni_3 in solid argon to be a bent structure with an apex angle predicted between 90^o and 100^o. The semiempirical calculations of Blyholder [107], extended Hückel calculations of Baetzold [39], and empirical PEF calculations of Erkoç [182] predicted the equilateral form for Ni_3 as most stable. Blyholder found that the equilateral form was more stable than the linear one by 1.7 eV. Reuse and Khanna [91], with a DFT calculation, found a triangular form with an apex angle 61^o as being most stable. In this work, we found the ground state to be an equilateral triangle with a bond length of 2.21 Å, which is not too different from the other literature values. Furthermore, our trial linear geometry for Ni_3 has appeared with an energy value which was significantly above from that of the equilateral one by 3.1 eV. We also note that our bond length of 2.21 Å for Ni_3 is significantly lower from that for Ni_2 dimer, 2.4948 Å. Koutecký [16] states that from theoretical and experimental results the conclusion can be drawn that in a gas phase the Ni_3 species is probably a *fluxional* molecule. As to the vibrational frequency, Moskovits and Hulse [42] attribute a system with a spacing of 202 cm^{-1} to Ni_3. Moskovits and DiLella [118] later observed Ni_3 with a

dominant frequency about resonance 232.3 cm^{-1}. The present calculated value of 227.8 cm^{-1} is in good agreement with these two experimental values.

Ti_3: We found the ground state to be a triangle with a bond length of 2.30 Å, an apex angle of 67.97^o, and a maximum–amplitude–vibration of 75.2 cm^{-1}. We have encountered only one theoretical calculation in the literature: Anderson [41], with the molecular orbital approximation, found the ground state to be an equilateral triangle with a bond length of 3.1 Å. We note that the present bond length of 2.30 Å for Ti_3 is greater from that of Ti_2 dimer, 1.8537 Å. It is also found that a trial linear geometry for Ti_3 has an energy which is about 2.8 eV above from that of the (isosceles) triangular one.

Heteronuclear trimers: For these species, as well as homonuclear ones discussed above, all the calculated results are given in Table 2.6. We have encountered neither experimental nor theoretical information about these heteronuclear species in the literature to compare. Data on polyatomic metal clusters was indeed very limited. To our best knowledge, the present calculated values are the first for these species. An interesting feature of Table 2.6 is that the optimized minimum energy structure of AlNiNi is linear in the given order. Furthermore, both AlNiNi and TiTiAl trimers have asymmetric structure.

Table 2.6: Trimers of $Al_kTi_lNi_m$ at minimum energy configurations. Bond lengths a and b are in Å, bond angle θ is in degree, and vibrational frequencies ω_n are in cm^{-1}. The geometry is as shown in Figure 2.2. The asterisked frequencies represent the vibrations with maximum amplitude.

A–B–C	a	b	θ	w_1	w_2	w_3	w_4
Al–Al–Al	2.6444	2.6444	60.00	200.7*	201.3	301.1	—
Ni–Ni–Ni	2.2184	2.2184	60.00	227.8	231.4*	333.4	—
Ti–Ti–Ti	2.3035	2.3035	67.97	75.2*	261.3	368.1	—
Al–Ni–Al	2.2907	2.2907	77.87	147.8	302.8*	358.4	—
Al–Ni–Ni	2.8152	2.3430	180.00	64.4	75.2	171.4*	245.3
Al–Ti–Al	2.8631	2.8631	64.35	139.0*	182.8	208.4	—
Ni–Ti–Ni	2.0346	2.0346	116.81	81.0	340.1	421.5*	—
Ti–Ti–Al	2.9985	2.6779	58.56	133.0	203.1*	251.1	—
Ti–Ni–Ti	2.3719	2.3719	51.27	143.6	284.7*	470.0	—
Ni–Al–Ti	2.3633	2.7302	151.99	45.0	160.9*	351.7	—

2.2.3.3 Energetics of clusters

We calculated the possible dissociation channels and the corresponding dissociation energies, which are presented in Tables 2.7 and 2.8. We define the dissociation energy of a particular dissociation channel XY $\rightarrow$ X + Y as $E_{\rm dis} = E^{\rm XY}_{\rm total} - E^{\rm X}_{\rm total} - E^{\rm Y}_{\rm total}$. From experimental point of view, this definition may be reversed. It is seen from Tables 2.7 and 2.8 that atomization energies of homonuclear trimers are, not surprisingly, greater than those of the corresponding dimers. Besides, homonuclear trimers, X_3, are seen to dissociate as $X_3 \rightarrow X_2 + X$, as expected. All but XTi_2, all the XY_2 type trimers dissociate as $XY_2 \rightarrow XY + Y$. XTi_2 type trimers, i.e. $AlTi_2$ and $NiTi_2$, prefer to fragment into $XTi_2 \rightarrow X + Ti_2$. NiAlTi trimer dissociates as NiAlTi $\rightarrow$ AlNi + Ti, consistent with the fact that AlNi dimer has the greatest binding energy. For Ni_2 and Ni_3 we found the dissociation energies to be -1.2581 and -4.6854 eV, respectively. These results contradict with the findings of Anderson [123] (using gas phase UV Ni atom spectra), Lian *et al.* [114] (the collision induced fragmentation of Ni_n^+ clusters), and Reuse and Khanna [91] (DFT calculations); they all found that the dissociation energy of Ni_3 was lower than that of Ni_2.

Table 2.7: Dissociation data of the most stable $Al_kTi_lNi_m$ microclusters: the possible dissociation channels and the corresponding dissociation energies (in eV). The asterisked rows represent the favorable dissociation for the corresponding clusters. Trimer structures are as shown in Figure 2.2.

Cluster A–B–C		Dissociation channel	Dissociation energy
Al–Al	→	2Al	−0.4531
Ti–Ti	→	2Ti	−2.8979
Ni–Ni	→	2Ni	−1.2581
Al–Ni	→	Al + Ni	−3.3511
Al–Ti	→	Al + Ti	−2.0708
Ni–Ti	→	Ni + Ti	−2.8032
Al–Al–Al	→	3Al	−2.6859
		Al_2 + Al	−2.2328*
Ni–Ni–Ni	→	3Ni	−5.9436
		Ni_2 + Ni	−4.6854*
Ti–Ti–Ti	→	3Ti	−5.8400
		Ti_2 + Ti	−2.9420*
Al–Ni–Al	→	Al_2 + Ni	−4.8000
		2Al + Ni	−5.2531
		AlNi + Al	−1.9020*

Table 2.8: Continuation of Table 2.7.

Cluster A–B–C		Dissociation channel	Dissociation energy
Al–Ni–Ni	→	Al + Ni_2	−3.6298
		Al + 2Ni	−4.8880
		AlNi + Ni	−1.5369*
Al–Ti–Al	→	Al_2 + Ti	−3.3556
		2Al + Ti	−3.8087
		Al + AlTi	−1.7379*
Ni–Ti–Ni	→	Ni_2 + Ti	−5.7217
		2Ni + Ti	−6.9799
		Ni + NiTi	−4.1766*
Ti–Ti–Al	→	Al + Ti_2	−3.0561*
		Al + 2Ti	−5.9540
		AlTi + Ti	−3.8832
Ti–Ni–Ti	→	Ni + Ti_2	−4.0595*
		Ni + 2Ti	−6.9575
		NiTi + Ti	−4.1542
Ni–Al–Ti	→	Al + Ni + Ti	−5.4357
		AlNi + Ti	−2.0846*
		AlTi + Ni	−3.3649
		Al + NiTi	−2.6324

We calculated HOMO–LUMO gaps of all the microclusters considered in this work, which are given in Table 2.9. Since the number of electrons in Al–Al, Ni–Ni, Ti–Ti, Ni–Ti, Ni–Ni–Ni, Ti–Ti–Ti, Al–Ni–Al, Ni–Ti–Ni, and Ti–Ni–Ti is even, this microclusters have only α–states; on the other hand, the remaining clusters have odd number of electrons hence they have both α– and β–states. The most striking feature seen from Table 2.9 is that the calculated HOMO–LUMO energy gap of dimers are relatively smaller than the corresponding ones for trimers, which may not be expected; but we should not hurry in drawing any conclusion from this result because both homonuclear dimers and the corresponding trimers are too small to be classified as conducting or not. Another feature is that the gap of α states are relatively larger than that of β states, except AlTiAl trimer.

The calculated excess charge and dipole moments of the trimers are given in Table 2.10. Because of their rotational symmetry, homonuclear trimers with equilateral–triangular structure, i.e. Al_3 and Ni_3, do not experience charge separations among the atoms, resulting in no dipole moments. All symmetric trimers, i.e., Ti_3, AlNiAl, AlTiAl, NiTiNi, and TiNiTi, have some excess (positive) charges equally distributed on the end atoms, and the negative charge on the center atom. The remaining trimers AlNiNi, TiTiAl (which has the largest dipole moment), and NiAlTi have no symmetry at all so that their charge separation do not exhibit any regular pattern. We note that all the trimers except Al_3 and Ni_3 bears a net

Table 2.9: Calculated HOMO, LUMO energies (in Hatree) and HOMO–LUMO gap (E_g) energies (in eV) of dimers and trimers.

Species	HOMO(α)	LUMO(α)	$E_g(\alpha)$	HOMO(β)	LUMO(β)	$E_g(\beta)$
Al–Al	−0.1416	−0.1176	0.6525	—	—	—
Ni–Ni	−0.1441	−0.1253	0.5124	—	—	—
Ti–Ti	−0.1118	−0.0776	0.9322	—	—	—
Al–Ni	−0.1786	−0.0847	2.5556	−0.1744	−0.0922	2.2362
Al–Ti	−0.1643	−0.0765	2.3888	−0.1479	−0.0837	1.7456
Ni–Ti	−0.1191	−0.0821	1.0054	—	—	—
Al–Al–Al	−0.1714	−0.1162	1.5020	−0.1681	−0.1184	1.3527
Ni–Ni–Ni	−0.1714	−0.0879	2.2718	—	—	—
Ti–Ti–Ti	−0.1376	−0.0749	1.7039	—	—	—
Al–Ni–Al	−0.1792	−0.0975	2.2239	—	—	—
Al–Ni–Ni	−0.1616	−0.0891	1.9736	−0.1607	−0.1499	0.2920
Al–Ti–Al	−0.1466	−0.1128	0.9205	−0.1706	−0.1101	1.6463
Ni–Ti–Ni	−0.1718	−0.0982	2.0046	—	—	—
Ti–Ti–Al	−0.1607	−0.0715	2.4272	−0.1579	−0.0899	1.8509
Ti–Ni–Ti	−0.1443	−0.0760	1.8580	—	—	—
Ni–Al–Ti	−0.1909	−0.0996	2.4854	−0.1427	−0.08750	1.5023

Table 2.10: Calculated excess charge (in units of electron charge) on atoms, and dipole moments (in Debye) of trimers.

A–B–C	$q(A)$	$q(B)$	$q(C)$	μ_x	μ_y	μ
Al–Al–Al	0.0000	0.0000	0.0000	0.0000	0.0000	0.0000
Ni–Ni–Ni	0.0000	0.0000	0.0000	0.0000	0.0000	0.0000
Ti–Ti–Ti	−0.0422	0.0845	−0.0422	0.0727	0.0000	0.0727
Al–Ni–Al	0.3407	−0.6815	0.3407	0.3952	0.0000	0.3952
Al–Ni–Ni	0.2068	0.1295	−0.3362	1.2073	0.0000	1.2073
Al–Ti–Al	0.1308	−0.2616	0.1308	2.0216	0.0000	2.0216
Ni–Ti–Ni	0.1746	−0.3492	0.1746	2.2309	0.0000	2.2309
Ti–Ti–Al	−0.1044	−0.1918	0.2962	2.2304	0.6519	2.3237
Ti–Ni–Ti	0.0274	−0.0548	0.0274	0.1591	0.0000	0.1591
Ni–Al–Ti	−0.3334	0.5133	−0.1800	1.2085	0.0426	1.2092

dipole moment, as expected. Here we should point out that the excess charge distribution pattern on atoms, both in sign and in amount, demonstrates a strong dependence on geometry. For example, the charge on Ni atom in NiTiNi is about +0.17 electron charge whereas in TiNiTi it is about −0.05 electron charge.

In concluding, compared with the experimental and the other theoretical results, the method of calculation and the basis set chosen in the first part of the doctoral study are seen to give reliable results for systems considered; therefore, it is quite appropriate to use the same method and basis set for other systems.

CHAPTER 3

EMPIRICAL POTENTIAL ENERGY FUNCTION FOR AlTiNi TERNARY SYSTEM

3.1 Introduction

The literature of last decades has witnessed many attempts devoted to predict energetically the most stable structures of small clusters. The methods used can be broadly classified into two groups, namely, computer simulations using empirical model potentials and *ab initio* calculations from first principles. But why a computer simulation based on a potential energy function (PEF) instead of an *ab initio* method? In spite of the advent of sophisticated computers, it is still not practical to handle systems containing more than a few heavy atoms using *ab initio* methods. It is generally accepted that in order to describe accurately the bonding phenomenon in metal clusters one needs high levels of theory [166]. Because of the partial occupancy of d orbitals in TMs, even in a simple case of homonuclear dimers of TMs, there is no unanimously accepted results, as we witnessed in Section 2.2. The seemingly most challenging problem in molecular

electronic *ab initio* methods is that as the system under study gets larger and larger, the number of molecular integrals to be evaluated increases in a tremendous manner. This in turn requires an expensive computational time. An efficient remedy for solving this problem is to introduce a reliable empirical model PEF. Computer simulations based on empirical PEFs have been used successfully to investigate the various bulk, surface, and cluster properties of numerous systems at the atomistic level [185]. Many of these simulations were based on empirical model potentials describing interactions among the atoms in the system under study [186]. It is likely that the use of empirical PEFs will continue its indispensability in material science computations.

3.2 Modeling & Simulation

A molecular–scale simulation involves a three–step procedure: (*i*) modeling individual particles, (*ii*) simulating the movements of a large number of the model particles, and (*iii*) analyzing the simulation data for the required collective phenomenon. Here are the words *modeling* and *simulation* that deserve further clarification. A *modeling* is an attempt to decouple and remove interactions that have little or no influence on the observables being studied. Thus a model is simpler than the system it mimics: it has access to fewer states. Decoupling interactions means relaxing constraints; and a model has access to some states not available

to the original system. In other words, a model is a subset or subsystem of the original system: outputs from a model will be consistent with those of the original system, but only for a restricted set of inputs. For those restricted inputs, since the model is a subsystem of the original one, states visited by the model correspond to those visited by the original system.

In contrast, a *simulation* is more complicated than the system it simulates: a simulation generally can reach many more states than the original system can. A simulation imposes constraints so that the simulated output is consistent with the output of the original system, at least for a restricted set of inputs. A simulation will typically bear no structural relation to the original system; for example, the way constraints are imposed in the simulation may differ from the mechanism that confines the original system to certain states. Hence, states in the simulation may bear no correspondence to states of the original system.

Here is an example to clarify these ideas. We identify a substance and its observables we want to study, say, thermodynamic properties of argon. Then we construct a model of the substance, say, the spherically symmetric, pairwise additive Lennard–Jones potential, which is a true model. The Lennard–Jones potential is simpler than the argon potential because argon atoms are not perfect spheres and their interactions are certainly not only pairwise additive. With the

model chosen, we then perform a simulation—but a simulation of what? It can only be a simulation of the model, of the Lennard–Jones substance. We do not simulate argon. The simulation is more complex than the model, but the added complexity does not add to the realism of the resulting observable outputs. In error are those who claim that molecular dynamics simulates argon, or water, or proteins, or whatever. We simulate molecular models of such substances.

3.3 Models for Atomistic Simulations

A computer simulation is valuable because it is applied to a precisely defined model for the material of interest. The model is actually composed of two parts: one for the interacting among the atoms making up the system and another for interactions between the atoms and their environments. The latter encompasses boundary conditions, which describe how the atoms interact with their surroundings. Characteristics of boundary conditions are largely dictated by the physical situation to be simulated.

The model for atomistic interactions is contained in an interatomic force law or, equivalently, an interatomic potential energy function (PEF). This PEF implicitly describes the geometric shapes of the individual atoms or, more precisely, their electron clouds. Thus when we specify a PEF, we establish the symmetry

of the atoms, whether they are rigid or flexible; how many interaction types are prevail among atoms, two–body interaction, three–body interaction, ...; and so on. A detailed characterization of interatomic PEF may be given analytically or numerically; in any case a quantitative form for PEF defines a molecular model and hence the form must be chosen before a simulation.

3.4 General Features of Potential Energy Functions

A PEF is a parametric function designated to describe the interactions among the atoms in a system. It is parameterized to give the empirical data for the system under consideration. Apart from the condition that a PEF must possess all physically required invariance properties, it is usually desired to have a small number of parameters because the more parameters a PEF has, the more time consuming the parametrization is. Furthermore, it is difficult to relate the observed structure back to the PEF parameters.

The Born–Oppenheimer approximation [187] provides us with an unambiguous definition of a PEF for the nuclei of a system. The PEF Φ of a system depends only on the positions of the nuclei and it implicitly contains the energy of the ground state electronic wave function that binds the nuclei together. If there is no external field acting on the system, then the PEF depends on the

relative positions of the nuclei (or, equivalently, atomic positions) and it can be expanded quite generally into a many–body series containing two–, three–, ..., N–body potentials which describe the interactions between two atoms, among three atoms, ..., among N atoms, respectively [188], like the multipole expansion in electrostatics:

$$\Phi\left(\mathbf{r}_1, \mathbf{r}_2, \ldots, \mathbf{r}_N\right) = \sum_{i<j}^{N} U_{ij}\left(\mathbf{r}_i, \mathbf{r}_j\right) + \sum_{i<j<k}^{N} W_{ijk}\left(\mathbf{r}_i, \mathbf{r}_j, \mathbf{r}_k\right) + \cdots + \sum_{i<j<k<\cdots<N}^{N} Z_{ijk\ldots N}\left(\mathbf{r}_i, \mathbf{r}_j, \mathbf{r}_k, \ldots, \mathbf{r}_N\right) , \tag{3.1}$$

where $\mathbf{r}_i$ is the position vector for the atom i, and N is the total number of atoms in the system. In practice, it is difficult to handle such an expansion in calculations; furthermore, it is not an easy task to define many–body atomic interactions. For these reasons the expansion is usually truncated after the three–body term [189]. Contributions of the truncated terms can sensitively be included in the PEF by inserting some linear combination parameters to the remaining two– and three–body terms [182, 190, 191]. All PEF parameters can be determined by making use of available experimental data and constraints imposed on the system. This is actually a hard step to achieve and requires skill and experience. For example, if a PEF is to be used for a bulk matter, the parameters are usually determined by considering the cohesive energy per atom and the stability condition $d\Phi/dV = 0$ at $T = 0$ K. If the so–parametrized PEF reproduces other experimental values such as bulk moduli, elastic constants, surface energies, etc.,

then it is said to reasonably represent the bulk matter under study [11]. A common situation is that one has not any experimental datum to determine the PEF parameters. What is done in that case is to resort to accurate first principles *ab initio* theoretical results. In any case, the main aim of parametrization is to obtain a fitting as accurate as possible for small systems (generally only for two– and three–atom systems). Once this is achieved, a well–constructed reliable PEF can be successfully used for larger systems, including bulk materials.

In general finding an appropriate PEF constitutes the most important and the most difficult part in the simulation of a system. It is necessary to describe the PEF of the system in terms of empirical or model potential functions with simple analytic forms. In the literature there are many such functions for two– and three–body interactions whose explicit functional forms for various systems were recently collected together in two reviews [192, 193].

3.5 Two–Body Potential Energy Functions

The potential energy functions used in molecular–scale simulations divide into two broad classes: those for *soft bodies*, for which the interatomic forces are continuous functions of the between molecules, and those for *hard bodies*, for which the forces are discontinuous. For hard bodies, the discontinuity in the

force extends to the interatomic potential; in particular, hard spheres of diameter σ interact through a PEF $u(r)$ of the form

$$u(r) = \begin{cases} \infty & r \leq \sigma \\ 0 & r > \sigma \end{cases} \tag{3.2}$$

which is shown in Figure 3.1. Thus hard spheres exert forces on one another only when they collide. Between collisions the spheres travel along straight lines at constant velocities, and so, rather than compute trajectories, the simulation algorithm computes the times of collision. The calculation is purely algebraic because collisions are taken to be perfectly elastic: during a collision no energy is transferred either to deform a sphere or to change its internal state. Thus two principles, conservation of linear momentum and conservation of kinetic energy, enable us to determine collision times.

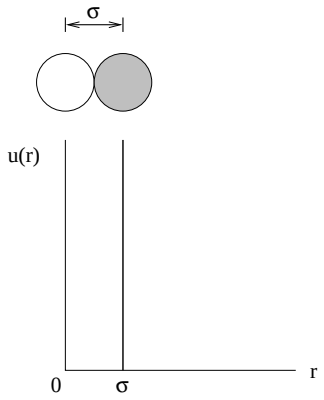

Figure 3.1: The pair PEF $u(r)$ for hard spheres

Although it is instructive, the hard–sphere potential is not realistic. What is needed is a model PEF that accounts both for short–range, repulsive overlap forces and for long–range, attractive dispersion forces. Short–range repulsive forces prevent the substance from collapsing onto itself, while long–range attractions deter disintegration of the substance (in the absence of a container). A well-known useful model for the soft–sphere pair potential is the Lennard–Jones potential:

$$u(r) = \text{const.} \left[\left(\frac{\sigma}{r} \right)^n - \left(\frac{\sigma}{r} \right)^m \right] . \tag{3.3}$$

The range and strength of repulsive and attractive forces determined by the values assigned to the integers n and m. The most popular choice is $n = 12$ and $m = 6$, leading to the *(12,6) Lennard–Jones pair PEF*:

$$U(r_{ij}) = \varepsilon_0 \left[\left(\frac{r_0}{r_{ij}} \right)^{12} - 2 \left(\frac{r_0}{r_{ij}} \right)^6 \right] . \tag{3.4}$$

where $r_{ij} = |\mathbf{r}_i - \mathbf{r}_j|$ is the interatomic distance between the atoms i and j. In Eq. (3.4) the first term inside the brackets represents the repulsive branch and the second term represents the attractive branch of the interaction potential between two atoms. $U(r_{ij}) = 0$ when the two atoms are infinitely far apart, i.e., when $r_{ij} = \infty$. Using $dU/dr_{ij} = 0$, it is readily seen that the minimum value of the energy is $-\varepsilon_0$ (i.e., the depth of the potential well is ε_0). This minimum occurs at $r_{ij} = r_0$ and this is the position of the static equilibrium. In Figure 3.2 the (12,6) Lennard–Jones pair PEF, $U(r)$, and the corresponding pair force, $F(r)$, are shown qualitatively.

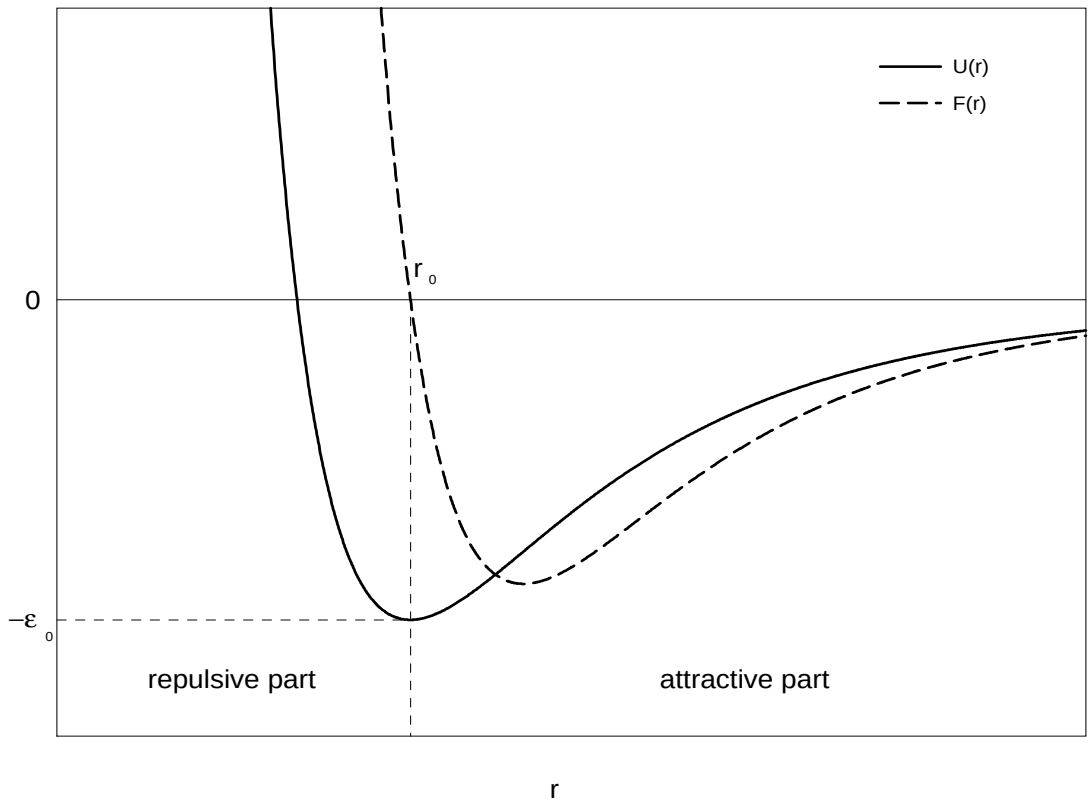

Figure 3.2: The (12,6) Lennard–Jones pair PEF, $U(r)$, and the corresponding pair force, $F(r)$.

Empirical two–body, or pair, potentials, like the LJ potential, have been utilized for years for a variety of bulk, surface, interface, and cluster simulations. We now know, however, that if the PEF of a system includes only two–body interaction, such a PEF does not stabilize open crystal structures; does not give the proper surface lattice plane spacing changes on relaxation; or does not provide the proper atomic configuration for trimers [194]. There are two ways to overcome the deficiency of a two–body interaction (not necessarily only LJ–type). One can scale the total energy into two parts as repulsive $U_{21}(r_{ij})$ and attractive $U_{22}(r_{ij})$ terms [195]:

$$\Phi = \sum_{i<j}^{N} U_{ij} = D_{21} \sum_{i<j}^{N} U_{21}(r_{ij}) + D_{22} \sum_{i<j}^{N} U_{22}(r_{ij}) \,. \tag{3.5}$$

The additional parameters D_{21} and D_{22} can then be determined analytically from the stability condition $d\Phi/dV = 0$ at $T = 0$ K. The combination $D_{21}U_{21}(r_{ij}) + D_{22}U_{22}(r_{ij})$ can be said to represent the *effective pair interaction*. The second way of overcoming the deficiency of a two–body interaction is to include a three–body interaction term in the PEF of the system. Any angular dependence of a PEF is essentially an expression of the many–body effect and thus the PEF needs at least a three–body potential for its description. Unfortunately, it is a very difficult task to derive a three–body atomic interaction from pure quantum mechanical means [196].

3.6 Empirical Potential Energy Function for AlTiNi Ternary System

Now we return to our AlTiNi ternary system. As usual we assume that, in the absence of external forces, there exists a PEF, $\Phi(\mathbf{r}_1, \mathbf{r}_2, \ldots, \mathbf{r}_N)$, describing the total potential energy of a system of N atoms as a functions of their positions and that this PEF can be expanded into the contributions from two–body, three–body, ... interactions, as given in Eq.(3.1). It is usually believed that this series is rapidly convergent [189] and that the first two terms give a reasonable approximation to the total interaction potential. (As we mentioned above, the contributions of the remaining terms, beyond the three–body term, may be forced to be included in the two– and three–body parts during the parametrization process.) In early applications, this expansion used to be truncated after the two–body term. However, it has been shown [197, 198] that the three–body term makes important contributions to the structure and stability of different microclusters, and is essential to a proper understanding of surface multilayer relaxation in crystals [199].

In this study, the expansion (3.1) has also been truncated after the second term so that only the two– and three–body interactions were included. The Lennard–Jones potential, Eq.(3.4), has been taken for the two–body part, and the Axilrod–Teller triple–dipole potential for the three–body part [200], their

explicit form respectively are

$$U_{ij} = \epsilon_0 \left[\left(\frac{r_0}{r_{ij}} \right)^{12} - 2 \left(\frac{r_0}{r_{ij}} \right)^{6} \right] \tag{3.6}$$

and

$$W_{ijk} = \frac{Z\,(1 + 3\cos\theta_i \cos\theta_j \cos\theta_k)}{(r_{ij}\, r_{ik}\, r_{jk})^3}\,, \tag{3.7}$$

where $r_{ij} = |\mathbf{r}_i - \mathbf{r}_j|$ is the interatomic distance between the atoms i and j; θ_i, θ_j, and θ_k are the angles of the triangle formed by the three atoms i, j, k; and Z is the three–body parameter which is a measure of the energy density in the three–body part. [For the information about the derivation of Eq.(3.7), see Ref. [196].] The combination of PEF given above, (LJ + AT), has proven its usefulness and was successfully used for different cluster systems as well as for surface and bulk properties of some materials [111, 200–204]. should emphasize here that, in the literature, this empirical many–body potential energy function, Eq.(3.1) with Eqs.(3.6) and (3.7), is the one which has the least number of parameters for a monatomic system, namely r_0, ϵ_0, and Z.

An important point is in order here. In the electronic properties of the elements containing many electrons, such as those in our work, relativistic effects play an important role. This fact is even more crucial in molecules. However, empirical potentials do not contain electronic information directly; they contain all kinds of contributions, nonrelativistic and/or relativistic, indirectly by using

accurate dimer, cluster, and bulk properties in their parametrization procedure. This approach has been used successfully before for elements such as nickel [206], copper [207], ZnCd binary [208, 209], and even for heavier elements such as silver [210], gold [211, 212], lanthanum [213], lutethium [214], uranium [215], and AuGaAs ternary [202, 204, 216] systems.

3.6.1 Parametrization of the Empirical Potential Energy Function for AlTiNi Ternary System

Making use of the available experimental data and the quantum mechanical calculation results for dimers and trimers of Al, Ni, and Ti (see Tables 2.1–2.3 and 2.5; we have not taken Table 2.4 into account because there was no available experimental data for the heteronuclear dimers of the elements under consideration), we have determined the parameters, (r_0, ϵ_0, Z) of the PEF, Eqs.(3.1,3.6,3.7), for the AlTiNi ternary system. The binding energy and the interatomic equilibrium distance for two–atom clusters, whereas the binding energy and the geometry for three–atom clusters have been taken into account during the parametrization process. The main objective was to re-obtain the geometry and the total energies of the dimers and trimers of the elements under consideration as close as those resulting from experiments and, at the same time, those resulting from the previous *ab initio* results. The so–obtained parameter set for the AlTiNi ternary

Table 3.1: Empirical potential energy function parameters determined for the AlTiNi ternary system.

Two–body parameters			Three–body parameters	
Dimer	ϵ_o (eV)	r_o (Å)	Trimer	Z (eV Å^9)
Al–Al	1.60	2.55	Al–Al–Al	3000.0
Ti–Ti	2.00	2.30	Ti–Ti–Ti	1760.0
Ni–Ni	2.20	2.22	Ni–Ni–Ni	1813.0
Al–Ti	1.70	2.70	Al–Al–Ti	6000.0
Al–Ni	1.70	2.25	Al–Al–Ni	1510.0
Ti–Ni	2.20	2.00	Al–Ti–Ti	500.0
			Al–Ni–Ni	3810.0
			Ti–Ti–Ni	600.0
			Ti–Ni–Ni	250.0
			Al–Ti–Ni	290.0

system is presented in Table 3.1. We should point out here that this parameter set can be more suitable for cluster applications; it is, not surprisingly, likely that it might not properly work for bulk properties. This is due to the fact that we have not made use of bulk properties in the parametrization procedure, instead we have used only the two– and three–atom properties mentioned above.

The mentioned parametrization procedure is not like the least–square fitting method; it is merely a numerical search being aimed to get predetermined geometry and energy of the system studied. We first reasonably fixed the two–body

parameters r_0 and ϵ_0 by making use of the experimental data and *ab initio* results, then we determined the three–body parameter Z. In the determination of Z, the two–body parameters were always kept fixed; however, the Z values for homonuclear systems were determined analytically, whereas for heteronuclear systems they are determined partly analytically and partly numerically by considering the predetermined total energy and geometry of the system considered.

CHAPTER 4

MOLECULAR DYNAMICS SIMULATIONS

This chapter is composed of three main sections. In the first section, we will give, at some length, introductory information about molecular dynamics method. In the second and third sections we will present the second and third parts of our study carried out by using both DFT calculations and molecular dynamics simulations.

4.1 Molecular Dynamics Methods

4.1.1 Introduction

Molecular dynamics (MD) methods are now widely accepted means for simulating molecular–scale models of matter. Although they were originally devised in the 1950s, with the advent of sophisticated computers, they only began to receive widespread attention in the mid–1950s. Today they continue to attract attention from researchers and they are now an indispensable tool in material science, solid and liquid state physics, physical chemistry, etc.

The essence of MD is simply solving the N–body problem of classical mechanics. Since the time of Newton, the N–body problem has been viewed important, but the reasons for its importance has evolved. At the present time, its importance stems from attempts to relate collective dynamics to single–particle dynamic, attempts motivated by the hope that the puzzling behavior of large collections of particles can be explained by examining the motions of individual particles.

Molecular dynamics simulations compute the motions of individual molecules (atoms) in models of solids, liquids, and gases. The key idea of MD simulation is *motion*, which describes how positions, velocities, and orientations change with time. Molecular dynamics simulation is the modern realization of an old idea in science that the behavior of a system can be computed if we have a set of initial conditions plus forces of interaction.

In the following, the commonly used simulation methods will be summarized and, because it is used in the present work, a detailed information will be given for MD method. The following information is basically compiled from the book *Lecture Notes on Simulations of Many–Particle Systems* by Ş. Erkoç [217].

4.1.2 Atomistic Computer Simulations

As we pointed out previously, the first two tasks of the dynamic modeling are (*i*) developing a model and (*ii*) using the model in a simulation. The first task, model development, includes choosing a form for the interatomic PEF. Once the basic physical behavior of the system is embodied in the PEF, large–scale numerical calculations, referred to as *atomistic computer simulations* (ACS), provide an iterative solution to the basic structural, energetic, and dynamical behavior of the interacting atoms. After we have chosen the model potential, we must derive appropriate equations of motion. In this chapter we tackle simulation of substances modeled as soft spheres, substances for which the potential is that proposed in the previous chapter, Eq.(3.1) with Eqs.(3.6) and (3.7).

Before entering the details of the MD method, it would be appropriate here to give some general information about the methods used in ACSs. There are four basic ACS methods: *Static method*, *Monte–Carlo method*, *lattice–dynamics method*, and *molecular–dynamics method*. The common property of all these methods is that their application to the determination of macroscopic properties from a microscopic description of the Born–Oppenheimer potential using numerical methods on high–speed computers.

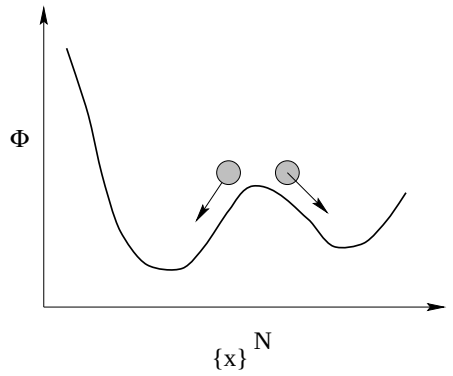

Figure 4.1: The static method, qualitatively. $\{x\}^N$ is portion of the level surface of the hypersurface of the PEF of the system.

4.1.2.1 The Static Method

The static method [218] is the simplest one. An initial configuration of the atoms of the input to the program and the forces on all the atoms are calculated from the PEF using

$$\mathbf{F}_i = -\nabla_i \Phi \,. \tag{4.1}$$

Then, all of the atoms are displaced in the direction of the net force acting on them, and the magnitude of this displacement is proportional to the magnitude of the force. Thus the static method traverses the gradient path from the initial configuration to the *closest* local critical point which may or may not be the global minimum, see Figure 4.1. Since the static method is able to find only stable minima, it can not be used for full thermodynamic calculations.

4.1.2.2 The Monte–Carlo Method

The Monte–Carlo Method [218–221] aspires to the generation of a large number of successive atomic configurations which, taken as a whole, approximate the canonical ensemble of the system of atoms. The constraints of constant volume and number of atoms are automatically satisfied by the use of periodic boundary conditions. The constraint of constant temperature is achieved through the following method. Small random displacements are applied to an atom and the PEF of the system is used to calculate the change in energy, $\Delta\Phi$, caused by this displacement. If $\Delta\Phi$ is negative, this displacement is accepted as a new configuration. If $\Delta\Phi$ is positive, then the Metropolis criterion is applied; that is, the Boltzman factor, $e^{-\Delta\Phi}$, is calculated for the temperature T at which the simulation is desired. This factor is then compared to a random number to probabilistically some configurations of higher energy to be included in the ensemble. Modification of this method can be used to generate other ensembles, such as a constant pressure and temperature ensemble. Figure 4.2 diagramatically shows the general feature of the Monte–Carlo method.

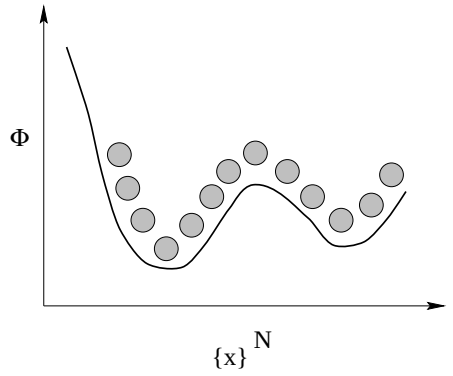

Figure 4.2: The Monte–Carlo method, qualitatively.

4.1.2.3 The Lattice–Dynamics Method

The lattice–dynamics method [223] is distinct from the other techniques in that it generates an analytic representation for the atomic motion in terms of harmonic functions (i.e., phonons), see Figure 4.3. This is accomplished by considering only small amplitude, low temperature vibrations of the atoms about some metastable point of the PEF hypersurface, so that the curvature of the hypersurface at that point suffices for characterizing the atomic motion. Although the applicability of this method is severely restricted compared to the Monte–Carlo and/or MD techniques, its advantage is that the phase space becomes analytically integrable, so that the entropy and related quantities can be directly obtained.

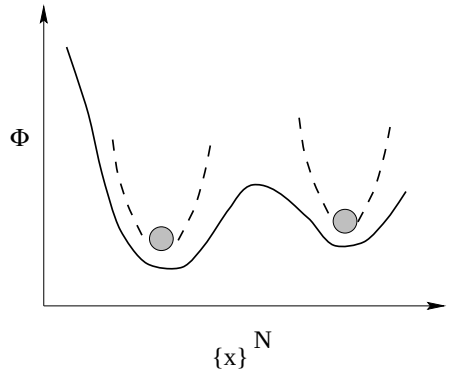

Figure 4.3: The lattice–dynamics method, qualitatively.

4.1.2.4 The Molecular Dynamics Method

The molecular dynamics method [223–226] attempts to numerically integrate the classical equations of motion,

$$\frac{\partial^2 \mathbf{x}_i}{\partial t^2} = -\frac{1}{m_i}\nabla_i \Phi\,, \qquad i = 1, 2, \ldots, 3N\,, \tag{4.2}$$

for a collection of N atoms interacting through a specific analytic PEF and subject to a periodic boundary conditions that constraint the volume and number of atoms. A variety of numerical algorithms are available for this purpose. When done with sufficient accuracy, the total energy in the system will be constant, thus the MD method generates a time–ordered series of atomic configurations which, taken as a whole, approximate the microcanonical ensemble for the system. Modification of the technique can allow constant pressure or temperature ensembles

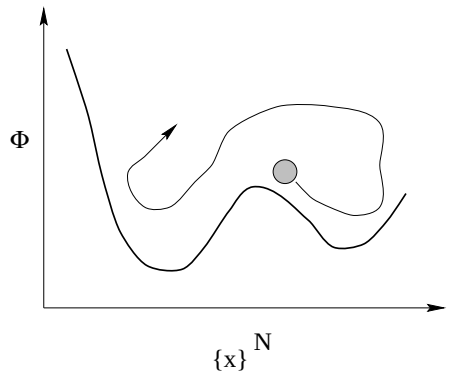

Figure 4.4: The molecular dynamics method, qualitatively.

to be generated. In addition, MD can be applied to the study of non–equilibrium and kinetic phenomena. Figure 4.4 diagramatically shows the general feature of the MD method.

4.1.3 An Important Algorithmic Feature: Truncated Potential

In a system of N atoms, the double sum in the pair potential, for example the one in Eq.(3.6), accumulates $\frac{1}{2}N(N-1)$ unique pair interactions. Thus if all pair interactions are sampled during a simulation, the number of such samples increases with the square of the number of atoms, N^2. Moreover, if the allowed range of interaction between atoms is increased, say from r to $r + \delta r$, then the

number of sampled interactions increases as r^2; that is,

$$N(r, \delta r) \approx \rho\, V(r, \delta r) \approx 4\pi\rho r^2\, \delta r\,. \tag{4.3}$$

Here ρ is the number density, $N(r, \delta r)$ is the number of atoms in a spherical shell of radius r and thickness δr, and $V(r, \delta r)$ is the volume of the shell.

From Figure 3.2 it is seen that the Lennard–Jones pair potential extends over a modest range of pair separations; as a result, we can achieve a considerable savings in computer time by neglecting pair interactions beyond some distance $r = R_{\text{cut}}$. The same considerations hold also for three–body interactions.

4.1.4 Details Of Molecular Dynamics Method

4.1.4.1 A General Look at the Method

What is done in an MD simulation can be simply summarized as follows:

1. Choose the initial configuration, calculate the total energy E using

$$\Phi = \Phi(\mathbf{r}_1, \mathbf{r}_2, \ldots, \mathbf{r}_N) \equiv E\,. \tag{4.4}$$

   (a) Determine velocities $\{\mathbf{v}_i\}$ considering Maxwell speed distribution for a given temperature T. (For constant temperature only—temperature rescaling.)

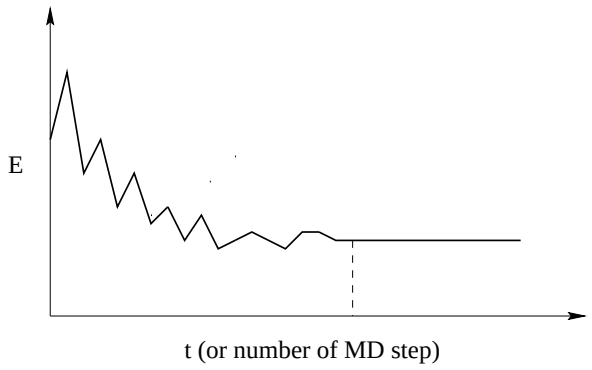

Figure 4.5: Variation of energy with respect to time (or number of MD steps).

(b) Move particles for a time step Δt, determine new configuration, calculate energy. (For relaxation only—without temperature rescaling.)

2. Calculate forces using

$$\mathbf{F}_i = -\nabla_i \Phi \,, \tag{4.5}$$

and calculate velocities using

$$\mathbf{F}_i = m_i \frac{d\mathbf{v}_i}{dt} \,. \tag{4.6}$$

3. Go to (a) or (b).

Figure 4.5 depicts typical energy variation with respect to time (or number of MD steps).

4.1.4.2 Details

In a Newtonian MD simulation one simply solves Newton's equations of motion for a collection of N particles interacting via an assumed PEF, Φ. Consider N particles inside a cubic box of volume $V = L^3$. Each time step the simulation starts with the calculation of the force for each particles, $\mathbf{F}_i = -\nabla_i \Phi$. In this evaluation the interaction between a pair of particles is ignored if their separation r is greater than a predetermined cut–off radius R_{cut}. The size of the computation cell and R_{cut} should satisfy $R_{\text{cut}} \leq L/2$.

The system is made pseudo–infinite by the application of periodic boundary conditions in the three cartesian directions, which is accomplished by the *nearest image convention* [228]. In evaluating the force on particle i due to particle j, we look at the image of j, j', which is nearest to i as shown in Figure 4.6. This is achieved by the transformation:

$$\text{if} \quad r_{ij_\alpha} > L/2 \qquad \text{then} \qquad r_{ij_\alpha} \leftarrow r_{ij_\alpha} - L\,, \tag{4.7}$$

$$\text{if} \quad r_{ij_\alpha} > -L/2 \qquad \text{then} \qquad r_{ij_\alpha} \leftarrow r_{ij_\alpha} + L\,, \tag{4.8}$$

where α stands for x, or y, or z.

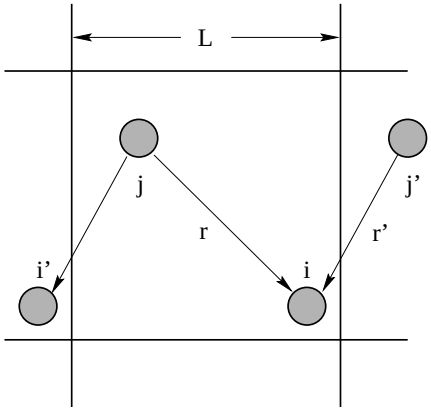

Figure 4.6: Nearest image model for periodic boundary condition.

Having obtained the total force on each particle, we integrate its equation of motion, $\mathbf{F}_i = m(\partial^2 \mathbf{r}_i / \partial t^2)$, between times $n\,\Delta t$ and $(n+1)\Delta t$ using a convenient numerical integration method, which we tackle in the following section. The kinetic energy and temperature of the system at step n is calculated using

$$K = \sum_i \frac{1}{2}\, m_i \, |v_i^n|^2 \tag{4.9}$$

and

$$T = \frac{2}{3}\,\frac{K}{N k_B}\,. \tag{4.10}$$

If the movement of a particle produced after solving the equation of motion takes it outside the calculation box, the periodic boundary conditions are applied to bring it back into the box by means of the transformation

$$\text{if} \quad r_{i\alpha} > L/2 \qquad \text{then} \qquad r_{i\alpha} \quad \leftarrow \quad r_{i\alpha} - L\,, \tag{4.11}$$

$$\text{if} \quad r_{i\alpha} > -L/2 \qquad \text{then} \qquad r_{i\alpha} \quad \leftarrow \quad r_{i\alpha} + L\,, \tag{4.12}$$

with the convention that the origin of the coordinates is at the center of the calculational box.

When the system is in thermal equilibrium, the total kinetic energy is about $\frac{3}{2}Nk_BT$, the velocity distribution remains Maxwelian, and at the same time, the particle displacement distribution becomes a Gaussian form.

The termination of the simulation can be decided by checking the variation of total energy of the system versus the number of time steps: when a smooth region is reached, as in Figure 4.5, the simulation is halted.

4.1.5 Algorithms for Molecular Dynamics

At this point we have a MD simulation of atoms whose PEF varies continuously with distances among atoms, i.e., atoms are treated as "soft–bodies". We are required a numerical method for solving differential equations with the known initial values. Most of the algorithms used in MD methods are based on the so–called *finite–difference methods*, which are classical tools for attacking initial–value problems.

Finite–difference methods replace differentials such as dx and dt with finite differences Δx and Δt; they replace differential equations with finite–difference equations; and over a small but finite time Δt, they assume the rate (or some known function of the rate) is constant.

Most of finite–difference methods stem from truncated Taylor expansions; the simplest one, for example, is *Euler's method*, which is a Taylor expansion truncated after the first–order term:

$$x(t + \Delta t) = x(t) + \Delta t\, \dot{x}(t)\,. \tag{4.13}$$

From the known (or estimated) value of x at t, this method estimates x at $t + \Delta t$ by extrapolating from $x(t)$ the straight line that has slope $\dot{x}(t)$, evaluated at t.

The most commonly used finite–difference methods are the *Runge–Kutta* (RK) methods [229, 230]. These methods have the structure of Euler's method, Eq.(4.13). The various RK methods differ from one another in how the slope $\dot{x}(t)$ is estimated. Each RK algorithm estimates the slope at points along Δt and then computes a weighted average to get a single value to be used in Eq.(4.13). Runge–Kutta methods have been little used in MD because, for large numbers of atoms, the RK algorithms are too slow; they have been used in simulations of systems involving a very few degrees of freedom [231].

Verlet's method [232] is the simplest finite–difference method that has been widely used in MD. The algorithm is a combination of two Taylor's expansions (up to the third order) for $x(t + \Delta t)$ and $x(t - \Delta t)$:

$$x(t + \Delta t) = 2\, x(t) - x(t - \Delta t) + \ddot{x}(t)\, \Delta t^2 + \mathcal{O}\left(\Delta t^4\right) . \tag{4.14}$$

In this approximation the acceleration $\ddot{x}$ is obtained from the interatomic forces and Newton's second law. Various schemes can be used to estimate velocities. One of them is

$$v(t) \approx \frac{x(t + \Delta t) - x(t - \Delta t)}{2\, \Delta t} . \tag{4.15}$$

We notice that Verlet's algorithm is a two–step method because it estimates $x(t + \Delta t)$ from the current position $x(t)$ and the previous position $x(t - \Delta t)$. Therefore it is not self–starting: initial positions $x(0)$ and velocities $v(0)$ are not enough to begin a calculation, and something must be done at $t = 0$ (say, a backward Euler method) to get $x(-\Delta t)$.

4.1.5.1 Predictor–Corrector Algorithms

As seen above, Verlet's algorithm uses positions and velocities from previously calculated steps. Another well-reputed algorithm, called *predictor–corrector algorithm* [233], runs reversely: it estimates positions and velocities for future steps.

Predictor–corrector algorithms are composed of three steps: prediction, evaluation, and correction. For just an example, from the current position $x(t)$ and velocity $v(t)$ the steps are as: (*i*) Predict the position $x(t + \Delta t)$ and velocity $v(t + \Delta t)$ at the end of a step. (*ii*) Evaluate the forces at $t + \Delta t$ using the predicted position. (*iii*) Correct the predictions using some combination of the predicted and previous values of position and velocity.

Predictor–corrector methods offer great flexibility in that many choices are possible for both the prediction and correction steps. They may be either one–step, in which case they are self–starting, or multistep methods, in which case something special must be done to start the calculation.

4.1.5.2 Nordsieck–Gear Predictor–Corrector Algorithm

This is the most commonly used algorithm in MD [234, 235]. To illustrate its *fifth–order* version in detail, we first make some definitions. Let $q_0(t)$ be one of the $3N$ coordinate components for an assembly of N atoms. If D is taken as the operator for the time derivative d/dt, the scaled derivatives of $q_0(t)$ will be

$$q_n(t) = \frac{1}{n!}\Delta t^n \, D^n q_0 \, . \tag{4.16}$$

The Nordsieck–Gear predictor–corrector algorithm consists of the following steps:

- *Predict* atomic position q_0 at time $t+\Delta t$ using a fifth–order Taylor expansion based on position and its derivatives at time t. Thus, the derivatives q_1, q_2, q_3, q_4, q_5 are needed at each step; these are also predicted at time $t + \Delta t$ by applying Taylor expansion at t:

$$
\begin{aligned}
q_0(t+\Delta t) &= q_0 + q_1 + q_2 + q_3 + q_4 + q_5 \\
q_1(t+\Delta t) &= q_1 + 2\,q_2 + 3\,q_3 + 4\,q_4 + 5\,q_5 \\
q_2(t+\Delta t) &= q_2 + 3\,q_3 + 6\,q_4 + 10\,q_5 \\
q_3(t+\Delta t) &= q_3 + 4\,q_4 + 10\,q_5 \\
q_4(t+\Delta t) &= q_4 + 5\,q_5 \\
q_5(t+\Delta t) &= q_5
\end{aligned}
$$

  where all the quantities on the right are evaluated at time t.

- *Evaluate* the associated interatomic force F on the atom concerned at time $t + \Delta t$ using the predicted position q_0.

- *Correct* the predicted position and its derivatives using the discrepancy Δq_2 between the predicted acceleration and that given by the evaluated force. With the forces at $t+\Delta t$ obtained in the previous step and Newton's second law can be used to determine the accelerations $q_2(t + \Delta t)$. The difference between the predicted and evaluated accelerations is then formed:

$$\Delta q_2 = \left[q_2(t+\Delta t) - q_2^P(t+\Delta t)\right] , \tag{4.17}$$

which leads to a *discrepancy function*

$$\phi = \frac{1}{2}\frac{F}{m}(\Delta t)^2 - q_2(t+\Delta t)\,. \tag{4.18}$$

In this algorithm, for second order differential equations, this discrepancy function is used to correct all predicted positions and their derivatives. They are

$$q_n^{\rm corr}(t+\Delta t) = q_n(t+\Delta t) + \alpha_n \phi\,, \qquad n = 0,1,2,3,4,5\,, \tag{4.19}$$

where

$$\alpha_0 = \frac{3}{16}\,, \quad \alpha_1 = \frac{251}{360}\,, \quad \alpha_2 = 1\,, \quad \alpha_3 = \frac{11}{18}\,, \quad \alpha_4 = \frac{1}{6}\,, \quad \alpha_5 = \frac{1}{60}\,.$$

The parameters α_n cause the algorithm to have a higher stability; they depend on the order of the Taylor series predictor. As to the integration time step Δt, it depends on the system studied and is usually on the order of 10^{-15} second.

In the present study, the seventh order predictor–corrector method has been used in the solutions of equations of motion.

4.2 $Al_kTi_lNi_m$ ($k+l+m=4$) Ternary Alloy Microlusters: Molecular Dynamics Simulations and Density Functional Theory Calculations

4.2.1 Introduction

The second part of our study is the continuation of the previous one, presented in Section 2.2, but this time $k+l+m=4$. In this study, structural and electronic properties of fifteen different microclusters of the type $Al_kTi_lNi_m$ ($k+l+m=4$) have been investigated theoretically. The elemental clusters (Al_4, Ti_4, Ni_4), their binary (Al_3Ni, Al_2Ni_2, $AlNi_3$, Al_3Ti, Al_2Ti_2, $AlTi_3$, Ni_3Ti, Ni_2Ti_2, $NiTi_3$), and ternary combinations (Al_2TiNi, $AlTi_2Ni$, $AlTiNi_2$) have been studied in their ground states.

This work is composed of two stages. In the first stage, we have parameterized a reliable empirical PEF for the AlTiNi ternary system. The PEF used in the calculations includes two– and three–body atomic interactions which were respectively represented by Lennard–Jones and Axilrod–Teller type functions. Then, performing MD simulations, we obtained and reported minimum energy configurations for the clusters. A discussion about the energetics of the species in both 1 K and 300 K then follows. We compared the energetically most stable geometries with the previously reported ones computed by various other approximate methods and estimated experimentally (available only for Al_4 and Ni_4). In the

second stage, in order to explore the electronic properties of the most stable clusters obtained from MD simulations, we have performed DFT calculations within the effective core potential (ECP) level with B3LYP exchange–correlation potential, the same as in the first part. The DFT calculations were carried out by using the GAUSSIAN 98 package [155]. For all the clusters considered, the possible dissociation channels and the corresponding dissociation energies, the calculated highest occupied molecular orbital (HOMO), lowest unoccupied molecular orbital (LUMO), and HOMO–LUMO gap energies are presented. The calculated dipole moments and excess charges on the atoms of the four–atom clusters are also given.

4.2.2 Results and Discussions

4.2.2.1 MD Simulations Results

Having fixed the empirical potential parameters, we have used the new potential in the simulations of four–atom clusters of the elements under consideration, $Al_kTi_lNi_m$ ($k+l+m=4$), by MD technique. Since clusters assume their geometry according to the local minima on the potential energy hypersurface (PES) of the system, a cluster should be expected to have as many "isomers" as the number of local minima, just like molecules. In order to "catch" the real minimum energy configuration of the system, corresponding to the global minimum on the PES hypersurface, one then must try as many initial configuration as possible *at low*

temperature. Although the difference in the interaction energy of the isomers is usually small, their structures may be greatly different. (Here an important point is in order: there exist some well–known standard methods to determine the global minimum–energy configuration of a system. For example, a single initial configuration can be optimized either through the simulated annealing or quenching, or through the conjugated gradient and steepest descend methods. There should be no doubt that it is more likely to find the global minimum–energy configuration of the system under consideration by starting with many randomly–chosen different initial configurations than by starting with only a single initial configuration optimized through the methods mentioned above [236].) For all these reasons, we have tried 1000 randomly generated initial configurations, within a volume of $7.5 \times 7.5 \times 7.5$ Å^3, for each cluster under consideration. Each configuration then was relaxed, as an isolated cluster, through the MD simulations at low temperature, 1 K. The one giving the minimum energy was then taken as the most stable structure for the cluster. The cluster geometry of the most stable structures obtained using the MD simulations are shown in Figure 4.7 (which correspond to the geometry of the cluster at the last MD step), the corresponding interatomic distances are given in Table 4.1.

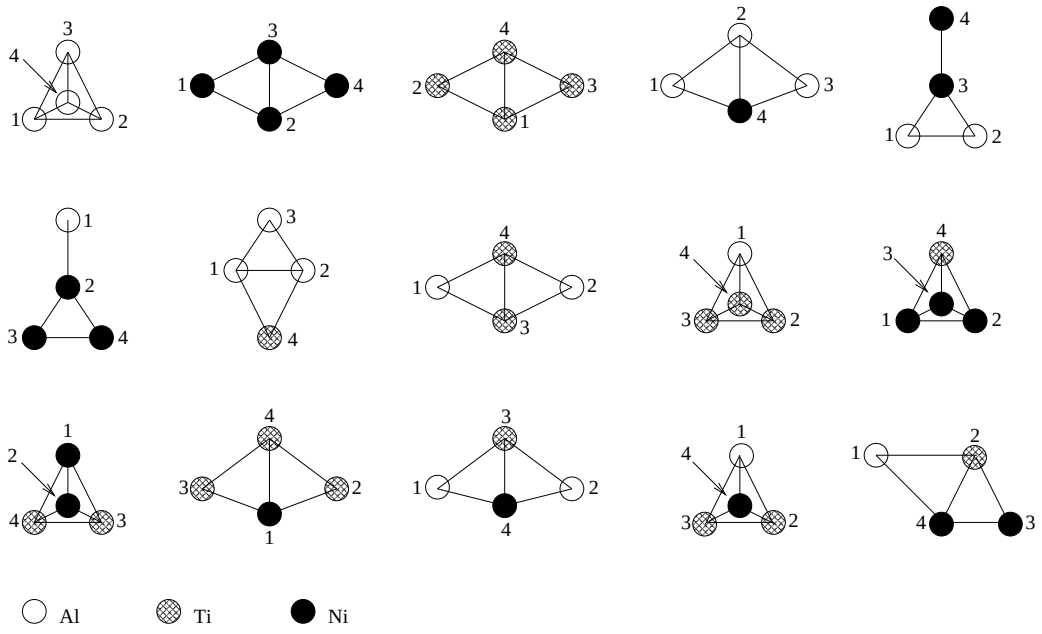

Figure 4.7: Structures of clusters optimized with use of the empirical potential via MD simulations.

Table 4.1: Interatomic distances (in Å) of the stable clusters obtained as the result of MD simulations. (d_{ij} is the distance between atoms i and j. The geometries of the clusters and the labels of the atoms are as shown in Figure 4.7.)

Cluster	Dimensionality	d_{12}	d_{13}	d_{14}	d_{23}	d_{24}	d_{34}
Al_4	3D	2.67	2.67	2.67	2.67	2.67	2.67
Ni_4	2D	2.29	2.29	3.88	2.43	2.29	2.29
Ti_4	2D	2.36	2.36	2.46	4.02	2.35	2.35
Al_3Ni	2D	2.63	4.25	2.28	2.63	2.35	2.28
Al_2Ni_2	2D	2.61	2.25	4.20	2.25	4.21	2.16
$AlNi_3$	2D	2.18	4.27	4.28	2.26	2.26	2.30
Al_3Ti	2D	2.71	2.60	2.78	2.60	2.78	4.64
Al_2Ti_2	2D	4.88	2.70	2.70	2.70	2.70	2.31
$AlTi_3$	3D	2.72	2.72	2.72	2.37	2.37	2.37
Ni_3Ti	3D	2.33	2.33	2.03	2.33	2.03	2.03
Ni_2Ti_2	3D	2.27	2.05	2.05	2.05	2.05	2.46
$NiTi_3$	2D	2.02	2.07	2.02	2.37	3.80	2.36
Al_2TiNi	2D	4.40	2.72	2.24	2.72	2.24	2.01
$AlTi_2Ni$	3D	2.73	2.73	2.27	2.37	2.04	2.04
$AlTiNi_2$	2D	2.76	4.13	2.21	2.03	2.01	2.20

Starting with many randomly–chosen different initial configurations assisted us in identifying the isomers of the clusters, so that we were able to determine the energy distribution of each species. Just for an example, for Al_4 case, 1000 initial random geometry resulted in four distinct energy values (so that four well-defined geometries), namely around 6.6 eV (equilateral pyramid), 6.5 eV (equilateral parallelogram), 5.9 eV (Y-shaped, like Al_2Ni_2 in Figure 4.7), and 5.3 eV (linear). We saw that each of the trial runs went into one of these four values, not into any other energy (geometry). This situation was similar for all the remaining clusters. We tabulated the energy distribution data in Table 4.2. As is seen from that table, the number of isomers varies from one species to another, according to their constituent atoms. As advertised previously, we saw indeed several "isomers" for each cluster, possessing geometries not similar at all each other. That there exist only a few, finite number of local minima is the result of the fact that we chose our working temperature as to be 1 K. At such a low temperature, it is natural for only low–energy states (geometries) to be populated. To see the effect of temperature on the energy levels (geometries) of the clusters, we performed another series of simulations at 300 K. We were again able to obtain the minimum energy–geometries obtained at 1 K with some small distortions. Because the increased temperature adds some small amount of kinetic energy to the atoms, the minimum–energies at 300 K were slightly larger (i.e. absolutely smaller) than those at 1 K (compare the third column with the last column in Table 4.3). The

most striking difference between the studies at 1 K and 300 K was that in the latter case there was no distinct energy values (so that no well–defined geometries) at all. For all the clusters considered, we witnessed the same situation at 300 K. Put another way, the increased temperature caused high–energy states (beside the low–energy states) to populate. To visualize this phenomenon clearly, we superimposed in Figure 4.8 the Gaussian-broadened distributions (for number of clusters possessing the energy between E and $E + dE$) of Al_4 clusters at 1 K and 300 K. It follows from this figure that the distinct energy values at 1 K (corresponds to peaks in dashed–line curve) disappear at 300 K (only one peak in solid curve). Secondly, we see that the majority of randomly–chosen different initial configurations result in structures with energy close to the global minimum. This means that 300 K for Al_4 cluster (and for others also) should not be considered as *high temperature*.

Clusters differ from molecules which usually possess definite compositions and definite geometries. As mentioned above, the properties of a cluster depend on the number of constituent atoms and so does the energetically most stable structure. Although a particular geometry may be more stable than any of several others, clusters generally can assume any of a number of different geometries. In low–temperature studies, like the present one, the number of distinct geometries is finite because the cluster does not have energy enough to pass over some "large"

Table 4.2: Energy distribution of the clusters studied. (E is the total interaction energies of possible isomers via MD simulation. n represents the total number of trials giving the same energy.)

Cluster	$-E(n)$					
Al_4	6.6 (12)	6.5 (151)	5.9 (567)	5.3 (270)		
Ti_4	7.9 (52)	7.3 (493)	6.7 (455)			
Ni_4	8.1 (14)	7.8 (326)	7.5 (565)	7.3 (27)	7.2 (45)	6.7 (23)
Al_3Ti	6.5 (46)	6.3 (40)	6.2 (221)	5.9 (320)	5.6 (200)	5.5 (154)
	5.4 (19)					
Al_2Ti_2	8.7 (409)	8.1 (19)	7.6 (230)	7.5 (262)	5.7 (76)	5.3 (4)
$AlTi_3$	9.5 (155)	9.0 (842)	5.3 (3)			
Al_3Ni	6.9 (72)	6.7 (59)	6.4 (48)	6.1 (288)	6.0 (203)	5.6 (100)
	5.3 (230)					
Al_2Ni_2	7.5 (164)	7.4 (81)	6.6 (505)	6.5 (21)	6.4 (74)	6.3 (30)
	6.0 (5)	5.4 (120)				
$AlNi_3$	7.8 (186)	7.5 (345)	7.4 (430)	5.7 (34)	5.6 (5)	
Ti_3Ni	9.0 (54)	8.4 (44)	7.9 (340)	7.3 (115)	7.1 (130)	6.7 (287)
Ti_2Ni_2	10.4 (294)	9.5 (267)	8.9 (3)	8.5 (283)	8.1 (2)	6.9 (8)
	6.8 (94)	6.7 (49)				
$TiNi_3$	10.4 (55)	10.3 (853)	10.2 (3)	9.5 (2)	9.3 (3)	9.1 (18)
	8.9 (7)	8.3 (1)	7.2 (58)			
Al_2TiNi	8.9 (317)	8.4 (23)	8.0 (141)	7.7 (130)	7.5 (275)	6.4 (1)
	5.5 (113)					
$AlTi_2Ni$	10.1 (180)	9.5 (159)	9.1 (658)	7.7 (1)	5.4 (2)	
$AlTiNi_2$	9.8 (604)	9.0 (1)	8.8 (20)	8.4 (1)	7.9 (365)	7.1 (6)
	6.7 (3)					

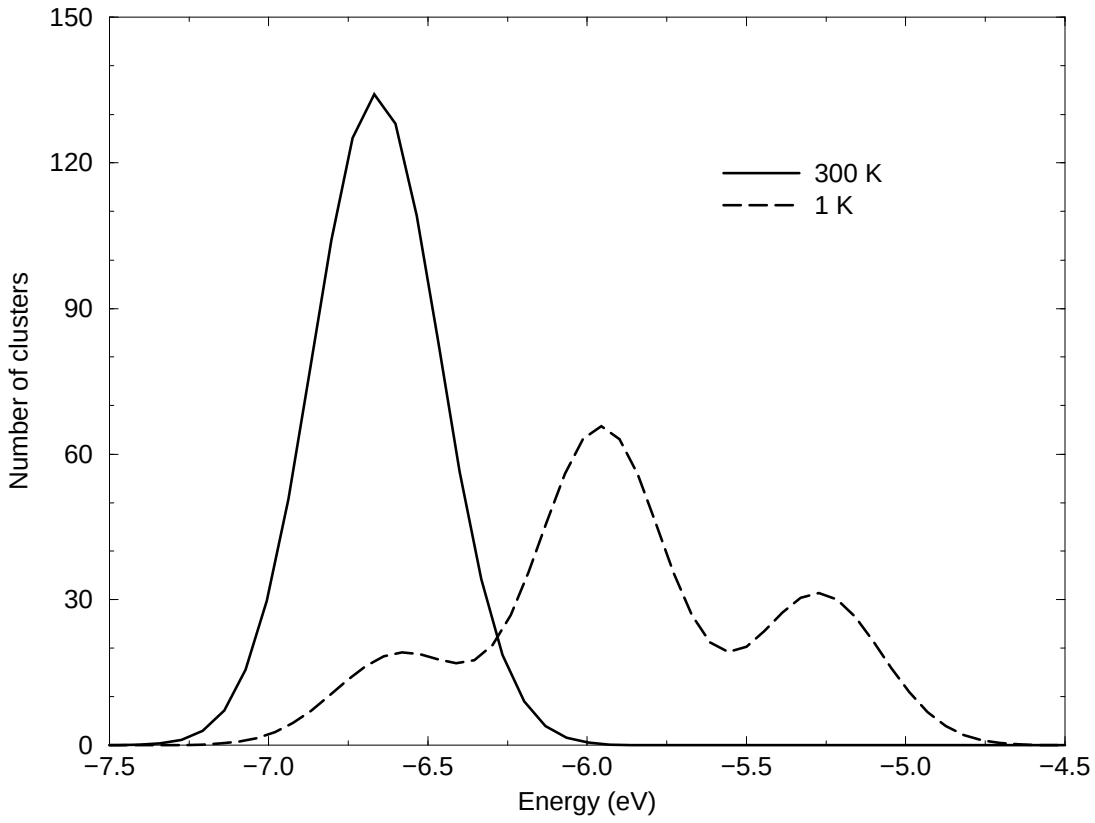

Figure 4.8: The Gaussian-broadened distributions (number of clusters possessing the energy between E and $E + dE$) of Al_4 clusters at 1 K and 300 K.

energy barriers on the potential energy surface. That is, the atoms are trapped inside some finite number of "deep" local minima. As the temperature increases, the cluster will have energy enough to pass over from any local minimum to another, deep or not; consequently, a cluster may assume many stable structures at high temperatures different from those in low temperatures.

Information about most of the clusters considered in this work does not exist in the literature. We have encountered data of only Al_4 and Ni_4 tetramers. Similar to the case in Section 2.2, we have again seen that there was no consensus about the question of whether these species was 2D or 3D. To our best knowledge, the present calculated values for the remaining thirteen clusters are the first to appear. In the following, we will compare the present results for Al_4 and Ni_4 with those from the literature. We will focus mainly on the structures of the four–atom clusters considered, not on the bond lengths.

Al_4: In this study, we found the most stable geometry of Al_4 to be a 3D tetrahedron with T_d symmetry (see Figure 4.7). Pacchioni and Koutecký [180] considered pseudopotential calculations and found that rhombic Al_4 was energetically most favorable. With an *ab initio* pseudopotential method, Upton [56] found that Al did not become 3D for Al_4, and the planar structures remained most stable. In his later perturbed electron drop model calculation, Upton [110]

reported that the Al_4 cluster having lowest energy is in a puckered rhombohedron structure which is between the square planar and tetrahedral geometries. Pettersson *et al.* [111] considered both *ab initio* and parametric empirical potential calculations for Al_n clusters, and they found the planar rhombus structure for Al_4 to be the lowest in energy. In the study of Erkoç [182] with a PEF, the tetrahedral form of Al_4 was reported to be most stable. In their empirical PEF calculation, Erkoç and Katırcıoğlu [183] calculated that the planar rhombus and the 3D tetrahedron structures were energetically very close to each other, but the tetrahedron geometry with T_d symmetry was slightly lower in energy. Jones [112], using DFT calculation, found that the planar rhombohedral structure (D_{2h}) was more stable. Employing MD technique, El–Bayyari and Erkoç [113] found a distorted tetrahedron as being most stable. Finally, with a first–principles calculation and a local orbital DFT study, Yang *et al.* [74] found a (nearly) rhombus as being most stable for Al_4.

Ni_4: Experimental observation of Parks *et al.* [237] showed that the structure of Ni_4 was not certain; it was probably two–dimensional such as rhombic. In this study, we also found the most stable geometry of Ni_4 to be a 2D rhombus (see Figure 4.7). In his extended Hückel and complete neglect of differential overlap (CNDO) calculations, Baetzold [39] reported a pyramidal structure for Ni_4 as most stable. In the literature, there are many studies showing the tetrahedron

geometry with T_d symmetry for Ni_4 energetically most favorable: Empirical PEF calculations of Erkoç [182, 191], Amerillas and Garzon [238], Nayak *et al.* [239]; effective medium calculations of Stave and DePristo [240], Wetzel and DePristo [241]; tight–binding MD calculations of Lathiotakis *et al.* [242], Bouarab *et al.* [243]; size–dependent empirical PEF calculation of Erkoç *et al.* [206]. A DFT calculation of Reuse and Khanna [91] gave the stable structure of Ni_4 as trigonal bipyramid and square. Finally, in their empirical PEF calculation, Hu *et al.* [244] found Ni_4 as trigonal pyramid.

4.2.2.2 Density Functional Theory Calculation Results

With the aim of predicting the electronic properties of the most stable clusters obtained from MD simulations, we have performed DFT calculations within the effective core potential (ECP) level [with B3LYP exchange–correlation contribution]. In Table 4.3 we present the interaction energy, $E_{\rm I}$(DFT), calculated by DFT method with the total potential energy, $E_{\rm T}$(MD), calculated by empirical potential (through MD simulations). The interaction energy $E_{\rm I}$(DFT) of the four–atom clusters was calculated using

$$E_{\rm I} = E_{\rm total}^{\rm ABCD} - E_{\rm total}^{\rm A} - E_{\rm total}^{\rm B} - E_{\rm total}^{\rm C} - E_{\rm total}^{\rm D}\,, \tag{4.20}$$

where $E_{\rm total}$ are the total energies obtained from the DFT calculations for four-atom (ABCD) and individual atoms (A, B, C, D). We see from Table 4.3 that

there are some small discrepancies between the two types of calculations, as one should expect. However, the discrepancy for Al_4 is quite large, which is an exceptional case. (This may be due to the fact that the minimum–energy configuration of Al_4 in this work has been determined by using MD method; it has not been optimized thoroughly by using DFT method. As a result, the optimized structure of Al_4 obtained from MD simulation might not correspond to the minimum–energy configuration which would be obtained using only DFT method. We now know that most of the DFT method gives the minimum energy configuration of Al_4 as being a rhombohedral structure, like in the Ref. [74]. Recall that the our result was a 3D tetrahedron.) Existence of small discrepancies the potential energies of the two methods should not be surprising. One should not expect the two energy values to have the same value: during the parametrization process of PEF, there were many quantities (bond length, interaction energies and geometries of dimers and trimers) to be re–obtained altogether as close as those resulting from experiments and, at the same time, those resulting from the previous *ab initio* results. This many–quantity–process indispensably creates some amount of discrepancy between the two types of energy values.

Table 4.3: Calculated interaction energy by DFT method, E_I(DFT), and total potential energy by empirical potential (through MD simulations at 1 K), E_T(MD). (Contributions of two– and three–body energies, E_2 and E_3, to total potential energy, E_T(MD), and their ratio are given separately. The last column gives total energy at 300 K through MD simulations, $-E_T^{300K}$(MD). Energies are in eV.)

Cluster	$-E_I$(DFT)	$-E_T$(MD)	$-E_2$	E_3	(E_3/E_2) $\times 100$	$-E_T^{300K}$(MD)
Al_4	2.9054	6.6494	9.0208	2.3715	$\sim$ 26	6.6448
Ti_4	9.4808	7.8733	9.7853	1.9120	$\sim$ 20	7.8674
Ni_4	6.7985	8.0877	10.5045	2.4168	$\sim$ 23	8.0767
Al_3Ti	5.6978	6.5162	8.0612	1.5451	$\sim$ 19	6.5106
Al_2Ti_2	5.2894	8.7285	8.8627	0.1343	$\sim$ 02	8.7240
$AlTi_3$	8.7790	9.5257	10.9172	1.3915	$\sim$ 13	9.5209
Al_3Ni	5.6401	6.8813	8.2493	1.3680	$\sim$ 17	6.8720
Al_2Ni_2	6.3613	7.4618	7.2686	-0.1933	$\sim$ 03	7.4335
$AlNi_3$	7.8628	7.7821	8.2394	0.4573	$\sim$ 06	7.7576
Ti_3Ni	7.3243	9.0458	10.6066	1.5608	$\sim$ 15	9.0413
Ti_2Ni_2	8.6911	10.3836	12.6011	2.2174	$\sim$ 18	10.3774
$TiNi_3$	8.8924	10.3685	12.7273	2.3588	$\sim$ 19	10.3634
Al_2TiNi	7.0054	8.8912	9.1088	0.2169	$\sim$ 02	8.8882
$AlTi_2Ni$	8.5650	10.0629	11.3728	1.3099	$\sim$ 12	10.0601
$AlTiNi_2$	8.2884	9.8224	10.0150	0.1926	$\sim$ 02	9.8199

In Table 4.3 we also give the contributions the two– and three–body energies, E_2 and E_3, to the total energy, $E_{\rm T}$(MD) and the percentage ratio of E_3 to E_2. It is seen that, for all clusters but Al_2Ni_2, the three–body interaction is positive. That the mentioned percentage ratio varies between 2% and 26% indicates that the contribution of the three–body energies to the total energy is not at all negligible. This point is one of the most important conclusion to be drawn from this work. As an aside, a comparison of the geometries in Figure 4.7 with the E_3 values in Table 4.3 shows no correlation.

We calculated the possible dissociation channels and the corresponding dissociation energies, which are tabulated in Tables 4.4–4.6. We define the dissociation energy of a dissociation process XY $\rightarrow$ X + Y as $E_{\rm dis} = E^{\rm XY}_{\rm total} - E^{\rm X}_{\rm total} - E^{\rm Y}_{\rm total}$. In calculating the dissociation energies, we used the total energy values obtained from the DFT calculations; the four–atom cluster values are given in Table 4.3, the three–atom, two–atom, and atomic energies were from the first part of our work, Section 2.2. We see from Tables 4.4–4.6 that, apart from Al_2Ti_2 and Al_2Ni_2, all the dissociation energies are negative, as should be. The positive ones should not be interpreted as simultaneous dissociations or as unstable clusters. This is due to the fact that, although the dimers and trimers of our previous work were calculated thoroughly by using DFT method, the tetramers of the present work were calculated by using first MD method and then DFT method. Consequently,

the optimized structures of Al_2Ti_2 and Al_2Ni_2 obtained from MD simulations might not correspond, at least in energy, to the minimum–energy configuration which would be obtained using only DFT method. Nevertheless, Tables 4.4–4.6 are illustrative and are believed to give reasonable trends for dissociation channels. It is seen for each cluster that atomization energies (dissociation to the constituent atoms) are, not surprisingly, the greatest among the other possible dissociation energies. Homonuclear tetramers X_4 are seen to dissociate as $X_4 \rightarrow X_3 + X$, as expected. Apart from Al_2Ni_2 and $AlTi_3$, the remaining Al–contained clusters prefer to fragment to give one Al atom firstly. Al_2Ni_2 dissociates to give two AlNi dimers, consistent of the fact that AlNi dimer has a large binding energy (3.3511 eV, from the previous work, Section 2.2). Except $AlNi_3$, all XY_3 type clusters dissociate as $XY_2 + Y$. For the NiTi containing species, we see that there is no priority for neither Ni nor Ti to dissociate first. If one combines this datum with the fact that Al has a relative larger preference to dissociate firstly, we may conjecture the following: If we continue to enlarge our AlTiNi ternary system, we expect most of Al atoms to occupy outermost part of the system, relatively few to place themselves in the NiTi–rich inner part.

Table 4.4: Possible dissociation channels and the corresponding dissociation energies (in eV) for the clusters studied. (DC: dissociation channel, DE: dissociation energy.)

Cluster		DC	DE	Cluster		DC	DE
Al_4	$\rightarrow$	$Al_3 + Al$	-0.2194	Al_2Ni_2	$\rightarrow$	$2AlNi$	$+0.3409$
		$2Al_2$	-1.9993			$Al_2Ni + Ni$	-1.1082
		$Al_2 + 2Al$	-2.4525			$AlNi_2 + Al$	-1.4733
		$4Al$	-2.9054			$AlNi + Al + Ni$	-3.0102
						$Al_2 + Ni_2$	-4.6501
Ti_4	$\rightarrow$	$Ti_3 + Ti$	-3.6408			$2Al + Ni_2$	-5.1032
		$2Ti_2$	-3.6849			$Al_2 + 2Ni$	-5.9082
		$Ti_2 + 2Ti$	-6.5829			$2Al + 2Ni$	-6.3613
		$4Ti$	-9.4808				
				Ti_2Ni_2	$\rightarrow$	$TiNi_2 + Ti$	-1.7112
Ni_4	$\rightarrow$	$Ni_3 + Ni$	-0.8549			$Ti_2Ni + Ni$	-1.7337
		$2Ni_2$	-4.2822			$2TiNi$	-3.0846
		$Ni_2 + 2Ni$	-5.5404			$Ti_2 + Ni_2$	-4.5350
		$4Ni$	-6.7985			$Ti_2 + 2Ni$	-5.7932
						$TiNi + Ti + Ni$	-5.8879
Al_2Ti_2	$\rightarrow$	$AlTi_2 + Al$	$+0.6646$			$2Ti + Ni_2$	-7.4330
		$2AlTi$	-1.1478			$2Ti + 2Ni$	-8.6911
		$Al_2Ti + Ti$	-1.4807				
		$Al_2 + Ti_2$	-1.9384	Al_3Ti	$\rightarrow$	$Al_2Ti + Al$	-1.8891
		$2Al + Ti_2$	-2.3915			$Al_3 + Ti$	-3.0119
		$AlTi + Al + Ti$	-3.2186			$Al_2 + AlTi$	-3.1739
		$Al_2 + 2Ti$	-4.8363			$AlTi + 2Al$	-3.6270
		$2Al + 2Ti$	-5.2894			$Al_2 + Al + Ti$	-5.2447
						$3Al + Ti$	-5.6978

Table 4.5: Continuation of Table 4.4.

Cluster		DC	DE	Cluster		DC	DE
Al_3Ni	$\rightarrow$	$Al_2Ni + Al$	-0.3870	$AlNi_3$	$\rightarrow$	$Ni_3 + Al$	-1.9192
		$Al_2 + AlNi$	-1.8359			$AlNi_2 + Ni$	-2.9748
		$AlNi + 2Al$	-2.2890			$Ni_2 + AlNi$	-3.2536
		$Al_3 + Ni$	-2.9541			$AlNi + 2Ni$	-4.5117
		$Al_2 + Al + Ni$	-5.1870			$Ni_2 + Al + Ni$	-6.6047
		$3Al + Ni$	-5.6401			$3Ni + Al$	-7.8628
Ti_3Ni	$\rightarrow$	$Ti_2Ni + Ti$	-0.3668	$TiNi_3$	$\rightarrow$	$TiNi_2 + Ni$	-1.9125
		$Ti_3 + Ni$	-1.4843			$Ni_3 + Ti$	-2.9488
		$Ti_2 + TiNi$	-1.6231			$Ni_2 + TiNi$	-4.8310
		$Ti_2 + Ti + Ni$	-4.4263			$TiNi + 2Ni$	-6.0891
		$TiNi + 2Ti$	-4.5210			$Ni_2 + Ti + Ni$	-7.6342
		$3Ti + Ni$	-7.3243			$3Ni + Ti$	-8.8924
$AlTi_3$	$\rightarrow$	$AlTi_2 + Ti$	-2.8250	Al_2TiNi	$\rightarrow$	$AlTiNi + Al$	-1.5697
		$Ti_3 + Al$	-2.9390			$AlTi + AlNi$	-1.5835
		$Ti_2 + AlTi$	-3.8103			$Al_2Ni + Ti$	-1.7523
		$Ti_2 + Al + Ti$	-5.8811			$Al_2Ti + Ni$	-3.1967
		$AlTi + 2Ti$	-6.7082			$AlNi + Al + Ti$	-3.6543
		$3Ti + Al$	-8.7790			$Al_2 + TiNi$	-3.7491
						$TiNi + 2Al$	-4.2022
						$AlTi + Al + Ni$	-4.9346
						$Al_2 + Ti + Ni$	-6.5523
						$2Al + Ti + Ni$	-7.0054

Table 4.6: Continuation of Table 4.4.

Cluster		DC	DE	Cluster		DC	DE
$AlTi_2Ni$	$\rightarrow$	$Ti_2Ni + Al$	-1.6075	$AlTiNi_2$	$\rightarrow$	$TiNi_2 + Al$	-1.3085
		$AlNi + Ti_2$	-2.3159			$AlNi + TiNi$	-2.1341
		$AlTi_2 + Ni$	-2.6109			$AlTiNi + Ni$	-2.8527
		$AlTiNi + Ti$	-3.1293			$AlNi_2 + Ti$	-3.4004
		$AlTi + TiNi$	-3.6909			$AlNi + Ti + Ni$	-4.9373
		$AlNi + 2Ti$	-5.2139			$AlTi + Ni_2$	-4.9595
		$Ti_2 + Al + Ni$	-5.6670			$TiNi + Al + Ni$	-5.4852
		$TiNi + Al + Ti$	-5.7617			$AlTi + 2Ni$	-6.2176
		$AlTi + Ti + Ni$	-6.4942			$Ni_2 + Al + Ti$	-7.0303
		$Al + 2Ti + Ni$	-8.5650			$Al + Ti + 2Ni$	-8.2884

Some computational details in the DFT calculations are presented in Table 4.7 which contains mainly the molecular properties, the basis set and spin information of the species considered. Basis information reflects the basis set used in the calculation, namely CEP–121G. The size of basis set is fixed for each element in CEP–121G. The accuracy of results depends surely on the basis set used. In the present study the basis set used is believed to be sufficient for the species under study [156–158].

Table 4.7: Some molecular properties of the clusters studied. N_b: number of basis functions with symmetry A; N_g: number of primitive Gaussians; N_α: number of α–electrons; N_β: number of β–electrons. The point group symmetry of all the clusters are C_1.

Cluster	N_b	N_g	N_α	N_β	Cluster	N_b	N_g	N_α	N_β
Al_4	48	64	6	6	$AlNi_3$	114	220	29	28
Ti_4	136	272	24	24	$TiNi_3$	136	272	33	33
Ni_4	136	272	36	36	Ni_2Ti_2	136	272	30	30
Al_3Ti	70	116	11	10	Ti_3Ni	136	272	27	27
Al_2Ti_2	92	168	15	15	Al_2TiNi	92	168	18	18
$AlTi_3$	114	220	20	19	$AlTi_2Ni$	114	220	23	22
Al_3Ni	70	116	14	13	$AlTiNi_2$	114	220	26	25
Al_2Ni_2	92	168	21	21					

The positions of the highest occupied molecular orbital (HOMO) and the lowest unoccupied molecular orbital (LUMO), and the HOMO–LUMO difference (or the frontier molecular orbital energy gap, E_g) bear some importance from spectroscopic point of view. Since the number of electrons in Al_4, Ti_4, Ni_4, Ni_3Ti, Ni_2Ti_2, $NiTi_3$, and Al_2TiNi is even, this clusters have only α–states; on the other hand, the remaining clusters have odd number of electrons hence they have both α– and β–states. HOMO, LUMO, and E_g of the systems studied are tabulated in Table 4.8. Some interesting features follow from this table: its $E_g(\alpha)$ value tempts us to say that Al_2Ti_2 cluster has the best metallic property, but we should remember that a four–atom cluster is too small to be classified as conducting or

not. Another feature is that the gap of α states are relatively larger than that of β states, except $AlTi_3$. An interesting situation draws attention: a replacement of one Al atom by a Ni atom increases the $E_g(\alpha)$ value of Al_2Ti_2 by about eight times. This may be due to the drastic change in the geometry in passing from Al_2Ti_2 to $AlTi_2Ni$. The same situation takes place also in passing from Al_2Ti_2 to Al_3Ti and/or to $AlTi_3$.

The calculated excess charge (Mulliken charges) and dipole moments of the four–atom clusters are given in Table 4.9. We note that all the clusters bear a net dipole moment according to their geometry and configurations of constituent atoms, as expected. Because of its rotational symmetry, homonuclear Al_4 tetramer with tetrahedral structure experiences relatively less charge accumulations on the atoms, compared to the other clusters. But its resulting dipole moment is, however, not small because of the distribution of the excess charges among the atoms. The same distribution concern makes the Ti_4 cluster possess the smallest dipole moment. One of the important outcomes of the charge data from this table is that in all heteronuclear clusters containing Al (i.e. Al_3Ti, Al_2Ti_2, $AlTi_3$, Al_3Ni, Al_2Ni_2, $AlNi_3$, Al_2TiNi, $AlTi_2Ni$, $AlTiNi_2$) we never see a negative charge accumulation on Al atoms. A very similar conclusion holds for Ni atoms in species Ni_3Ti, Ni_2Ti_2, $NiTi_3$. Another interesting feature is the

Table 4.8: HOMO, LUMO energies (in Hatree) and HOMO–LUMO gap (E_g) energies (in eV) of the clusters studied, calculated by DFT method.

Cluster	HOMO(α)	LUMO(α)	$E_g(\alpha)$	HOMO(β)	LUMO(β)	$E_g(\beta)$
Al_4	−0.1511	−0.1281	0.6239	—	—	—
Ti_4	−0.1477	−0.0878	1.6324	—	—	—
Ni_4	−0.1614	−0.1175	1.1940	—	—	—
Al_3Ti	−0.1715	−0.1128	1.5959	−0.1640	−0.1156	1.3184
Al_2Ti_2	−0.1474	−0.1392	0.2253	—	—	—
$AlTi_3$	−0.1549	−0.0973	1.5695	−0.1558	−0.0906	1.7741
Al_3Ni	−0.1450	−0.1200	0.6803	−0.1520	−0.1308	0.5761
Al_2Ni_2	−0.1665	−0.1189	1.2955	—	—	—
$AlNi_3$	−0.1653	−0.1027	1.7034	−0.1509	−0.1042	1.2716
Ti_3Ni	−0.1448	−0.0903	1.4838	—	—	—
Ti_2Ni_2	−0.1488	−0.1033	1.2400	—	—	—
$TiNi_3$	−0.1304	−0.1016	0.7839	—	—	—
Al_2TiNi	−0.1537	−0.1033	1.3722	—	—	—
$AlTi_2Ni$	−0.1663	−0.0992	1.8253	−0.1580	−0.0969	1.6629
$AlTiNi_2$	−0.1582	−0.1039	1.4789	−0.1557	−0.1022	1.4552

Table 4.9: Excess charge (in units of electron charge) on atoms, and dipole moments (in Debye) of the clusters studied, calculated by DFT method. Refer to Figure 4.7 for the labels of atoms.

Cluster	q_1	q_2	q_3	q_4	μ_x	μ_y	μ_z	μ
Al_4	−0.027	0.027	−0.027	0.027	0.867	1.623	0.884	2.042
Ti_4	0.079	−0.087	−0.084	0.092	0.070	0.156	−0.042	0.176
Ni_4	0.062	0.056	0.021	−0.138	−1.636	−0.266	0.006	1.657
Al_3Ti	0.156	0.128	0.018	−0.303	−3.623	0.188	0.132	3.630
Al_2Ti_2	0.367	0.356	−0.334	−0.389	0.349	−0.081	0.011	0.358
$AlTi_3$	0.450	−0.094	−0.154	−0.203	−0.095	0.418	−2.907	2.938
Al_3Ni	0.279	0.280	0.277	−0.837	−0.122	0.920	−0.095	0.933
Al_2Ni_2	0.281	0.280	−0.580	0.018	−0.358	−0.002	−0.003	0.358
$AlNi_3$	0.400	−0.393	−0.013	0.006	0.858	0.356	0.039	0.930
Ti_3Ni	1.241	−0.368	−0.475	−0.398	0.061	2.278	0.002	2.279
Ti_2Ni_2	0.373	0.372	−0.371	−0.374	−0.006	0.011	1.750	1.750
$TiNi_3$	0.057	0.041	0.081	−0.179	0.460	0.058	2.593	2.635
Al_2TiNi	0.339	0.339	−0.361	−0.318	−0.000	3.512	0.000	3.511
$AlTi_2Ni$	0.259	−0.365	−0.362	0.469	−2.501	0.021	−0.378	2.530
$AlTiNi_2$	0.341	−0.261	0.146	−0.226	−0.562	0.895	0.009	1.057

unexpected situation between the symmetry of the structure and the charge distribution in clusters Ti_4 and Ni_4. We see that although the charge accumulation in Al_4 is commensurate with its geometry, the similar expected situation does not occur in Ti_4 and Ni_4: charges on the atoms of each of these clusters do not show any correlation with their geometry at all.

We have thus come to the end of the second part of our doctoral study. In these two studies, our aim was to determine the basic building blocks for the AlTiNi ternary clusters. We investigated systematically the simpler potential candidates for the building blocks, namely Al_2, Ti_2, Ni_2, AlTi, AlNi, TiNi, Al_3, Ti_3, Ni_3, Al_2Ti, $AlTi_2$, Al_2Ni, $AlNi_2$, Ti_2Ni, $TiNi_2$ (Section 2.2); and the more involved candidates Al_4, Ti_4, Ni_4, Al_3Ti, Al_2Ti_2, $AlTi_3$, Al_3Ni, Al_2Ni_2, $AlNi_3$, Ti_3Ni, Ti_2Ni_2, $TiNi_3$, Al_2TiNi, $AlTi_2Ni$, $AlTiNi_2$ (this section). In the latter, we investigated structural and electronic properties of $Al_kTi_lNi_m$ $(k+l+m=4)$ clusters by performing MD simulations and DFT calculations (within the B3LYP and effective core potential level). We first parametrized an empirical potential energy function (PEF) for the AlTiNi ternary system. We then determined stable structures of the clusters by MD simulations. We presented the possible dissociation channels and electronic properties, calculated by DFT method, of the stable clusters. We predicted that if the AlTiNi system was gradually enlarged, most of the Al atoms were expected to be distributed themselves in the outermost part of the system, relatively few to occupy in the NiTi–rich inner part. In the next part of our study we will see if this is the case or not.

4.3 Structural and Energetic Features of $Al_nTi_nNi_n$ (n = 1–16) Nanoparticles: Molecular Dynamics Simulations

4.3.1 Introduction

This is the last part of our doctoral study, which is the continuation of our previous two works (Sections 2.2 and 4.2). The general objective in our research series is to explore the clustering phenomenon in economically promising AlTiNi ternary alloy systems which is believed to lead valuable insights into the evolution from small clusters to bulk material. In this regard, we continue our research with this work. Here we theoretically investigated the structural and energetic features of the energetically most stable nanoparticles of the type $Al_nTi_nNi_n$ (n = 1–16), which were supposedly in their ground states. Using the previously parameterized empirical PEF for the AlTiNi ternary system (Section 4.2), we performed MD simulations. We obtained and reported minimum–energy configurations.

4.3.2 Results and Discussions

Since this work is the continuation of especially the second part, we used the same potential as in Section 4.2 in the simulations of the nanoparticles under consideration, $Al_nTi_nNi_n(n = 1–16)$, by MD technique. Because of the reasons explained previously (Subsection 4.2.2.1), in order to increase the chance of catching the "real" minimum–energy configuration of the system, corresponding to the global minimum on the PES hypersurface, we tried 1000 randomly generated initial configurations for each nanoparticle of different n value. These initial random geometries are generated within a cube of volume ranging from $(2.5\times2.5\times2.5)$ Å^3 for $n = 1$ to $(13 \times 13 \times 13)$ Å^3 for $n = 16$. Each configuration then was relaxed through the MD simulations as an isolated system; the one giving the minimum energy was *accepted* as the most stable structure for that nanoparticle. Indeed, we have again observed that as n increased, the number of local minima increased drastically, as expected. To give an idea, there were 936 runs (out of 1000 trials) giving the same minimum–energy configuration for $n = 1$, 120 runs for $n = 2$, 6 runs for $n = 3$; and there were only 1 run for each of the remaining n values. It is always a great trouble in this type of systems to answer the question "how can one decide that one particular configuration corresponds to the *global minimum* on the PES hypersurface?" Actually the answer is simple: "one cannot!" We can never ensure that, even after $n = 2$, our findings are the *global minima*. The only thing to do is to investigate the configuration of the same n numerous

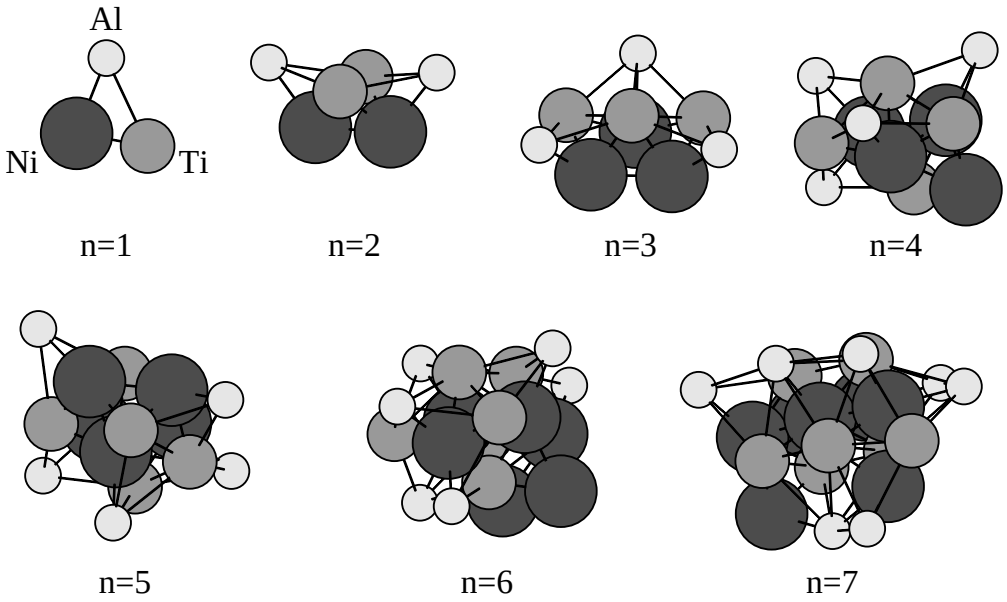

Figure 4.9: Optimum geometries of $Al_nTi_nNi_n$ $(n = 1 - 7)$ nanoparticles.

times, for instance, 10000, 100000 times; then to compare all the results and finally to choose the minimum one. But even in this case the *global minimum* may remain elusive. Fortunately, in our all cases, energies of most of the lowest minima were very close to each other and choosing the very lowest one is very likely to give intimately the properties of the global minimum. The geometries of the most stable structures obtained from the MD simulations are qualitatively shown in Figures 4.9–4.11. Tables 4.10 and 4.11 present the related quantitative information about the nanoparticles studied.

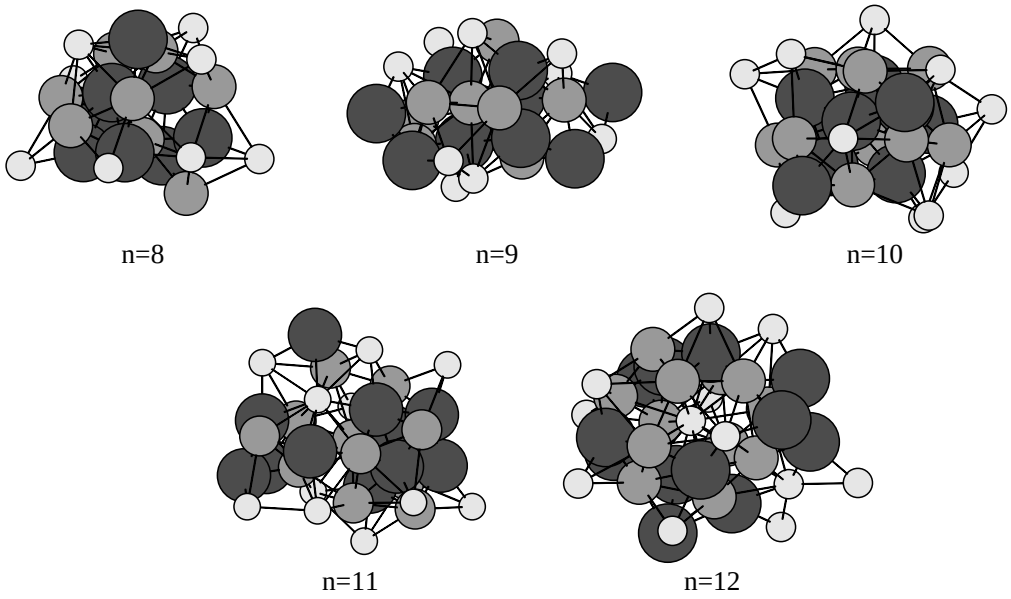

Figure 4.10: Optimum geometries of $Al_nTi_nNi_n$ $(n = 8 - 12)$ nanoparticles.

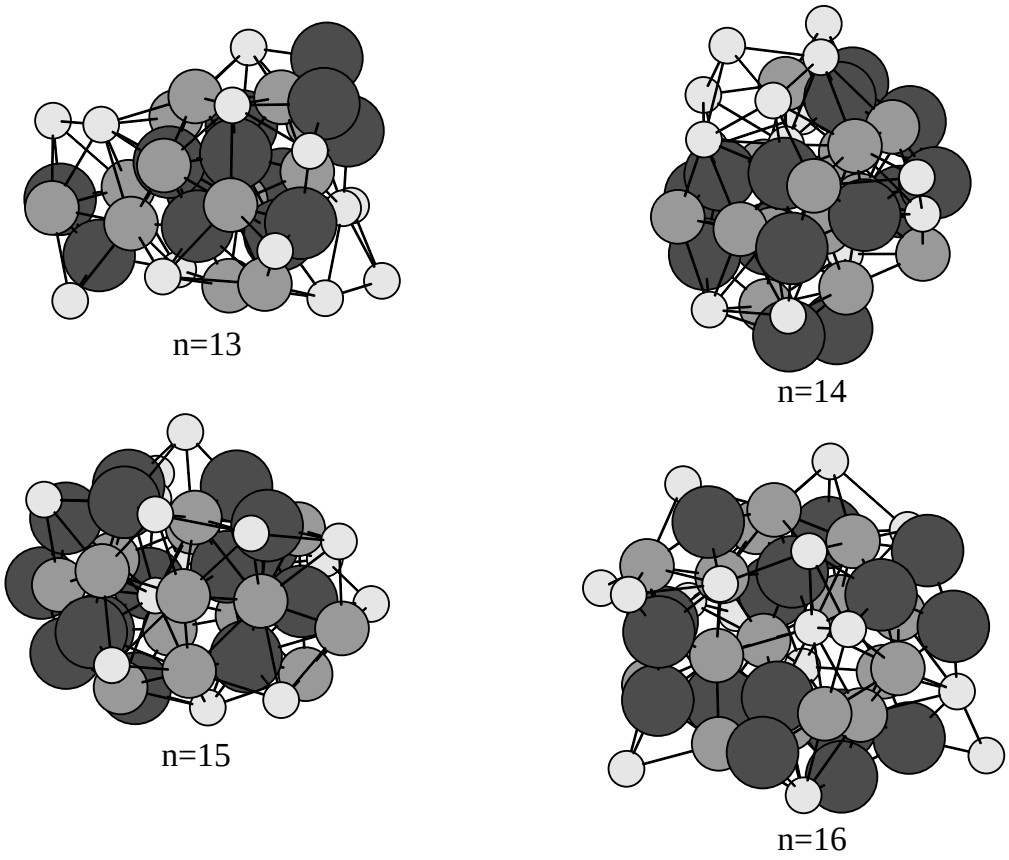

Figure 4.11: Optimum geometries of $Al_nTi_nNi_n$ $(n = 13 - 16)$ nanoparticles.

Table 4.10: Average interatomic distances for the neighboring atoms in the $Al_nTi_nNi_n$ nanoparticles. The distances are in Å.

$Al_nTi_nNi_n$ n	Al–Al	Al–Ti	Al–Ni	Ti–Ti	Ti–Ni	Ni–Ni
1	—	2.718	2.259	—	2.006	—
2	—	2.763	2.217	2.387	2.071	2.192
3	—	2.785	2.203	2.430	2.070	2.275
4	—	2.790	2.202	2.476	2.070	2.315
5	—	2.803	2.180	2.525	2.067	2.323
6	—	2.788	2.219	2.464	2.059	2.357
7	2.883	2.851	2.235	2.449	2.083	2.292
8	2.811	2.804	2.258	2.432	2.079	2.334
9	2.893	2.828	2.220	2.432	2.079	2.300
10	2.687	2.775	2.305	2.455	2.063	2.352
11	2.791	2.794	2.251	2.473	2.061	2.315
12	2.744	2.753	2.301	2.423	2.062	2.275
13	2.728	2.788	2.297	2.450	2.090	2.318
14	2.757	2.797	2.260	2.430	2.078	2.276
15	2.702	2.785	2.263	2.435	2.075	2.300
16	2.716	2.780	2.269	2.425	2.080	2.303

Table 4.11: Energetics of most stable $Al_nTi_nNi_n$ nanoparticles. Calculated total potential energy by empirical potential (through MD simulations), E_T^n; contributions of two– and three–body energies, E_2^n and E_3^n, to total potential energy and their percentage ratio, $(E_3^n/E_2^n) \times 100$; contributions of elemental energies, E_{Al}^n, E_{Ti}^n, E_{Ni}^n, to total potential energy. The values within the parentheses are energies per particle, see the text. Energies are in eV.

n	$-E_T^n$	$-E_2^n$	E_3^n	$\frac{E_3^n}{E_2^n} \times 100$	$-E_{Al}^n$	$-E_{Ti}^n$	$-E_{Ni}^n$
1	5.41 (1.80)	5.60	0.19	~ 3	1.64 (1.64)	1.89 (1.89)	1.89 (1.89)
2	20.23 (3.37)	22.95	2.71	~ 12	5.09 (2.55)	7.87 (3.94)	7.27 (3.63)
3	35.93 (3.99)	42.82	6.89	~ 16	8.56 (2.85)	13.99 (4.66)	13.39 (4.46)
4	52.67 (4.39)	66.45	13.78	~ 21	11.67 (2.92)	20.52 (5.13)	20.48 (5.12)
5	70.04 (4.67)	89.26	19.22	~ 22	14.78 (2.96)	27.61 (5.52)	27.65 (5.53)
6	87.03 (4.84)	114.43	27.40	~ 24	20.04 (3.34)	35.23 (5.87)	31.77 (5.30)
7	103.90 (4.95)	141.37	37.47	~ 27	24.10 (3.44)	42.56 (6.08)	37.24 (5.32)
8	122.01 (5.08)	162.49	40.48	~ 25	27.88 (3.49)	50.37 (6.30)	43.75 (5.47)
9	138.98 (5.15)	186.01	47.03	~ 25	34.72 (3.86)	57.62 (6.40)	46.63 (5.18)
10	158.61 (5.29)	218.63	60.03	~ 28	36.30 (3.63)	65.39 (6.54)	56.92 (5.69)
11	175.40 (5.32)	234.46	59.06	~ 25	44.71 (4.07)	72.33 (6.58)	58.35 (5.31)
12	192.75 (5.35)	252.44	59.69	~ 24	48.90 (4.08)	83.88 (6.99)	59.98 (5.00)
13	211.12 (5.41)	293.56	82.44	~ 28	51.12 (3.98)	88.98 (6.85)	71.02 (5.46)
14	229.93 (5.47)	309.84	79.92	~ 26	61.81 (4.42)	94.01 (6.72)	74.11 (5.29)
15	248.70 (5.53)	335.14	86.44	~ 26	62.48 (4.17)	104.35 (6.96)	81.87 (5.46)
16	265.55 (5.53)	358.68	93.13	~ 26	67.71 (4.23)	112.38 (7.02)	85.47 (5.34)

In Figures 4.9–4.11, the Al atoms were drawn as the smallest, the Ti atoms as larger, and the Ni atoms as the largest, somewhat accordingly to their atomic numbers. To give an idea about the size of the minimum–energy nanoparticles, the maximum distance between any two atoms is 2.718 Å for $n = 1$, and 12.213 Å for $n = 16$. Apart from $n = 2$ and $n = 3$ cases, it is hardly possible to speak of any geometrical symmetry of the systems. This was expected because these nanoparticles are too small to be considered as being bulk and hence as having well–defined symmetrical structures. One interesting feature seen from the figures that, except in $n = 12$, $n = 15$, and $n = 16$ cases, most of the Al atoms occupy the outermost part of the system. The similar reverse fashion holds for the Ni atoms: most of them occupy the innermost part. The remaining Ti atoms are usually between these two regions. In other words, we may see the formation of the systems as though first the Ni atoms assembled to form the inner core part of the nanoparticles, then the Ti atoms tried to cover this Ni–core, and then the Al atoms distributed on the Ni–Ti rich part. This trend appears almost in all the nanoparticles considered. For the distribution of the Al atoms, the figures tempt us to say that the Al atoms starts to mix with the Ni–Ti mixture at $n = 12$ case. The existence of Al atom in the inner part for $n = 15$ and $n = 16$ cases implies us to predict that it is highly likely for the Al atoms to find places to themselves in the inner part of the system for cases of n greater than 16.

In Table 4.10 we tabulated the average interatomic distances for the atoms within the *first neighboring range*. With the expression *first neighboring range* we mean that, for the sake of clarity and simplicity, we only give the average interatomic distances, r, limited to ranges $0 < r < 3.0$ Å for Al–Al and Al–Ti bonds, $0 < r < 2.5$ Å for Al–Ni and Ni–Ni bonds, $0 < r < 2.6$ Å for Ti–Ti bonds and $0 < r < 2.2$ Å for Ti–Ni bonds. Commensurate with Figures 4.9–4.11, it is seen from Table 4.10 that there is no Al–Al bond till $n = 7$ case within the first neighboring range. The nearest–neighbor distance in the bulk aluminum is 2.864 Å [245]. This bulk value is comparable with our average Al–Al bond lengths which are roughly in the range from 2.7 to 2.9 Å. As to Al–Ti bonds it is seen that the average bond length steadily increases from $n = 1$ to $n = 5$ case; beginning from $n = 6$, it smoothly fluctuates about 2.80 Å. In Al–Ni bonds we see a persistent and smooth fluctuation about 2.25 Å. Like Al–Ti bond lengths, the average Ti–Ti bond length increases from $n = 1$ to $n = 5$ case, then fluctuates about 2.43 Å to compare with 2.95 Å [245], the nearest–neighbor distance in the bulk titanium. These situation results in the conclusion that our model underestimates the Ti–Ti bond length as compared to that in bulk. In Ti–Ni bond lengths we see a very smooth fluctuation about 2.07 Å. And finally, we again see an average bond length steadily increasing from $n = 1$ to $n = 6$ case, and then a smooth fluctuation about 2.31 Å, to compare with 2.489 Å [245], the nearest–neighbor distance in the bulk nickel. A general feature seen from

Table 4.10 that all above mentioned bond lengths less fluctuate as n increases, especially beginning from $n = 10$ case. Apart from the possibly fortuitous Al–Al case, we see that the average bond lengths are not harmonious with those of bulk. This situation should not to be regretted because, as we pointed out earlier, our parameter set is suitable for cluster properties, not for bulk.

In Table 4.11 we present energetic features of the nanoparticles obtained as most stable. It is seen that the total energy of the system, E_{T}; the two–body energy contribution, E_2; and the individual elemental energy contributions, E_{Al}, E_{Ti}, E_{Ni} are all negative and they demonstrate a steadily decreasing behavior, as expected. To get a better understanding, we also give within the parentheses average energies per particle, $E^n_{\mathrm{T}}/3n$, E^n_{Al}/n, E^n_{Ti}/n, and E^n_{Ni}/n. In Figure 4.12 we plotted these average energies with respect to n. We see from the plotting that all four energies are decreasing as n increases in such a way that they at first drop sharply, then go down gradually. Their trends show that they finally level off to some well-defined energies. These are all expected. Probably prohibitively, we can compare this trend with the cohesive energies of Al, Ti, and Ni from bulk, which are respectively 3.39, 4.85, and 4.44 eV/atom [245]. Our possible offlevel values are roughly 4.5, 7.5, and 5.5 eV/atom, not harmonious with bulk values. This is expected because of two reasons: first, our offlevel values are from AlTiNi–type nanoparticles, not from individual elemental clusters; second, at a

Figure 4.12: Variation of average interaction energies per particle versus cluster size.

cost of repeating, our parameter set is not appropriate for the bulk applications. What important here is the same ordering of cohesive energies obtained from both source: $E_{\mathrm{Ti}}^{\mathrm{coh}} < E_{\mathrm{Ni}}^{\mathrm{coh}} < E_{\mathrm{Al}}^{\mathrm{coh}}$. If we had rescale our parameters using known elemental bulk properties, we would probably cohesive energy values closer to the experimental ones.

In Table 4.11 we also give the contributions the two– and three–body energies, E_2 and E_3, to the total energy, E_T and the percentage ratio of E_3 to E_2. It is seen that, for all nanoparticles the three–body interaction energy is positive. It also follows from this table that the contribution of the three–body interaction also levels off to some fixed value between 26% and 28% . More importantly, that the mentioned percentage ratio varies between 3% to 28% indicates that the contribution of the three-body energies to the total energy is not at all negligible, as the same case as that in Section 4.2.2.2.

As we pointed out earlier, clusters occupy the intermediate region between atoms and bulk matter. If the number of atoms making up a cluster is large, and also the atoms themselves contain many electrons, as our case in this study, one cannot apply, at least for the time being, *ab initio* quantum methods because clusters are too big to handle properly. On the other hand, one cannot apply solid state physics methods because clusters are much smaller than small solids

that we can conceive of. The same situation exists from experimentalists' point of view. The clusters considered in this work may be produced experimentally but their structural and electronic analyses, if possible, may not be an easy task because of the fact that our clusters are not homonuclear and, even worse, two of the elements we considered are transition metals. Nevertheless, this study can be seen a preliminary work for possible future experimental studies. We did not attempt to calculate fundamental frequencies since this is computationally very expensive even for 4– or 5–atom clusters; and frequencies to be calculated were so many that we decided not to deal with them within the scope of this work.

In this study we presented our theoretical computational outcomes on the structural and energetic features of the most stable $Al_nTi_nNi_n$ $(n = 1 - 16)$ nanoparticles via MD technique. We believe that the structural features obtained in this treatise are reasonable and reliable. The trends seen in energetics of the systems studied appeared to be correct although, not surprisingly, the numerical values are not harmonious with those of bulk.

CHAPTER 5

CONCLUSIONS

5.1 A General Look

In this doctoral study, structural and electronic properties of AlTiNi ternary cluster systems are studied theoretically. Due to their physical, chemical, metallurgical, and economical importance, we deal with the microclusters of aluminum, nickel and titanium in various combinations, $Al_kTi_lNi_m$ $(k+l+m=2-4)$, and with the nanoparticles of type $Al_nTi_nNi_n$ $(n=1-16)$.

This work consists of three main parts. In the first part of our study, we investigated structural and electronic properties of 16 different microclusters of the type $Al_kNi_lTi_m$; $k+l+m=n)$; $(n=2,3)$. We studied the dimers (Al_2, Ti_2, Ni_2), trimers (Al_3, Ti_3, Ni_3) of aluminum, titanium, and nickel, and their binary combinations (AlNi, AlTi, NiTi, Al_2Ni, AlNi2, Al_2Ti, Ni_2Ti, $AlTi_2$, $NiTi_2$), and the ternary combination (AlTiNi) in their ground states. We performed the density functional theory (DFT) calculations. We have presented the literature with our results as an article titled **Structural and electronic properties**

of $Al_kNi_lTi_m$; $k+l+m=n$); $(n=2,3)$ microclusters: density functional theory calculations [H. Oymak, Ş. Erkoç, Phys. Rev. A **66**, 033202 (2002)], where we reported the calculated spectroscopic constants (binding energy D_e, equilibrium interatomic separation r_e, and fundamental frequency w_e) of the dimers, the minimum energy configurations of the trimers (bond lengths and bond angle, as well as their fundamental frequencies w_n). For all the microclusters considered, we presented the possible dissociation channels and the corresponding dissociation energies, the calculated HOMO (highest occupied molecular orbital), LUMO (lowest unoccupied molecular orbital), and HOMO–LUMO gap energies. We also gave the calculated dipole moments and excess charges on the atoms of the trimers. We compared the calculated values with the previously reported ones computed by various other approximate methods and estimated experimentally.

The second part of our study is the continuation of the first part: we studied structural and electronic properties of $Al_kNi_lTi_m$ $(k+l+m=4)$ by performing molecular–dynamics simulations (MD) and DFT calculations. The elemental clusters (Al_4, Ti_4, Ni_4), their binary (Al_3Ni, Al_2Ni_2, $AlNi_3$, Al_3Ti, Al_2Ti_2, $AlTi_3$, Ni_3Ti, Ni_2Ti_2, $NiTi_3$), and ternary combinations (Al_2TiNi, $AlTi_2Ni$, $AlTiNi_2$) have been studied in their ground states. Using the previous part's results and the related experimental data from the literature, a reliable empirical potential energy function (PEF) for AlTiNi ternary system has been developed. Then,

this PEF was applied to the four–atom AlTiNi microclusters for the determination of stable structures by employing MD simulations. The energetics of the clusters at 1 K and 300 K were also studied in this stage. Finally, the possible dissociation channels and electronic properties of the obtained clusters were calculated by the DFT method. In this part we placed the main emphasis on MD results. We have provided the literature with our results as an article titled **AlTiNi Ternary Alloy Clusters: Molecular Dynamics Simulations and Density Functional Theory Calculations** [Ş. Erkoç, H. Oymak, J. Phys. Chem. B **107**, 12118, 2003], where we reported minimum energy configurations and compared them with the previously reported ones (available only for Al_4 and Ni_4), dissociation channels and dissociation energies, the calculated HOMO, LUMO, HOMO–LUMO gap energies, and the calculated dipole moments and excess charges on the atoms of the four–atom clusters.

Within the scope of the first two parts of our study, we encountered in the literature of microclusters many experimental and theoretical studies focused on elemental clusters of aluminum, nickel but very limited for elemental titanium clusters. To our best knowledge, there is no study for the rest of the clusters mentioned above. Therefore, exploring the uncertain geometrical and electronic properties of the remaining microclusters was our aim the first two parts.

In the last part of our study, with the aim of getting valuable insights into the evolution from small clusters to bulk material, we theoretically investigated the structural and energetic features of the energetically most stable nanoparticles of the type $Al_nTi_nNi_n$ (n = 1–16). Using the previously parametrized empirical PEF for the AlTiNi ternary system, we performed MD simulations. We have presented the literature with our results as an article titled **Structural and energetic features of $\mathbf{Al_nTi_nNi_n}$ (n = 1–16) nanoparticles: molecular–dynamics simulations** [H. Oymak, Şakir Erkoç, Modelling Simul. Mater. Sci. Eng. **12**, 109 (2004)], where we reported the obtained minimum–energy configurations; we gave the average interatomic distances making a bond analysis and compared them with bulk; we stated the general trend toward the bulk; and finally some analysis about the energetic features.

We must here stress that our outcomes should not be taken for granted; they should be understood merely as *predictions* based on the CEP–121G basis functions and B3LYP exchange–correlation functional used in the first and second part of our study and on the PEF parameters for AlTiNi ternary system used in the second and third part.

It follows from the results of the present work that the present PEF works very well for the cluster properties of Al–Ti–Ni ternary systems. It will be scientifically and practically interesting to extend the present work to investigation of the surface and bulk properties of some Al–Ti–Ni binary and ternary systems by making use of the same PEF. An important point is in order here: since the present PEF has been parametrized to give primarily the cluster properties of Al–Ti–Ni ternary system, it may not give the proper surface and bulk properties as good as the cluster properties. If this is the case, one should modify the PEF by re–adjusting only the three–body intensity parameters Z, not the two–body parameters. This can be achieved by considering some of the surface and bulk characteristics, such as surface energy, surface reconstruction, surface multilayer relaxation, bulk stability condition, cohesive energy, elastic constants, phonon frequencies, etc.

In Section 1.1 we pointed out that one of the most important reason of the intense interest in the Al–Ti–Ni binary and ternary intermetallics was their shape–memory–alloy (SMA) properties. Unfortunately the cluster and nanoparticle systems considered in this work are too small to attach any SMA property to them. The possible thing to do is to parameterize the PEF for some Al–Ti–Ni binary and ternary systems to give primarily their bulk properties, as described in the previous paragraph. Then a specific system can be studied in different sizes and

especially in different temperatures; it is likely that the outcomes will shed light on the SMA properties of the system.

5.2 Afterword

Finally we have come to the end of this study. Before closing, it would be appropriate here to mention briefly the task of quantum mechanical methods in cluster research. At the time being there are denumerably many researchers around world who are after a theory, or a formalism, or an algorithm, or what it is called, which is capable of giving appropriate, reasonable, and/or accurate answers to some frequently asked questions. Some of them which are listed as follows [16]:

- At what cluster size do the typical metallic properties, such as high electronic and/or thermal conductivity, start to appear?
- At which rate does the ionization potential of clusters converge to the bulk work function?
- At which rate does the average binding energy per atom in a cluster converge cohesion energy of a crystal?
- Is the geometric arrangement of particles in cluster similar to that in the crystal or crystal surface or are, on the contrary, the geometric features of

clusters very specific?

- Is it possible to obtain the most stable cluster by adding more atoms or atom groups at proper places to a smaller stable cluster or, oppositely, should the cluster undergo deep qualitative arrangements during its growth?

- Is cluster stability a monotonic function of cluster size?

- If mass spectroscopy is used for the detection of clusters, the experimentalists very often find especially high abundances for certain cluster sizes in the mass spectra. What are the reasons for the appearance of these "magic numbers"?

- .....

A reliable theory for electronic structure is expected to give at least the basic starting point to answer all these questions. Quantum mechanical methods are now capable at least of answering the *qualitative* explanation and prediction of the electronic structure and properties of small stable molecular and cluster systems which are urged by modern chemistry and atomic & molecular physics. Unfortunately a reliable investigation of atomic and molecular systems with unusual fundamental properties needs much more elaborate quantum mechanical methods unless the system under consideration is indeed quite small. The applicability of sophisticated methods is still limited only to small systems. What

is worse is that experimentally most frequently studied and scientifically and practically most interesting small atomic clusters are made up of heavy atoms possessing large number of electrons. The situation is more serious in the case of transition metal clusters. As we stated earlier, clusters occupy the intermediate region between atoms and bulk matter. If the atoms making up cluster contain many electrons, as our case in the last part of our study, one cannot apply properly, at least for the time being, *ab initio* quantum methods because clusters are too big to handle properly. On the other hand, one cannot apply solid state physics methods because clusters are much smaller than small solids we can conceive of. What is needed is a tool which is particularly designated to study in this "no man's land". We believe that reliable empirical model potential energy functions are capable of dealing with these not too small nor big systems.

In this study we presented our theoretical computational outcomes on the structural and energetic features of Al–Ti–Ni ternary microclusters and nanoparticles via DFT and MD techniques. We believe that the structural and electronic features obtained in this treatise are reasonable and reliable so that the present study is a preliminary work in this "no man's land".

REFERENCES

[1] B. Huneau, P. Rogl, K. Zeng, R. S.–Fetzer, M. Bohn, J. Bauer, Intermetallics **7**, 1337 (1999).

[2] K. Zeng, R. S.–Fetzer, B. Huneau, P. Rogl, J. Bauer, Intermetallics **7**, 1347 (1999).

[3] D. Farkas, D. Roqueta, A. Vilette, K. Ternes, Modelling Simul. Mater. Sci. Eng. **4**, 359 (1996).

[4] A. Pasturel, C. Colinet, D. N. Manh, A. T. Paxton, M. van Schilfgaarde, Phys. Rev. B **52**, 15176 (1995).

[5] J. Y. Rhee, B. N. Harmon, D. W. Lynch, Phys. Rev. B **59**, 1878 (1999).

[6] T. Hong, T. J. W.–Yang, A. J. Freeman, T. Oguchi, Jian–hua Xu, Phys. Rev. B **41**, 12462 (1990).

[7] S. Lauer, Z. Guan, H. Wolf, Th. Wichert, Hyperfine interactions **120/121**, 307 (1999).

[8] Y. Du, N. Clavaguera, Journal of Alloys and Compounds **237**, 20 (1996).

[9] M. Widom, J. A. Moriarty, Phys. Rev. B **8967**, 58 (1998).

[10] Ş. Erkoç in *Proceedings of the International Conference on Advances in Materials and Materials Processing (ICAMMP–2002)*, edited by N. Chakraborti and U.K. Chatterjee (Tata McGraw–Hill, New Delhi, 2002).

[11] Ş. Erkoç in *Proceedings of the International Conference on Designing of Interfacial Structures in Advanced Materials and their Joints (DIS'02)*, edited by M. Naka (Osaka University, 2002).

[12] H. Oymak, Ş. Erkoç, Phys. Rev. A **66**, 033202 (2002).

[13] Ş. Erkoç and H. Oymak, J. Phys. Chem. B **107**, 12118 (2003).

[14] H. Oymak, Ş. Erkoç, Modelling Simul. Mater. Sci. Eng. **12**, 109 (2004).

[15] W. Weltner, Jr.; R. J. Van Zee, Annu. Rev. Phys. Chem. **35**, 291 (1984).

[16] J. Koutecký, P. Fantucci, Chem. Rev. **86**, 539 (1986).

[17] M. D. Morse, Chem. Rev. **86**, 1049 (1986).

[18] T. Halıcıoğlu, C. W. Bauschlicher, Jr; Rep. Prog. Phys. **51**, 883 (1988).

[19] K. Balasubramanian, Chem. Rev. **90**, 93 (1990).

[20] W. A. de Heer, Rev. Mod. Phys. **65**, 611 (1993).

[21] M. Brack, Rev. Mod. Phys. **65**, 677 (1993).

[22] E. R. Hilf, F. Kammer, K. Wien, Eds., *PDMS and Clusters*, Springer–Verlag, Berlin, 1986.

[23] S. Sugano, Y. Nishina, S. Ohnishi, Eds., *Microclusters*, Springer–Verlag, Berlin, 1987.

[24] D. R. Salahub, In *Ab Initio Methods in Quantum Chemistry–II*, Adv. Chem. Phys. Vol. LXIX, K. P. Lawley, Ed., John Wiley & Sons Ltd. 1987.

[25] M. Moskovits, Ed., *Metal Clusters*, John Wiley & Sons Ltd.

[26] P. Jena, B. K. Rao, S. N. Khanna, Eds., *Physics and Chemistry of Small Clusters*, NATO ASI Series, Series B: Physics Vol. 158, Plenum Press, New York, 1987.

[27] G. Pacchioni, P. S. Bagus, F. Parmigiani Eds., *Cluster Models for Surface and Bulk Phenomena*, NATO ASI Series, Series B: Physics Vol.283, Plenum Press, New York, 1992.

[28] G. G.–Moraga, *Cluster Chemistry*, Springer–Verlag, Berlin, 1993.

[29] P. J. Reynolds, Ed., *On Clusters and Clustering*, North–Holland, Amsterdam, 1993.

[30] H. Haberland, Ed., *Clusters of Atoms and Molecules*, Springer–Verlag, Berlin, 1994.

[31] H. Haberland, Ed., *Clusters of Atoms and Molecules II*, Springer–Verlag, New York, 1994.

[32] J.–P. Connerade, Ed., *Correlations in Clusters and Related Systems*, World Scientific, Singapore, 1996.

[33] P. Jena, S. N. Behera, Eds., *Clusters and Nanostructured Materials*, Nova Science Publishers, Inc., New York, 1996.

[34] R. D. Adams, F. A. Cotton, Eds., *Catalysis by Di– and Polynuclear Metal Clusters Complexes*, Wiley–Vch, New York, 1998.

[35] G. N. Chuev, V. D. Lakhno, A.P. Nefedov, Eds., *Progress in the Physics of Clusters*, World Scientific, Singapore, 1999.

[36] K.–H. M.–Broer, Ed., *Metal Clusters at Surfaces*, Springer, Berlin, 2000.

[37] G. Schmid, *Clusters and Colloids*, VCH Verlagsgesellschaft mbH, Weinheim, 1994.

[38] M. L. Cohen, in Ref.[23], pp.2.

[39] R. C. Baetzold, J. Catal. **29**, 129 (1973).

[40] H. Huber, G. A. Ozin, W. J. Power, J. Am. Chem. Soc. **98**, 6508 (1976).

[41] A. B. Anderson, J. Chem. Phys. **64**, 4046 (1976).

[42] M. Moskovits, J. E. Hulse, J. Chem. Phys. **66**, 3988 (1977).

[43] I. Shim, J. P. Dahl, H. Johansen, Int. J. Quantum. Chem. **15**, 311 (1979).

[44] J. O. Noell, M. D. Newton, P. J. Hay, R. L. Martin, F. W. Bobrowicz, J. Chem. Phys. **73**, 2360 (1980).

[45] H. Basch, M. D. Newton, J. W. Moskovitz, J. Chem. Phys. **73**, 4492 (1980).

[46] A. Wolf, H.-H. Schmidtke, Int. J. Quantum. Chem. **18**, 1187 (1980).

[47] M. D. Morse, G. P. Hansen, P. R. R. Langridge–Smith, Lan–Sun Zheng, M. E. Geusic, D. L. Michalopoulos, R. E. Smalley J. Chem. Phys. **80**, 5400 (1984).

[48] H. Knözinger, in Ref.[27], pp.131.

[49] E. J. Baerends, in Ref.[27], pp.189.

[50] S. J. Riley, in Ref.[31], pp.221.

[51] J. Belloni, J. Amblard, J. L. Marignier, M. Mostafavi, in Ref.[31], pp.290.

[52] A. B. Anderson, R. Hoffmann, J. Chem. Phys. **61**, 4545 (1974).

[53] C. F. Melius, J. W. Moskovitz, A. P. Mortola, M. B. Baillie, M. A. Ratner, Surface Sci. **59**, 279 (1976).

[54] J. L. Whitten, T. A. Pakkanen, Phys. Rev. B **21**, 4357 (1980).

[55] J. L. Whitten, Phys. Rev. B **24**, 1810 (1981).

[56] T. H. Upton, Phys. Rev. Lett. **56**, 2168 (1986).

[57] P. Mlynarski, D. R. Salahub, J. Chem. Phys. **95**, 6050 (1991).

[58] O. Kühnholz, M. Grodzicki, in Ref.[22], pp.198.

[59] P. S. Bagus, G. Pacchioni, in Ref.[27], pp.233.

[60] P. E. M. Siegbahn, M. A. Nygren, U. Wahlgren, in Ref.[27], pp.267.

[61] G. F. Tantardini, in Ref.[27], pp.389.

[62] R. Fournier, N. Russo, D. R. Salahub, M. Toscano, in Ref.[27], pp.433.

[63] H. Sellers, A. Ulman, Y. Shnidman, J. E. Eilers, in Ref.[27], pp.441.

[64] H. Burtscher, H. C. Siegmann, in Ref.[31], pp.272.

[65] H. Hövel, L. S. O. Johansson, B. Reihl, in Ref.[36], pp.37.

[66] H. C. Siegmann, in Ref.[27], pp.17.

[67] R. R. Lucchese, W. H. Marlow, in Ref.[29], pp.143.

[68] H. E. Stanley, A. Coniglio, S. Havlin, J. Lee, S. Schwarzer, in Ref.[29], pp.345.

[69] S. B. DiCenzo, G. K. Wertheim, in Ref.[31], pp.361.

[70] A. Perez, P. Mélinon, V. Paillard, V. Dupuis, P. Jensen, A. Hoareau, J. P. Perez, J. Tuaillon, M. Broyer, J. L. Vialle, M. Pellarin, B. Baugenard, J. Lerme, in Ref.[33], pp.319.

[71] H. Brune, in Ref.[36], pp.67.

[72] O. Sinanoğlu, J. Chem. Phys. **75**, 493 (1981).

[73] O. Sinanoğlu, Chem. Phys. Lett. **81**, 188 (1981).

[74] S. H. Yang, D. A. Drabold, J. B. Adams, A. Sachdev, Phys. Rev. B **47**, 1567 (1993).

[75] L. Jansen, R. Block, in Ref.[22], pp.151.

[76] G. S. Anagnostatos, in Ref.[26], pp.151.

[77] B. P. Feuston, R. K. Kalia, P. Vashishta, in Ref.[26], pp.283.

[78] T. P. Martin, T. Bergmann, H. Göchlich, T. Lange, in Ref.[27], pp.3.

[79] C. Yannouleas, E. Vigezzi, P. F. Bortignon, R. A. Broglia, in Ref.[27], pp.41.

[80] H. Müller, H. G.–Fritsche, L. Skala, in Ref.[30], pp.114.

[81] M. F. Jarrold, in Ref.[30], pp.315.

[82] E. E. B. Campbell, in Ref.[30], pp.331.

[83] T. D. Märk, O. Echt, in Ref.[31], pp.155.

[84] P. Jena, S. N. Khanna, B. K. Rao, in Ref.[33], pp.1.

[85] W. A. de Heer, in Ref.[36], pp.1.

[86] U. Heiz, W.–D. Schneider, in Ref.[36], pp.237.

[87] J. R. Morris, D. M. Deaven, K. M. Ho, Phys. Rev B **53**, R1740(1996).

[88] Ş. Erkoç, R. Shaltaf, Phys. Rev A **60**, 3053 (1999).

[89] H. Oymak, Ş. Erkoç, Int. J. Mod. Phys. **12**, 293 (2001).

[90] D. M. Cox, J. Trevor, R. L. Whetten, E. A. Rohlfing, A. Kaldor, J. Chem. Phys. **84**, 4651 (1986).

[91] F. A. Reuse, S. N. Khanna, Chem. Phys. Lett. 234, 77 (1995).

[92] R. E. Benfield, in Ref.[26], pp.401.

[93] P. Milani, W. de Heer, A. Châtelain, in Ref.[27], pp.67.

[94] L. A. Bloofield, J. P. Bucher, D. C. Douglass, in Ref.[29], pp.193.

[95] G. C. Papaefthymiou, in Ref.[29], pp.209.

[96] K. M. Unruh, C. L. Chien, P. Sheng, in Ref.[29], pp.303.

[97] S. N. Khanna, in Ref.[33], pp.265.

[98] P. J. Jensen, K. H. Bennemann, in Ref.[33], pp.277.

[99] W. Wernsdorfer, in Ref.[36], pp.211.

[100] C. Cossé, M. Fouassier, T. Mejean, M. Tranquille, D. P. DiLella, M. Moskovits, J. Chem. Phys. **73**, 6076 (1980).

[101] L. Skala, H. Müller, in Ref.[22], pp.144.

[102] W. Klein, H. Gould, in Ref.[29], pp.243.

[103] A. W. Castlemann, Jr., in Ref.[31], pp.77.

[104] D. A. Jelski, T. T. Rantala, T. F. George, in Ref.[29], pp.47.

[105] M. A. El–Sayed, in Ref.[29], pp.69.

[106] P. B. Armentrout, J. B. Griffin, J. Conceição in Ref.[35], pp.198.

[107] G. Blyholder, Surf. Sci. **42**, 429 (1974).

[108] G. Pacchioni, D. Plavšić, J. Koutecký, Ber. Bunsenges. Phys. Chem. **87**, 503(1983).

[109] C. W. Bauschlicher, Jr.; H. Partridge, S. R. Langhoff, P. R. Taylor, S. P. Walch, J. Chem. Phys. **86**, 7007 (1987).

[110] T. H. Upton, J. Chem. Phys. **86**, 7054 (1987).

[111] L. G. L. Pettersson, C. W. Bauschlicher, Jr.; T. Halicioğlu, J. Chem. Phys. **87**, 2205 (1987).

[112] R. O. Jones, Phys. Rev. Lett. **67**, 224 (1991).

[113] Z. El–Bayyari, Ş. Erkoç, Phys. Stat. Sol. (b) **170**, 103 (1992).

[114] L. Lian, C. –X. Su, P. B. Armentrout, J. Chem. Phys. **96**, 7542 (1992).

[115] J. Jortner, Z. Phys. D **24**, 247 (1992).

[116] G. M. Pastor, K. H. Bennemann, in Ref.[30], pp.86.

[117] M. Springborg, *Methods of Electronic–Structure Calculations: From Molecules to Solids*, John Willey and Sons, Surrey, 2000.

[118] M. Moskovits, D. P. DiLella, J. Chem. Phys. **72**, 2267 (1980).

[119] G. Mahler, in Ref.[22], pp.135.

[120] R. Chang, *Chemistry*, McGraw–Hill Inc., New York, 1981.

[121] T. H. Upton, W. A. Goddard III, J. Am. Chem. Soc. **100**, 5659 (1978).

[122] T. C. De Vore, A. Ewing, H. F. Franzen, V. Calder, Chem. Phys. Lett. **35**, 78 (1975).

[123] A. B. Anderson, J. Chem. Phys. **66**, 5108 (1977).

[124] R. E. Honig, J. Chem. Phys. **21**, 573 (1953) (In Ref. [43]).

[125] J. Drowart, R. E. Honig, J. Phys. Chem **61**, 980 (1957) (In Ref. [43]).

[126] J. Franzen, H. Hintenberger, Z. Naturforsch **16a**, 535 (1961) (In Ref. [43]).

[127] R. F. K. Herzog, W. P. Poschenrieder, F. G. Satkiewicz, Rad. Eff. **18**, 199(1973) (In Ref. [43]).

[128] J. M. Brom, Jr., W. D. Hewett, Jr., W. Weltner, Jr., J. Chem. Phys. **62**, 3122 (1975) (In Ref. [43]).

[129] T. A. Ford, H. Huber, W. Klotzbücher, E. P. Kündig, M. Moskovits, G. A. Ozin, J. Chem. Phys. **66**, 524 (1977) (In Ref. [43]).

[130] J. C. Miller, L. Andrews, Chem. Phys. Lett. **50**, 315 (1977) (In Ref. [43]).

[131] R. A. Teichman III, E. R. Nixon, J. Chem. Phys. **67**, 2470 (1977) (In Ref. [43]).

[132] J. E. Hulse, M. Moskovits, Surface Sci. **57**, 125 (1976) (In Ref. [43]).

[133] M. Moskovits, J. E. Hulse, Surface Sci. **61**, 302 (1976) (In Ref. [43]).

[134] Ş. Erkoç, *Lecture Notes on Molecular Physics*, (unpublished).

[135] R.G. Parr and W. Yang, *Density-Functional Theory of Atoms and Molecules*, Oxford University Press, New York, 1989.

[136] L. H. Thomas, Proc. Cambridge Phil. Soc. **23**, 542 (1926).

[137] E. Fermi, Rend. Acad. Lincei **6**, 602 (1927).

[138] P. Gombas, *Die statistische Theorie des Atoms und ihre Anwendungen*, Springer-Verlag, Vienna, 1949.

[139] E. Clementi, IBM J. Res. Develop. Suppl. **9**, 2 (1965).

[140] Ş. Erkoç, Int. J. Mod. Phys. C **11**, 1 (2000).

[141] P. Hohenberg and W. Kohn, Phys. Rev. **136**, B864 (1964).

[142] W. Kohn and L. J. Sham, Phys. Rev. **140**, A1133 (1965).

[143] Ş. Erkoç and H. J. F. Jansen, Phys. Rev. A **59**, 2490 (1999).

[144] F. Bloch, Z. Physzik, **57**, 545 (1929).

[145] P. A. M. Dirac, Proc. Camb. Phil. Soc. **26**, 376 (1930).

[146] E. Fermi, Z. Physzik, **48**, 73 (1928).

[147] J. C. Slater, Phys. Rev. **81** 385 (1951).

[148] J. C. Slater, *The Self–Consisten Field for Molecules and Solids: Quantum Theory of Molecules and Solids*, Vol. 4, McGraw–Hill, New York, 1974.

[149] J. M. Seminario, in *Modern Density Functional Theory: A Tool for Chemistry*, Theoretical and Computational Chemistry, Vol. 2, Eds. J. M. Seminario and P. Politzer, Elsevier Science B. V., 1995.

[150] A. D. Becke, Phys. Rev. A **33**, 3098 (1988).

[151] C. Lee, W. Yang, and R. G. Parr, Phys. Rev. B **37**, 785 (1988).

[152] B. G. Johnson, in *Modern Density Functional Theory: A Tool for Chemistry*, Theoretical and Computational Chemistry, Vol. 2, Eds. J. M. Seminario and P. Politzer, Elsevier Science B. V., 1995.

[153] J. K. Labanowski, J. W. Andzelm, *Density Functional Methods in Chemistry*, Springer, New York, 1991.

[154] S. J. Vosko, L. Wilk, and M. Nusair, Can. J. Phys. **58**, 1200 (1980).

[155] Gaussian–98 Rev. A.9 package, Gaussian Corporation.

[156] W. J. Stevens, H. Basch, and M. Krauss, J. Chem. Phys. **81**, 6026 (1984).

[157] W. J. Stevens, M. Krauss, H. Basch, and P. G. Jasien, Can. J. Chem. **70**, 612 (1992).

[158] T. J. Cundari and W. J. Stevens, J. Chem. Phys. **98**, 5555 (1993).

[159] G. E. Scuseria, J. Chem. Phys. **97**, 7528 (1992).

[160] C. Sosa, C. Lee, J. Chem. Phys. **98**, 8004 (1993).

[161] K. P. Huber, G. Herzberg *Constants of Diatomic Molecules*, Van Nostrand Reinholb Comp. New York, 1979.

[162] K. A. Gingerich, Faraday Symp. Chem. Soc. **14**, 109 (1980).

[163] M. F. Cai, T. P. Djugan, V. E. Bondybey, Chem. Rev. Lett. **155**, 430 (1989).

[164] H. Basch, W. J. Stevens, M. Krauss, Chem. Phys. Lett. **109**, 212 (1984).

[165] A. D. Becke, J. Chem. Phys. **84**, 4524 (1986).

[166] C. W. Bauschlicher, Jr.; L. G. M. Pettersson, J. Chem. Phys. **87**, 2198 (1987).

[167] K. K. Sunil, K. D. Jordan, J. Phys. Chem. **92**, 2774 (1988).

[168] J. S. Tse, J. Mol. Struct. **165**, 21 (1988).

[169] A. Kant, J. Chem. Phys. **41**, 1872 (1964).

[170] F. Ahmed, E. R. Nixon, J. Chem. Phys. **71**, 3547 (1979).

[171] J. Ho, M. L. Polak, K. M. Ervin, W. C. Lineberger, J. Chem. Phys. **99**, 8542 (1986).

[172] W. F. Cooper, G. A. Clark, C. R. Hare, J. Phys. Chem **76**, 2268 (1972).

[173] J. Harris, R. O. Jones, J. Chem. Phys. **70**, 830 (1979).

[174] A. Kant, S. –S. Lin, J. Chem. Phys. **51**, 1644 (1969).

[175] V. D. Fursova, A. P. Klyagina, A. A. Levin, G. L. Gutsev, Chem. Phys. Lett. **116**, 317 (1985).

[176] W. B. Pearson, *A Handbook of Lattice Spacings and Structures of Metals and Alloys*; Pergamon Press, Elmsford, N. Y., 1958.

[177] M. F. Jarrold, in Ref.[30], pp.288.

[178] A. P. Sutton, *Electronic Structure of Materials*, Clarendon Press, Oxford, 1996.

[179] J. A. Howard, R. Sutcliffe, J. S. Tse, H. Dahmane, B. Mile, J. Phys. Chem. **89**, 3595 (1985).

[180] G. Pacchioni, J. Koutecký, Ber. Bunsenges. Phys. Chem. **88**, 242 (1984).

[181] H. Basch, Chem. Phys. Lett. 136, 289 (1987).

[182] Ş. Erkoç, Phys. Stat. Sol. (b) **152**, 447 (1989).

[183] Ş. Erkoç, Ş. Katırcıoğlu, Phys. Stat. Sol. (b) **152**, K37 (1989).

[184] S. P. Walch, J. Chem. Phys. **86**, 5082 (1987).

[185] G. Ciccotti, D. Frenkel, and I. R. McDonald, *Simulation of Liquids and Solids: Molecular Dynamics and Monte–Carlo Methods in Statistical Mechanics*, North–Holland, 1989.

[186] R. M. Nieminen, M. J. Pusha, and M. J. Manninen, *Many–Atom Interactions in Solids*, Springer–Verlag, 1990.

[187] J. M. Ziman, *Principles of the Theory of the Solids*, Cambridge: Cambridge University Press, Section 6.10, 1965.

[188] O. Sinanoğlu, Adv. Chem. Phys. **12**, 283 (1967).

[189] J. N. Murrell, S. Carter, S. C. Farantos, P. Huxley, and A. J. C. Varandas, *Molecular Potential Energy Functions*, Wiley, 1984.

[190] Ş. Erkoç, Phys. Stat. Sol. (b) **155** 461 (1989).

[191] Ş. Erkoç, Phys. Stat. Sol. (b) **161** 211 (1990).

[192] Ş. Erkoç, *Physics Reports* **278**, 79 (1997).

[193] Ş. Erkoç, in *Annual Reviews of Computational Physics IX*, D. Stauffer (Ed.) World Scientific, Singapore, 2001.

[194] W. A. Tiller, J. Crystal Growth **70**, 13 (1984).

[195] Ş. Erkoç, Z. Phys. D **32**, 257 (1994).

[196] M. L. Klein, J. A. Venables (Eds.), *Rare Gas Solids*, Vol.1, Academic Press, London, 1976, pp.132.

[197] T. Halıcıoğlu and P. J. White, J. Vacuum Sci. Technol. **17**, 1213 (1980).

[198] T. Halıcıoğlu and P. J. White, Surf. Sci. **106**, 45 (1981).

[199] T. Halıcıoğlu, H. Ö. Pamuk, and Ş. Erkoç, Surface Sci. **143**, 601 (1984).

[200] B. M. Axilrod and E. Teller J. Chem. Phys. **11**, 299 (1943).

[201] Ş. Erkoç, T. Halıcıoğlu, and H. Ö. Pamuk, Surface Sci. **169**, L273 (1986).

[202] D. K. Choi, T. Takai, Ş. Erkoç, T. Halıcıoğlu, and W. A. Tiller, J. Crystal Growth **85**, 9 (1987).

[203] Ş. Erkoç and Katırcıoğlu, Chem. Phys. Lett. **147**, 476 (1988).

[204] Ş. Erkoç, T. Halıcıoğlu, and W. A. Tiller, Phys. Stat. Sol. (b) **156**, K105 (1989).

[205] H. Oymak, Ş. Erkoç, Chem. Phys. **300**, 277 (2004).

[206] Ş. Erkoç, B. Güneş, and P. Güneş, Int. J. Mod. Phys. C **11**, 1013 (2000).

[207] C. Özdoğan and Ş. Erkoç *Z. Phys. D* **41**, 205 (1997).

[208] L. Amirouche and Ş. Erkoç, *Phys. Rev. A* **68**, 043203 (2003).

[209] L. Amirouche and Ş. Erkoç, *Phys. Stat. Sol. (b)* **241**, 292 (2004).

[210] Ş. Erkoç and T. Yilmaz, *Physica E* **5**, 1 (1999).

[211] Ş. Erkoç, *Physica E* **8**, 210 (2000).

[212] T. Bastug, M. Hirata, S. Varga, B. Fricke, Ş. Erkoç, and T. Mukoyama, *Adv. Quantum Chem.* **37**, 353 (2001).

[213] Ş. Erkoç, T. Bastug, M. Hirata, and S. Tachimori, *Chem. Phys. Lett.* **314**, 203 (1999).

[214] T. Bastug, Ş. Erkoç, M. Hirata, and S. Tachimori, *Phys. Rev. A* **59**, 3690 (1999).

[215] Ş. Erkoç, T. Bastug, M. Hirata, and S. Tachimori, *Jap. Phys. Soc. J.* **68**, 440 (1999).

[216] Ş. Erkoç, L. Amirouche, and L. Rouaiguia, *Int. J. Mod. Phys. C* **13**, 759 (2002).

[217] Ş. Erkoç, *Lecture Notes on Simulations of Many–Particle Sytems* (unpublished).

[218] R. Bennett, in *Diffusion in Solids: Recent Developments*, Eds. A. S. Nowick, J. J. Burton, Academic Press, New York, 1975.

[219] N. Metropolis, *et al.,* J. Chem. Phys. **21**, 1087 (1953).

[220] *Methods in Comp. Phys.*, Vol. 1, B. Alder *et al.,* (Eds.), Academic Press, New York, 1963.

[221] W. W. Wood, and J. J. Erpenbeck, Ann. Rev. Phys. Chem. **27**, 319 (1976).

[222] *Monte–Carlo Methods in statistical Methods*, Second Edition, K. Binder (Ed.), Springer–Verlag 1986.

[223] *Methods in Comp. Phys.*, Vol. 15, G. Gilat (Ed.), Academic Press, New York, 1976.

[224] W. G. Hoover and W. T. Ashust, in *Theoretical Chem.: Advances and Perspectives*, Vol. 1, H. Eyring and D. Hendersen (Eds.), Academic Press, New York, 1975.

[225] D. Beeman, J. Comp. Phys. **20**, 130 (1976).

[226] D. J. Evans and G. P. Morriss Comp. Phys. Rep. **1**, 297 1984.

[227] J. M. Haile, *Molecular Dynamics Simulation*, John Wiley & Sons, Inc. Toronto, 1992.

[228] P. Schöfield, Comp. Phys. Comm. **5**, 17 (1973).

[229] S. L. Ross, *Differential Equations*, Third Edition, John Wiley, Toronto, 1984.

[230] F. Hildebrand, *Introduction to Numerical Analysis*, Second Edition, McGraw–Hill, New York, 1974.

[231] W. G. Hoover, *Molecular Dynamics*, Lecture Notes in Physics, Vol. 258, Springer–Verlag, Berlin, 1986; in Ref. [227].

[232] L. Verlet, Phys. Rev. **159**, 98 (1967); in Ref. [227].

[233] A. Rahman, hys. Rev. **136** (2A), 405 (1964); in Ref. [227].

[234] A. Nordsieck, Math. Compute. **16**, 22 (1962).

[235] C. W. Gear, *Numerical Initial Value Problems in Ordinary Differential Equations*, NJ: Prentice–Hall, Englewood Cliffs), 1971.

[236] H. Oymak, M.S. Thesis, pp. 52, Thesis, Middle East Technical University, Ankara, 1999.

[237] E. K. Parks, L. Zhu, J. Ho, and S. J. Riley, J. Chem. Phys. **100**, 7206 (1994).

[238] A. P. Amerillas and I. Garzon, Phys. Rev. B **54**, 10362 (1996).

[239] S. K. Nayak, S. N. Khanna, B. K. Rao, and P. Jena, J. Phys. Chem. A **101**, 1072 (1997).

[240] M. S. Stave and A. E. DePristo, J. Chem. Phys. **97**, 3386 (1992).

[241] T. L. Wetzel and A. E. DePristo, J. Chem. Phys. **105**, 572 (1996).

[242] N. N. Lathiotakis, A. N. Andriotis, M. Menon, and J. Connolly, J. Chem. Phys. **104**, 992 (1996).

[243] S. Bouarab, A. Vega, M. J. Lopez, M.P. Inigues, and J. A. Alanso, Phys. Rev. B **55**, 13279 (1997).

[244] W. J. Hu, L. M. Mei, and H. Li, Solid State Commun. **100**, 129 (1996).

[245] C. Kittel, *Introduction to Solid State Physics*; Seventh Edition, Wiley, New York, 1996.

VITA

Hüseyin Oymak was born in Denizli, Turkey, in 1971. He got his B.S. degree in physics and physics education at Middle East Technical University (METU) in Ankara, Turkey, in 1999. He was awarded for being ranked first among all graduates of bachelor's degree programs at METU in the 1998–1999 academic year. He obtained his M.S. degree in physics in the same university in 2000. Since August 1999, he has been posted as research assistant at METU. At the present time he is the co-auther of nine research papers published in international refeered journals:

1. Ş. Erkoç and H. Oymak, "Rules for the distribution of point charges on a conducting disk", Phys. Rev. E **62**, 3075 (2000).

2. H. Oymak and Ş. Erkoç, "Distribution of point charges on a thin conducting disk", Int. J. Mod. Phys. C **11**, 891 (2000).

3. H. Oymak and Ş. Erkoç, "Energetics and stability of discrete charge distribution on the surface of a sphere", Int. J. Mod. Phys. C **12**, 293 (2001).

4. Ş. Erkoç and H. Oymak, "Energetics and stability of discrete charge distribution on a conducting disk", Phys. Lett. A **290**, 28 (2001).

5. H. Oymak and Ş. Erkoç, "Structural and electronic properties of $Al_kTi_lNi_m$ $(k+l+m=2,3)$ microclusters: density functional theory calculations", Phys. Rev. A **66**, 33202 (2002).

6. Ş. Erkoç and H. Oymak, "AlTiNi ternary alloy clusters: molecular–dynamics simulations and density–functional–theory calculations", J. Phys. Chem. B **107**, 12118 (2003).

7. H. Oymak and Ş. Erkoç, "Structural and energetic features of $Al_nTi_nNi_n$ $(n=1-16)$ nanoparticles: molecular-dynamics simulations", Modelling Simul. Mater. Sci. Eng. **12**, 109 (2004).

8. H. Oymak and Ş. Erkoç, "Titanium Coverage on a Single-Wall Carbon Nanotube: Molecular Dynamics Simulations", Chem. Phys. **300**, 277 (2004).

9. Z. El–Bayyari, H. Oymak, and H. Kökten, "On the structural and energetic features of small metal clusters: Ni_n, Cu_n, Pd_n, Pt_n, and Pb_n; $n=3-13$", Int. J. Mod. Phys. C **xx**, xxx (2004) (in press).